



Michigan Technological University
Create the Future Digital Commons @ Michigan Tech

Dissertations, Master's Theses and Master's
Reports - Open

Dissertations, Master's Theses and Master's
Reports

2012

COORDINATION CHEMISTRY OF BIS(BENZYL)PHOSPHINATE

John S. Maass

Michigan Technological University

Follow this and additional works at: <https://digitalcommons.mtu.edu/etds>


 Part of the [Chemistry Commons](#)

Copyright 2012 John S. Maass

Recommended Citation

Maass, John S., "COORDINATION CHEMISTRY OF BIS(BENZYL)PHOSPHINATE", Master's Thesis,
Michigan Technological University, 2012.
<https://doi.org/10.37099/mtu.dc.etds/468>

Follow this and additional works at: <https://digitalcommons.mtu.edu/etds>

 Part of the [Chemistry Commons](#)

COORDINATION CHEMISTRY OF BIS(BENZYL)PHOSPHINATE

By

John S. Maass

A THESIS

Submitted in partial fulfillment of the requirements for the degree of

MASTER OF SCIENCE

In Chemistry

MICHIGAN TECHNOLOGICAL UNIVERSITY

2012

© 2012 John S. Maass

This thesis has been approved in partial fulfillment of the requirements for the Degree of
MASTER OF SCIENCE in Chemistry.

Department of Chemistry

Thesis Advisor: *Rudy L. Luck*

Committee Member: *Bahne C. Cornilsen*

Committee Member: *Jaroslav Drelich*

Department Chair: *Sarah A. Green*

Table of Contents

Acknowledgements.....	v
Preface	vi
Abbreviations.....	vii
List of Figures	ix
List of Tables	xiii
Abstract.....	xiii
Chapter 1 Background	1
1.1 Introduction.....	2
1.2 Properties of Phosphinic Acids and Phosphate Ligands.....	2
1.3 Coordination Chemistry of Phosphinates	6
1.4 Purpose of Work	9
References.....	10
Chapter 2 Vanadium Trimers.....	13
2.1 Syntheses, x-ray structural characterizations and thermal stabilities of two nonclassical ferromagnetic trinuclear vanadium (IV) complexes; $(V_3(\mu_3-O)_2)(\mu_2-O_2P(CH_2C_6H_5)_2)_6(H_2O)$ and $(V_3(\mu_3-O)_2)(\mu_2-O_2P(CH_2C_6H_5)_2)_6(py)$ and polymeric complexes of stoichiometry $(VO(O_2PR_2)_2)_\infty$, $R_2 = Ph_2$ and $o-(CH_2)_2(C_6H_4)$	14
2.2 Abstract.....	15
2.3 Introduction.....	16
2.4 Experimental.....	18
2.5. Results and Discussion	26
References.....	47
Supplemental Data.....	51
Chapter 3 Tungsten and Vanadium Cubanes.....	68
3.1 Expanding molecular transition metal cubane clusters of the form $[M_4(\mu_3-O)_4]^{12+}$: Syntheses, spectroscopic and structural characterizations of molecules $M_4(\mu_3-$ $O)_4(O_2P(Bn)_2)_4(O_4)$, $M = V^V$ and W^V	69
3.2 Abstract.....	70

3.3 Results and Discussion	70
3.4 Notes and references	78
Supplemental Data	83
Chapter 4 Cobalt Dimers	94
4.1 Syntheses and structures of three complexes of formulae $[L_3Co(\mu_2-O_2P(Bn)_2)_3CoL'] [L'']$, featuring octahedral and tetrahedral cobalt(II) geometries; variable temperature magnetic susceptibility measurement and analysis on $[(py)_3Co(\mu_2-O_2PBn_2)_3Co(py)][ClO_4]^{1,2}$	95
4.2 Abstract	96
4.3 Results and Discussion	97
References	104
Supplemental Data	108
Chapter 5 Conclusion	126
1.1 Conclusion	127
Appendix	130
License agreement for Chapter 2	131
License agreement for Chapter 3	132
License agreement for Chapter 4	133

Acknowledgements

I would like to thank my advisor Dr. Rudy L. Luck. Dr. Luck let me pursue my own research interests as an undergraduate from which I learned the rewards of scientific discovery. Dr. Luck and I have managed to amass a large catalog of publications from my work as an undergraduate and graduate student.

I would also like to thank both Dr. Cornilsen and Dr. Drelich for taking the time to serve on my masters committee. I am also very grateful to have worked with Dr. Linsheng Feng, Dr. Louis Pignotti and Zhichao Chen.

Finally, I would like to thank my parents who supported me throughout my academic career.

Preface

This thesis is comprised of five different chapters. Chapter 1 is an introductory chapter. Chapters 2-4 are the manuscripts of previously published papers. All of these papers were the work of multiply authors. Each manuscript contains its own figure, equation and reference numbering. Chapter 5 is a conclusion of the work.

Chapter 2 is the manuscript of a paper published in *Inorganic Chemistry*. The author of this dissertation was responsible for the synthetic work along with much of the spectrometry. Zhichao Chen measured the TGA, DSC and X-ray powder diffraction of some of the compounds. Richard E. P. Winpenny and Floriana Tuna measured the temperature dependant variable magnetic data and helped with interrupting the results. Matthias Zeller collected the X-ray crystallographic data. The writing of the paper was a collaborative effort between Rudy L. Luck, Zhichao Chen and the author of this dissertation.

Chapter 3 is the manuscript of a communication published in *Dalton Transactions*. The author of this dissertation was responsible for the synthetic work along with much of the spectrometry. Zhichao Chen was responsible for checking the preparation of the vanadium compound along with exploring different synthetic routes. Matthias Zeller collected the X-ray crystallographic data. The writing of the paper was a collaborative effort between Rudy L. Luck and the author of this dissertation.

Chapter 4 is the manuscript of a communication published in *Inorganic Chemistry*. The author of this dissertation was responsible for the synthetic work along with much of the spectrometry. Bart M. Bartlett and Tanya M. Breault were responsible for measuring the temperature dependent variable magnetic data. Hiroshi Sakiyama was responsible for the interpolation of the magnetic data along with the theoretical calculations. Matthias Zeller collected the X-ray crystallographic data. The writing of the paper was a collaborative effort between Rudy L. Luck and the author of this dissertation.

Abbreviations

1,5-COD	1,5-cyclooctadiene
Å	angstrom
Acac	acetylacetonate
Anal. Calc.	Analysis Calculated
Bn	benzyl
^t BuOOH	tertiary butyl hydroperoxide
^t BuOH	tertiary butyl alcohol
cp*	pentamethylcyclopentadienyl
cyclam	1,4,8,11-tetraazacyclotetradecane
DSC	differential scanning calorimetry
EtOH	ethanol
FTIR	Fourier Transformation Infrared
<i>g</i>	dimensionless magnetic moment
IR	Infrared
<i>J</i>	intramolecular exchange interaction
Ph	phenyl
Pr ⁱ	isopropyl
Me	methyl
mmol	millimole
mol	mole
NMR	nuclear magnetic resonance
Oe	magnetic field strength
Ph	phenyl

Py	pyridine
pz	pyrazolyl
TGA	thermogravimetric analysis
Tert	tertiary
THF	tetrahydrofuran
TIP	temperature independent paramagnetism
UV-vis	ultraviolet-visible
X_m	magnetic susceptibility
Δ	energy gap between states
δ	NMR shift in ppm
κ	orbital reduction factor
θ	Weiss constant
ν	distortion parameter
λ	spin-orbit coupling factor
μ_B	magnetic susceptibility
σ^*	antibonding sigma orbital

List of Figures

Figure 1.1. The structures of (a) phosphoric acid, (b) phosphonic acid, (c) phosphinic acid and (d) a phosphine oxide are displayed.....	3
Figure 1.2. The lewis structure of a generic phosphinic acid (a) along with a figure displaying the hyperconjugation that occurs between the lone pairs on the oxygen and the empty σ^* orbitals on the phosphorus (b) is shown.....	4
Figure 1.3. The lewis structure of a generic phosphinate and carboxylate (a) and carboxylate with its resonance structure (b) are drawn here.	5
Figure 1.4. The potential bonding modes of phosphinates to one or more metal center is shown in this figure.....	6
Figure 1.5. A diagram of poly-bis(μ -dihexylphosphinato)copper(II) is drawn in which the R group is a hexyl moiety.....	7
Figure 2.1. POV-Ray rendered Platon	22
Fig. 2.2 A POV-Ray rendered drawing of an ORTEP-3	29
Figure 2.3. POV-Ray rendered drawings of ORTEP-3.....	30
Figure 2.4. POV-Ray rendered drawings of ORTEP-3.....	32
Figure 2.5. POV-Ray rendered Mercury ³³ produced overlay of the “(V ₃)” cores of the major orientation of 1 (light or yellow) in crystal A and the H ₂ O adduct (dark or blue) in crystal B on the left and an overlay of 2 from crystal B (light or yellow) and that of pure 2 (dark or blue).	33
Figure 2.6. POV-Ray rendered Mercury ³³ produced illustration of 2 from crystal B (left) and pure 2 (right) with the V2 and V3 atoms located in similar positions depicting the different orientation of the py ligands.....	33
Figure 2.7. Measured and calculated χ_M and χ_{MT} against T for compound X.....	42
Figure 2.8. DSC thermograms (5 °C min ⁻¹ , N ₂ atmosphere) for 1 (a, top curve) and 2 (b, bottom curve).	45
Figure 2.S1. FTIR spectrum (neat) of VO(acac) ₂	53
Figure 2.S2. FTIR spectrum (neat) of VO(acac) ₂ (py).....	53
Figure 2.S3. FTIR spectrum (neat) of (V ₃ (μ_3 -O)O ₂)(μ_2 -O ₂ P(CH ₂ C ₆ H ₅) ₂) ₆ (H ₂ O) (1).	54
Figure 2.S7. FTIR spectrum (neat) of (VO(O ₂ P(<i>o</i> -(CH ₂) ₂ (C ₆ H ₄))) _∞ (5).....	58
Figure 2.S8. FTIR spectrum (neat) of crystal B.	59
Figure 2.S9. X-ray powder diffraction patterns for complexes 3 – 5 at 295 °C.	60
Figure 2.S10. TGA curve of (VO(O ₂ PPh ₂) ₂) _∞ (3) at a heating rate of 10°C/min.....	61
Figure 2.S11. TGA curve of VO(acac) ₂ at a heating rate of 5 °C min ⁻¹	61

Figure 2.S12. TGA curve of VO(acac) ₂ (py) at a heating rate of 5 °C min ⁻¹	62
Figure 2.S13. DSC thermogram of VO(acac) ₂ (py) at a heating rate of 5 °C min ⁻¹	62
Figure 2.S14. TGA curve of diphenylphosphinic acid at a heating rate of 10 °C min ⁻¹	63
Figure 2.S15a. TGA curve of (V ₃ (μ ₃ -O)O ₂)(μ ₂ -O ₂ P(CH ₂ C ₆ H ₅) ₂) ₆ (H ₂ O), 1, at a heating rate of 10 °C min ⁻¹	64
Figure 2.S16a. TGA curve of (V ₃ (μ ₃ -O)O ₂)(μ ₂ -O ₂ P(CH ₂ C ₆ H ₅) ₂) ₆ (py), 2, at a heating rate of 10 °C min ⁻¹	65
Figure 2.S17. FTIR spectrum of the residue obtained after heating 1 at 600 °C.	65
Figure 2.S18. DSC thermogram of (V ₃ (μ ₃ -O)O ₂)(μ ₂ -O ₂ P(CH ₂ C ₆ H ₅) ₂) ₆ (H ₂ O), 1, at a heating rate of 5 °C min ⁻¹	66
Fig. 3.1 Mercury ²¹ drawing of 1 with 50% probability ellipsoids.....	74
Fig. 3.2 Mercury ²¹ drawing of 2 with 50% probability ellipsoids.....	76
Figure 3.S1. Elemental analyses on 1 and 2.....	85
Figure 3.S2. ¹ H NMR spectrum of V ₄ (μ ₃ -O) ₄ (O ₂ P(Bn) ₂) ₄ (O ₄), 1, in CDCl ₃	86
Figure 3.S3. ¹ H NMR spectrum of W ₄ (μ ₃ -O) ₄ (O ₂ P(Bn) ₂) ₄ (O ₄), 2, in CDCl ₃	86
Figure 3.S4. ³¹ P{ ¹ H} NMR spectrum of V ₄ (μ ₃ -O) ₄ (O ₂ P(Bn) ₂) ₄ (O ₄), 1, in CDCl ₃	87
Figure 3.S5. ³¹ P{ ¹ H} NMR spectrum of W ₄ (μ ₃ -O) ₄ (O ₂ P(Bn) ₂) ₄ (O ₄), 2, in CH ₂ Cl ₂	88
Figure 3.S7. IR spectrum of W ₄ (μ ₃ -O) ₄ (O ₂ P(Bn) ₂) ₄ (O ₄), 2.....	89
Figure 3.S9a. TGA curve of V ₄ (μ ⁴ -O) ₄ (μ ² -O ₂ P(CH ₂ C ₆ H ₅) ₂) ₄ (O ₄), 1, at a heating rate of 10 °C min ⁻¹	90
Figure 3.S9b. TGA curve of V ₄ (μ ₄ -O) ₄ (μ ₂ -O ₂ P(CH ₂ C ₆ H ₅) ₂) ₄ (O ₄), 1, at a heating rate of 10 °C min ⁻¹	90
Figure 3.S10a. TGA curve of W ₄ (μ ₃ -O) ₄ (μ ² -O ₂ P(CH ₂ C ₆ H ₅) ₂) ₄ (O ₄), 2, at a heating rate of 10 °C min ⁻¹	91
Figure 3.S10b. TGA curve of W ₄ (μ ₃ -O) ₄ (μ ₂ -O ₂ P(CH ₂ C ₆ H ₅) ₂) ₄ (O ₄), 2, at a heating rate of 10 °C min ⁻¹	91
Figure 3.S11a. TGA curve of Mo ₄ (μ ₃ -O) ₄ (μ ² -O ₂ P(CH ₂ C ₆ H ₅) ₂) ₄ (O ₄), 3, at a heating rate of 10 °C min ⁻¹	92
Figure 3.S11b. TGA curve of Mo ₄ (μ ₃ -O) ₄ (μ ₂ -O ₂ P(CH ₂ C ₆ H ₅) ₂) ₄ (O ₄), 3, at a heating rate of 10 °C min ⁻¹	92
Figure 3.S12. IR spectrum of the final product from the decomposition of V ₄ (μ ₃ -O) ₄ (O ₂ P(Bn) ₂) ₄ (O ₄), 1 at 600 °C.....	93
Figure 3.S13. IR spectrum of the final product from the decomposition of W ₄ (μ ₃ -O) ₄ (O ₂ P(Bn) ₂) ₄ (O ₄), 2 at 600 °C.....	93

Figure 3.S14. IR spectrum of the final product from the decomposition of $\text{Mo}_4(\mu_3\text{-O})_4(\text{O}_2\text{P}(\text{Bn})_2)_4(\text{O}_4)$, 3 at 600 °C.....	94
Figure 4.1. Thermal ellipsoid drawing of 1 (one orientation).	100
Figure 4.2. Temperature dependence of χ_M vs T and $\chi_M T$ vs T for 1 with data represented by open circles and the solid line the fit obtained using the parameters described in the text.	103
Figure 4.S1. FTIR spectra of complex 1 (neat).....	111
Figure 4.S2. FTIR spectra of complex 2 (neat).....	112
Figure 4.S3. FTIR spectra of complex 3 (neat).....	112

List of Tables

Table 2.1. Crystal data and refinement details of crystals A containing 1, B containing 2 and 1 in a 78.3(6):21.7(6) respective ratio and pure 2.	25
Table 2.2. Selected bond distances for major components, i.e., major orientation for 1, 2 from crystal B and pure 2. Equivalent distances are on the same horizontal line.....	34
Table 2.3. Selected bond angles for 1 (major orientation), 2 from crystal B and pure 2.	35
Table 2.4. Comparison of core bonding distances in $(V_3(\mu_3-O)O_2)(\mu_2-O_2P(CH_2C_6H_5)_2)_6H_2O$, 1, $(V_3(\mu_3-O)O_2)(\mu_2-O_2P(CH_2C_6H_5)_2)_6py$, pure 2, $(V_3(\mu_3-O)O_2)(C_6H_5CO_2)_6(THF)$, 6 ¹⁹ and $[(V_3(\mu_3-O)O_2)((C_2H_5O)_2PO_2)_6 \cdot CH_3CN]$, 7. ⁵	37
Table 2.5. Comparison of core bonding angles in $(V_3(\mu_3-O)O_2)(\mu_2-O_2P(CH_2C_6H_5)_2)_6H_2O$, 1, $(V_3(\mu_3-O)O_2)(\mu_2-O_2P(CH_2C_6H_5)_2)_6py$, pure 2, $(V_3(\mu_3-O)O_2)(C_6H_5CO_2)_6(THF)$, 6 ¹⁹ and $[(V_3(\mu_3-O)O_2)((C_2H_5O)_2PO_2)_6 \cdot CH_3CN]$, 7. ⁵	38
Table 2.6. Magnetic moments of oxovanadium phosphinate compounds.....	41
Table 2.S1. Raw Data for the Magnetic Susceptibilities for 1-5 and VO(acac) ₂	52
Table 3.1 Selected distances and bond angles for 1, 3 and 2.	77
Table 4.1. Magnetic parameters.	102

Abstract

The work presented in this dissertation deals with the coordination chemistry of the bis(benzyl)phosphinate ligand with vanadium, tungsten and cobalt. The long term goal of this project was to produce and physically characterize high oxidation state transition metal oxide phosphinate compounds with potential catalytic applications.

The reaction of bis(benzyl)phosphinic acid with $\text{VO}(\text{acac})_2$ in the presence of water or pyridine leads to the synthesis of trimeric vanadium(IV) clusters ($\text{V}_3(\mu_3\text{-O})\text{O}_2)(\mu_2\text{-O}_2\text{P}(\text{CH}_2\text{C}_6\text{H}_5)_2)_6(\text{H}_2\text{O})$ and $(\text{V}_3(\mu_3\text{-O})\text{O}_2)(\mu_2\text{-O}_2\text{P}(\text{CH}_2\text{C}_6\text{H}_5)_2)_6(\text{py})$. In contrast, when diphenylphosphinic acid or 2-hydroxyisophosphindoline-2-oxide were reacted with $\text{VO}(\text{acac})_2$, insoluble polymeric compounds were produced. The trimeric clusters were characterized using FTIR, elemental analysis, single crystal diffraction, room temperature magnetic susceptibility, thermogravimetric analysis and differential scanning calorimetry. The variable-temperature, solid-state magnetic susceptibility was measured on $(\text{V}_3(\mu_3\text{-O})\text{O}_2)(\mu_2\text{-O}_2\text{P}(\text{CH}_2\text{C}_6\text{H}_5)_2)_6(\text{py})$. The polymeric compounds were characterized using FTIR, powder diffraction and elemental analysis.

Two different cubane clusters made of tungsten(V) and vanadium(V) were stabilized using bis(benzyl)phosphinate. The oxidation of $(\text{V}_3(\mu_3\text{-O})\text{O}_2)(\mu_2\text{-O}_2\text{P}(\text{CH}_2\text{C}_6\text{H}_5)_2)_6(\text{H}_2\text{O})$ with $^t\text{BuOOH}$ led to the formation of $\text{V}_4(\mu_3\text{-O})_4(\mu_2\text{-O}_2\text{P}(\text{Bn})_2)_4(\text{O}_4)$. $\text{W}_4(\mu_3\text{-O})_4(\mu_2\text{-O}_2\text{P}(\text{Bn})_2)_4(\text{O}_4)$ was produced by heating $\text{W}(\text{CO})_6$ in a 1:1 mixture of EtOH/THF at 120 °C. Both compounds were characterized using single crystal diffraction, FTIR, ^{31}P -NMR, ^1H -NMR and elemental analysis. $\text{W}_4(\mu_3\text{-O})_4(\mu_2\text{-O}_2\text{P}(\text{Bn})_2)_4(\text{O}_4)$ was also characterized using UV-vis.

Cobalt(II) reacted with bis(benzyl)phosphinate to produce three different dinuclear complexes. $[(py)_3Co(\mu_2-O_2P(Bn)_2)_3Co(py)][ClO_4]$, $(py)_3Co(\mu_2-O_2P(Bn)_2)_3Co(Cl)$ and $(py)(\mu_2-NO_3)Co(\mu_2-O_2P(Bn)_2)_3Co(py)$ were all characterized using single crystal diffraction, elemental analysis and FTIR. Room temperature magnetic susceptibility measurements were performed on $[(py)_3Co(\mu_2-O_2P(Bn)_2)_3Co(py)][ClO_4]$ and $(py)_3Co(\mu_2-O_2P(Bn)_2)_3Co(Cl)$. The variable-temperature, solid-state magnetic susceptibility was also measured on $[(py)_3Co(\mu_2-O_2P(Bn)_2)_3Co(py)][ClO_4]$.

Chapter 1 Background

1.1 Introduction

Previous work in Dr. Luck's laboratory focused on the synthesis of high oxidation state transition metal oxide complexes and their applications as catalysts. Much of this work was focused on alcohol isomerization and epoxidation catalysts.^{1,2} Recently, we have started to explore the coordination chemistry of phosphinates and the catalytic applications of high oxidation state metal oxide phosphinate compounds as epoxidation catalysts.³⁻⁵ The work done in this dissertation is an extension of this research focusing mainly on the structural characterization of high oxidation state metal oxide phosphinate compounds.

1.2 Properties of Phosphinic Acids and Phosphinate Ligands

Phosphinic acids are of the general formula $R_2P(O)OH$ where R can be hydrogen, an alkyl group, an aryl group or some combination of any two. They are related to other phosphorus(V) compounds, which are shown in Figure 1, such as phosphine oxides, phosphonic acids and phosphorus acid in that the hydroxyl group on the phosphinic acid is replaced with another R group for a phosphine oxide, one of the R groups on the phosphinic acid is replaced by a hydroxyl group for phosphonic acid or both of the R groups on the phosphinic acid are replaced with hydroxyl groups for phosphorus acid. Industrially, these types of phosphorus compounds and their esters are used for the separation and purification of different metals. Mixtures of bis(2,4,4-trimethylpentyl)phosphinic acid and tri(2,4,4-trimethyloctyl)phosphine oxide are sold by

Cytec Industries Inc. with the name Cyanex 272 and are used for the extraction and purification of different metals. Notably, Cyanex 272 is most commonly used in the separation of cobalt from nickel.⁶ Despite their extensive use in the purification of different metals, the coordination chemistry of phosphinic acids is relatively unexplored.

Although phosphinic acids and related compounds are generally drawn with a phosphorus-oxygen double bond as in the case of Figure 1, this is in fact not correct. The phosphorus-oxygen bond is best modeled as a short σ -bond in which the oxygen

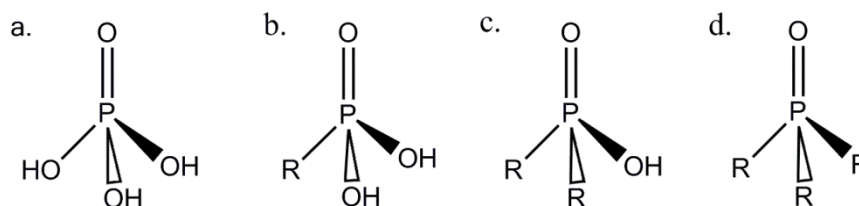


Figure 1.1. The structures of (a) phosphoric acid, (b) phosphonic acid, (c) phosphinic acid and (d) a phosphine oxide are displayed.

carries a negative charge and the phosphorus contains a positive charge as displayed in figure 2.⁷ Hyperconjugation occurs between the three lone pairs on the oxygen and empty σ^* orbitals on the phosphorus atom, further stabilizing the bond. The implication of this excess electron density accumulated on the oxide of the phosphinic acid is an increase in the electron donating capability to metal centers from the oxide. This makes them ideal ligands for stabilizing high oxidation state transition metals.

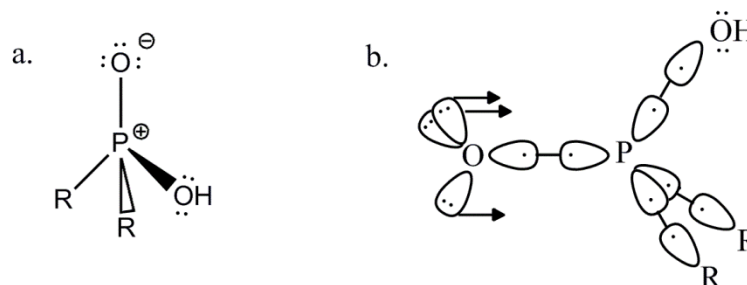


Figure 1.2. The lewis structure of a generic phosphinic acid (a) along with a figure displaying the hyperconjugation that occurs between the lone pairs on the oxygen and the empty σ^* orbitals on the phosphorus (b) is shown.

To a certain extent, phosphinic acids are structurally related to carboxylic acids which is shown in Figure 3a. Both compounds are organic oxoacids in which the acidic moiety consists of an oxide and hydroxide bonded to a central atom that is electron deficient. Due to this deficiency, the hydroxyl group can ionize relatively easily to form either a phosphinate or carboxylate anion and a proton. Where carboxylic and phosphinic acids differ is in their geometry and nature of their bonding. Phosphinic acids are always tetrahedral in shape with four different moieties bonding to the central phosphorus atom. The identities of the two moieties that are not the oxide or hydroxide can have profound effects on the steric nature of the phosphinic acids. If both groups were, for example, tert-butyl alkyl groups, the steric crowding around the oxygen atoms would increase and this could change how the phosphinic acid or phosphinate coordinates to metal atoms.⁸ Carboxylic acids on the other hand, are trigonal planar compounds with only three moieties bonded to the central carbon atom. The identity of the one moiety that is not the hydroxide or oxide can also have similar steric effects on the coordination of the

carboxylic acid or carboxylate to metal atoms. Unlike the O=P bond, the O=C double bond in carboxylic acids is in fact a true double bond consisting of one σ -bond and one π -bond. The carboxylate anion, when compared to the phosphinate anion, would have less electron density spread over its two oxygens due to its resonance structures. This would presumably decrease the amount of electron density that can be donated to a metal center potentially lowering its effectiveness in stabilizing high oxidation state metals.

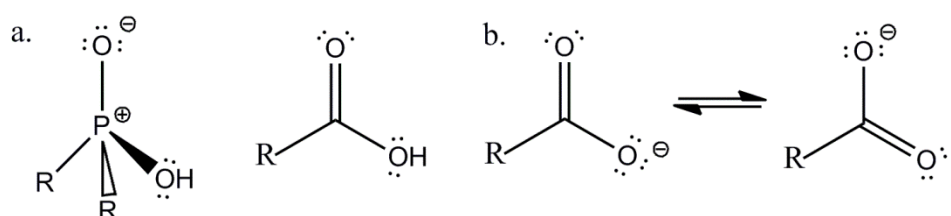


Figure 1.3. The lewis structure of a generic phosphinate and carboxylate (a) and carboxylate with its resonance structure (b) are drawn here.

Due to their geometry, phosphinates can potentially have many different coordination modes. Figure 4 lists some of the more obvious modes. One of the simplest coordination modes is when only one of the oxygen atoms on the phosphinate is bonding to a metal center and the second oxygen is left free dangling off the metal as shown in Figure 4a. Another possibility would be when the phosphinate acts as a chelating ligand with both oxygens bonded to the same metal center as displayed in Figure 4b. The third possibility would be when the two oxygens of the phosphinate bridge between two metal centers creating multi-nuclear clusters which is shown in figure 4c. The bridging coordination mode is the most commonly observed mode in metal phosphinate compounds as will be seen later in the discussion. Coordination compounds containing

multiply metals centers are of particular interest due to their prevalence in nature as the active sites in many enzymes.⁹

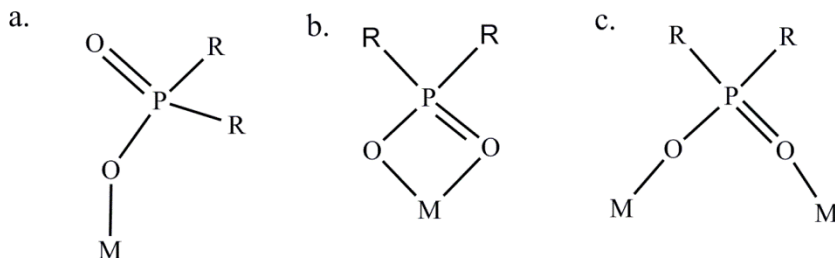


Figure 1.4. The potential bonding modes of phosphinates to one or more metal center is shown in this figure. (a) Shows only one of its oxygens coordinated to the metal center, (b) shows the phosphinate behaving as a chelating ligand and (c) depicts a phosphinate bridging two metal centers.

1.3 Coordination Chemistry of Phosphinates

Despite their favorable attributes, one of the main factors that prohibits the use of phosphinates as ligands is their tendency to form polymers with most metals.¹⁰ These inorganic polymers tend to be insoluble in water and most common organic solvents. This insolubility greatly inhibits the study of possible catalytic applications of metal phosphinate compounds as well as rendering the structural characterization of these compounds somewhat difficult. Despite their insolubility, some of these polymers have been characterized by single crystal X-ray diffraction. Their crystal structures verified that these polymers were 1-dimensional infinite polymers with the polymeric backbone made up of metal centers bridged by phosphinate ligands. For example, copper(II) was found to form a polymer with bis(hexyl)phosphinate in which each copper atom was in a

distorted square planar coordination environment and two phosphinates bridged between each copper.¹¹ A diagram of the polymer is displayed in Figure 5. Copper(II) was also found to form another polymer with dimethylformylamide and methylphenylphosphinate or dimethylformylamide in which each copper atom was octahedrally coordinated and was bridged by two phosphinates and one dimethylformylamide.¹² Other metal phosphinate polymers made with metals such as cobalt, manganese and other transition metals have been characterized by single crystal diffraction with similar structures.¹³⁻¹⁵ In all of the metal phosphinate polymers, the phosphinate ligand is always bridging between two metal centers. This preference for bridging metal centers is also observed in molecular phosphinate clusters.

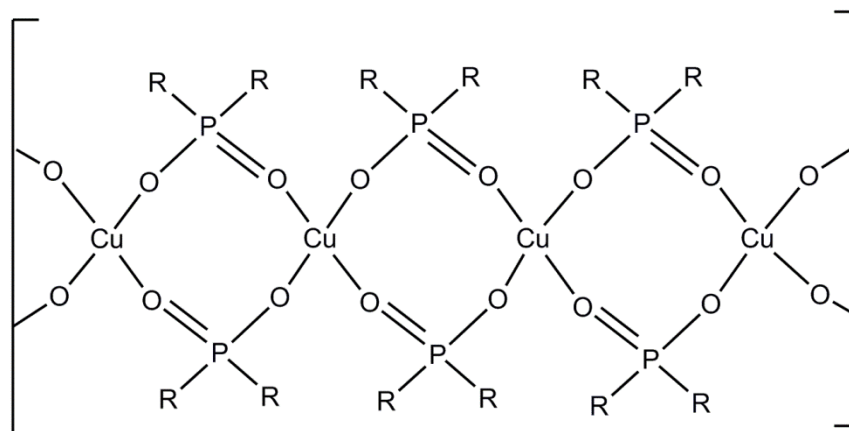


Figure 1.5. A diagram of poly-bis(μ -di-hexylphosphinato)copper(II) is drawn in which the R group is a hexyl moiety.

Although phosphinates have a strong tendency to form insoluble polymers with transition metals, molecular clusters can be synthesized in some cases if other ligands are also present. These ligands can block the formation of polymeric compounds by

occupying coordination sites on the metal centers and thus preventing the formation of the repeating bridging phosphinates which are the backbone of the polymer. The types of ligands that can be used to inhibit the formation of polymeric compounds are not limited to one type. Compounds containing organometallic ligands such as carbon monoxide in the case of $\text{Ru}_2(\text{O}_2\text{PR}_2)_2(\text{CO})_4(\text{PPh}_3)_2$ ($\text{R} = \text{Me}$ or Ph) or cyclopentadienyl as in the case of $[(\eta^5\text{-C}_5\text{H}_5)\text{TiCl}_2(\mu_2\text{-Ph}_2\text{PO}_2)]_2$ have been characterized.^{16,17} Nitrogen bases, which are strong sigma donors, have also been used to stop the polymerization of metal phosphinates. For example, hydrotris(pyrazolyl)borate was used along with bis(phenyl)phosphinate to synthesize a vanadium(IV) dimer $[\text{HB}(\text{pz})_3\text{VO}(\mu_2\text{-Ph}_2\text{PO}_2)]_2$.¹⁸ Alkoxides and oxides have also been used to prepare molecular phosphinates such as in the case of a tetrameric titanium cluster of the general formula $[\text{Ti}(\mu_3\text{-O})(\text{OPr}^i)(\mu_2\text{-Ph}_2\text{PO}_2)]_4$, which contains both oxides and alkoxides, or in the case of a tetrameric manganese species, $(\text{Mn}(\mu_3\text{-O}))_4(\mu_2\text{-Ph}_2\text{PO}_2)_6$, which only contains oxides along with bis(phenyl)phosphinate.^{19,20} Although more examples of molecular metal phosphinate clusters exist, the total amount of characterized species is very small when compared to more common ligands such as carboxylates or even phosphonic acids.

The applications of the previously mentioned molecular metal phosphinate compounds are generally in the area of catalysis. One compound of note is the tetrameric manganese oxide cluster, $(\text{Mn}(\mu_3\text{-O}))_4(\mu_2\text{-Ph}_2\text{PO}_2)_6$, stabilized by bis(phenyl)phosphinate. This compound was synthesized as a model compound for the active site of the enzyme referred to as the water oxidation complex(WOC) which is an integral part of photosynthesis. As one could assume by its name, the WOC oxidizes

H₂O to form stoichiometric amounts of electrons, oxygen gas and protons. Although the tetramer does not perfectly mimic the active site of the enzyme, it was still found to be a highly active catalyst and has been used in several water oxidation materials and devices.²¹⁻²³ The catalyst itself must undergo multiply redox processes in order to accomplish the oxidation. This required a ligand capable of stabilizing the manganese metal centers in different oxidation states to maintain the integrity of the catalyst. It also required a ligand that was resistant to oxidation by the manganese metal centers themselves due to their high oxidation states. Bis(phenyl)phosphinate was found not only be resistant to oxidation by the manganese, but it was also able to stabilize the metal center as it went through several oxidation states during the catalytic process. This in large demonstrated the usefulness of phosphinates as ligands to stabilize metal centers in high oxidation states.

1.4 Purpose of Work

Previously in our lab, we discovered that the reaction of bis(benzyl)phosphinate with MoO₂(acac)₂ in ethanol at different temperatures leads to two different compounds.²⁴ A mixed valence Mo(VI/V) flat tetramer was produced when the temperature was kept around 70 °C and a different Mo(V) cubic tetramer was produced when the reaction was conducted at 120 °C in a sealed tube. When we tried to reproduce these results with other phosphinates such as bis(phenyl)phosphinate, 2-hydroxyisophosphindoline-2-oxide or bis(chloromethyl)phosphinate only the cubic

tetramer was obtained no matter what the temperature was. To account for this difference we rationalized that the steric flexibility of the benzyl groups was the key factor.

Although we are not exactly sure as to the precise effect the steric bulk of the benzyl group, there was no clear reason as to why the other phosphinates did not work other than the differences in their physical structure. Regardless of the exact reason, this lead us to the conclusion that the coordination chemistry of bis(benzyl)phosphinate could be fundamentally different than other phosphinates.

In this work we explore the coordination chemistry of bis(benzyl)phosphinate with vanadium, tungsten and cobalt with an acute interest in high oxidation state transition metal clusters. Given our assumption of the unique steric nature of bis(benzyl)phosphinate and the ability of phosphinates to stabilize metal centers in high oxidation states, we hypothesized that using bis(benzyl)phosphinate as a ligand would allow us to synthesis new and unique clusters with potential applications in catalysis. The compounds produced in this work were analyzed by a variety of techniques including single crystal diffraction, x-ray powder diffraction, IR, NMR, UV-vis and variable temperature magnetic susceptibility.

References

- (1) Wang, G.; Jimtaisong, A.; Luck, R. L. *Organometallics* **2004**, *23*, 4522.
- (2) Jimtaisong, A.; Luck, R. L. *Inorganic Chemistry* **2006**, *45*, 10391.
- (3) Feng, L.; Luck, R. *J Chem Crystallogr* **2011**, *41*, 1317.

- (4) Jimtaisong, A.; Feng, L.; Sreehari, S.; Bayse, C.; Luck, R. *Journal of Cluster Science* **2008**, *19*, 181.
- (5) Feng, L.; Maass, J. S.; Luck, R. L. *Inorganica Chimica Acta* **2011**, *373*, 85.
- (6) Tait, B. K. *Hydrometallurgy* **1993**, *32*, 365.
- (7) Lyssenko, K. A.; Grintselev-Knyazev, G. V.; Antipin, M. Y. *Mendeleev Communications* **2002**, *12*, 128.
- (8) Mason, G. W.; Lewey, S. *Journal of Inorganic and Nuclear Chemistry* **1974**, *36*, 911.
- (9) Turowski, P. N.; Armstrong, W. H.; Roth, M. E.; Lippard, S. J. *Journal of the American Chemical Society* **1990**, *112*, 681.
- (10) Svetlana, V. V.; Vinogradova, O. V. *Russian Chemical Reviews* **1975**, *44*, 510.
- (11) Haynes, J. S.; Oliver, K. W.; Rettig, S. J.; Thompson, R. C.; Trotter, J. *Canadian Journal of Chemistry* **1984**, *62*, 891.
- (12) Betz, P.; Bino, A. *Inorganica Chimica Acta* **1988**, *147*, 109.
- (13) Du, J.-L.; Rettig, S. J.; Thompson, R. C.; Trotter, J. *Canadian Journal of Chemistry* **1991**, *69*, 277.
- (14) Cicha, W. V.; Haynes, J. S.; Oliver, K. W.; Rettig, S. J.; Thompson, R. C.; Trotter, J. *Canadian Journal of Chemistry* **1985**, *63*, 1055.
- (15) Pitts, J. J.; Robinson, M. A.; Trotz, S. I. *Journal of Inorganic and Nuclear Chemistry* **1969**, *31*, 3685.

- (16) Barnes, C. M.; Bohle, D. S.; Madsen, S. K. *Inorganic Chemistry* **1994**, *33*, 6411.
- (17) Dorn, H.; Vejzovic, E.; Lough, A. J.; Manners, I. *Canadian Journal of Chemistry* **2002**, *80*, 1650.
- (18) Dean, N. S.; Bond, M. R.; O'Connor, C. J.; Carrano, C. J. *Inorganic Chemistry* **1996**, *35*, 7643.
- (19) Guerrero, G.; Mehring, M.; Hubert Mutin, P.; Dahan, F.; Vioux, A. *Journal of the Chemical Society, Dalton Transactions* **1999**, 1537.
- (20) Ruettinger, W. F.; Campana, C.; Dismukes, G. C. *Journal of the American Chemical Society* **1997**, *119*, 6670.
- (21) Brimblecombe, R.; Koo, A.; Dismukes, G. C.; Swiegers, G. F.; Spiccia, L. *ChemSusChem* **2010**, *3*, 1146.
- (22) Brimblecombe, R.; Chen, J.; Wagner, P.; Buchhorn, T.; Dismukes, G. C.; Spiccia, L.; Swiegers, G. F. *Journal of Molecular Catalysis A: Chemical* **2011**, *338*, 1.
- (23) Ruettinger, W. F.; Dismukes, G. C. *Inorganic Chemistry* **2000**, *39*, 1021.
- (24) Maass, J.; Zeller, M.; Holmes, D.; Bayse, C.; Luck, R. *Journal of Cluster Science* **2011**, *22*, 193.

Chapter 2 Vanadium Trimers

2.1 Syntheses, x-ray structural characterizations and thermal stabilities of two nonclassical ferromagnetic trinuclear vanadium (IV) complexes; $(V_3(\mu_3-O)O_2)(\mu_2-O_2P(CH_2C_6H_5)_2)_6(H_2O)$ and $(V_3(\mu_3-O)O_2)(\mu_2-O_2P(CH_2C_6H_5)_2)_6(py)$ and polymeric complexes of stoichiometry $(VO(O_2PR_2)_2)_\infty$, $R_2 = Ph_2$ and $o-(CH_2)_2(C_6H_4)$ ^{1,2}

John S. Maass,^a Zhichao Chen,^a Matthias Zeller,^b Floriana Tuna,^c Richard E. P. Winpenny,^c Rudy L. Luck^{a,*}

^a*Department of Chemistry, Michigan Technological University, 1400 Townsend Drive, Houghton, MI 49931, USA*

^b*Department of Chemistry, Youngstown State University, 1 University Plaza, Youngstown, OH 44555, USA*

^c*School of Chemistry, The University of Manchester, Oxford Road, Manchester, M13 9PL, UK.*

¹“Reprinted with permission from Maass, J. S.; Chen, Z.; Zeller, M.; Tuna, F.; Winpenny, R. E. P.; Luck, R. L. *Inorganic Chemistry* **2012**, *51*, 2766. Copyright 2012 American Chemical Society.”

² License agreement for reproduction is provided in the Appendix

2.2 Abstract

The preparation and structural characterization of two trinuclear vanadium complexes, $(V_3(\mu_3-O)O_2)(\mu_2-O_2P(CH_2C_6H_5)_2)_6(H_2O)$, **1**, and $(V_3(\mu_3-O)O_2)(\mu_2-O_2P(CH_2C_6H_5)_2)_6(py)$, **2**, are reported. In these nonclassical structures, the planar central core consists of the three vanadium atoms arranged in the form of an acute quasi-isosceles triangle with the central oxygen atom multiply-bonded to the vanadium atom at the center of the vertex angle and weakly interacting with the two other vanadium atoms on the base sites, each of which contain one external multiply-bonded oxygen atom. Reacting $VO(acac)_2$ in the presence of diphenylphosphinic acid affords $(VO(O_2PPh_2)_2)_\infty$, **3**, while 2-hydroxyisophosphindoline-2-oxide at room temperature in CH_2Cl_2 affords $((H_2O)VO(O_2Po-(CH_2)_2C_6H_4)_2)_\infty$, **4**, and at 120 °C in EtOH yields $(VO(O_2P(o-(CH_2)_2(C_6H_4)))_\infty$, **5** on the basis of elemental analyses. The thermal and chemical stability of the complexes were assessed by thermogravimetric analysis (TGA) and differential scanning calorimetry (DSC) measurements. The bond strengths of the vanadium atoms to the OH_2 ligand in **1** and to the NC_5H_5 ligand in **2** were assessed at 10.7 and 42.0 kJ/mol respectively. Room temperature magnetic susceptibility measurements reveal magnetic moments for trinuclear **1** and **2** at 3.02(1) and 3.05(1) $\mu_B/mole$, and also close to spin only values (1.73 μ_B) values for **3**, **4** and **5** at 1.77(2), 1.758(7) and 1.77(3) μ_B , respectively. Variable-temperature, solid-state magnetic susceptibility measurements were conducted on complex **2** in the temperature range 2.0 to 298 K and at an applied field of 0.5 T. Magnetization measurements at 2 and 4 K confirmed the ferromagnetism.

Key words: vanadium(IV) trimers, magnetic susceptibility, thermal stability, dibenzylphosphinate, crystal structures

* Corresponding author. Tel.: 906 487 2309. E-mail address: rluck@mtu.edu

2.3 Introduction

We have previously detailed the formation of tetrameric clusters of molybdenum(V) stabilized by phosphinate ligands and described their capabilities as catalysts for the epoxidation of olefins.¹⁻³ More recently, we communicated the syntheses and single crystal structures of vanadium(V) and tungsten(V) tetrameric clusters.⁴ Vanadium is worthy of exploration as it is a catalyst for the industrial production of maleic anhydride,⁵ it is the active metal central in some halogenating enzymes of marine organisms,⁶ some vanadium compounds have been found to be effective in treating diabetes,⁷ and, more relevant, there is a very large quantity of oxovanadium compounds stabilized by phosphonic acids⁸ but not many containing phosphinate ligands.⁹⁻¹² In that regard, the diphenylphosphinate ligand was previously utilized as a model for the interaction of phosphate ligands with oxo-bridged di-Fe proteins^{13, 14} and in reactions with Co which resulted in polymers.¹⁵ We were most interested in studying how oxidovanadium(IV), VO^{2+} , would coordinate with different phosphinate ligands.

To the best of our knowledge, the only compounds reported that contain phosphinate ligands coordinated to oxidovanadium(IV) characterized by crystallography are dimeric compounds of the general formula $[(\text{VO})_2(\mu\text{-L})_2(\text{HB}(\text{pz})_3)_2]$ (L = diphenylphosphinate or monophenylphosphinate)⁹ and $[(\text{VO})_2(\mu\text{-L}_1)_3(\text{L}_2)_2]\text{NO}_3$ (L₁ = diphenylphosphinate or bis(4-methoxyphenyl)phosphinate, L₂ = 2,2'-bipyridine¹⁰ or 1,10-phenanthroline)¹¹ and the 2D-layered diphosphate, $[\text{VO}(\text{O}_2(\text{C}_6\text{H}_5)\text{PCH}_2\text{P}(\text{C}_6\text{H}_5)\text{O}_2)]$.¹² Interestingly, trinuclear vanadium clusters have been reported stabilized by carboxylate groups. For example, five compounds of the trinuclear formulation $[\text{V}_3\text{O}(\text{RCO}_2)_6\text{L}_3]^{0,+}$, two with valencies II, III, III and three with III, III, III, were reported as containing a

central oxo ligand in the center of an equilateral “V₃” triangle of *D*_{3h} symmetry referred to as classical.^{16, 17} A less symmetrical example (i.e., containing an almost centrally located oxo ligand but one V···V distance at 3.068(2) Å is shorter than the other two at 3.43(2) and 3.349(2) Å) of this type of trinuclear cluster is [Et₃NH][V^{III}₃(μ₃-O)(Salox)₂(HSalox)(Salmp)], where H₂Salox = salicylaldoxime and H₃Salmp = 2-(bis(salicylideneamino)methyl)phenol.¹⁸ In contrast, the less symmetrical [V₃(μ₃-O)O₂]⁶⁺ core, in which the central oxygen atom is doubly bonded to one vanadium atom, weakly bonded to the other two vanadium atoms and all vanadium atoms exhibited valencies of IV, was earlier reported for the compounds (V₃(μ₃-O)O₂)(μ₂-O₂CC₆H₅)₆(THF),¹⁹ [(V₃(μ₃-O)O₂)((C₂H₅O)₂PO₂)₆·CH₃CN]⁵ and [(V₃(μ₃-O)O₂)(BrC(CH₃)COO)₆(HOⁱPr)].²⁰ Here the three vanadium atoms are in the form of quasi-isosceles triangles displaying C_{2v} symmetry or the nonclassical form. The [V₃(μ₃-O)O₂]⁶⁺ cation was stabilized by the six bridging benzoate or diethylphosphate molecules and either a THF or CH₃CN ligand was bonded *trans* to the V=O_{center} bond. As stated,^{5, 19} these compounds do not contain true “M₃(μ₃-O)” cores in which the central oxygen atom in the “(V₃(μ₃-O)O₂)” moiety is located equidistant from the three metal atoms, but they are a cluster of three oxidovanadium(IV) ions. This difference is due to the fact that the oxygen atoms are more strongly bonded to the more positively charged vanadium (IV) atoms (i.e., as (V≡O)₃).

We report here on the use of dibenzylphosphinate ligands to synthesize the compounds (V₃(μ₃-O)O₂)(μ₂-O₂P(CH₂C₆H₅)₂)₆(H₂O), **1**, and (V₃(μ₃-O)O₂)(μ₂-O₂P(CH₂C₆H₅)₂)₆(py), **2**. These both contain asymmetrical centrally located oxo ligands,

i.e., the nonclassical forms which display C_{2v} symmetry. Reactions between $\text{VO}(\text{acac})_2$ and diphenylphosphinic acid resulted an intractable substance analyzing as $(\text{VO}(\text{O}_2\text{PPh}_2)_2)_\infty$, **3**, while reactions with 2-hydroxyisophosphindoline-2-oxide²¹ at room temperature in CH_2Cl_2 affords $((\text{H}_2\text{O})\text{VO}(\text{O}_2\text{P}(o\text{-(CH}_2)_2(\text{C}_6\text{H}_4)))_\infty$, **4**, and at 120 °C in EtOH yields $(\text{VO}(\text{O}_2\text{P}(o\text{-(CH}_2)_2(\text{C}_6\text{H}_4)))_\infty$, **5**. The crystal structures of **1**, a co-crystallized mixture consisting of 21.7(6)% **1** and 78.3(6)% **2** and pure **2**, and the thermal gravimetric analysis (TGA), differential scanning calorimetry (DSC), room temperature magnetic susceptibility measurements on **1-5** and the variable temperature magnetic susceptibility measurement for complex **2** are described.

2.4 Experimental

2.4.1. General Method

Chemicals were purchased from Aldrich Chemicals and solvents were used as received. Elemental analyses were conducted by Galbraith Laboratories, Knoxville, TN. IR spectra were recorded on a PerkinElmer Spectrum One spectrometer (neat). The TGA and DSC analyses were conducted on Shimadzu TGA-50 and DSC-50 analyzers and under a slow N_2 (not O_2 exclusive) stream. Magnetic measurements were conducted on a Johnson Matthey Auto MSB instrument. The powder diffraction X-ray data were obtained using a Scintag XDS-2000 θ/θ diffractometer. Dibenzylphosphinic acid and hydroxyisophosphindoline-2-oxide,²¹ diphenylphosphinic acid,²² $\text{VO}(\text{acac})_2$ ²³ and $\text{VO}(\text{acac})_2(\text{py})$ ^{23, 24} were prepared according to the cited literature. Their FTIR spectra are presented as Figs. S1 and S2 for $\text{VO}(\text{acac})_2$ and $\text{VO}(\text{acac})_2(\text{py})$ respectively. The

variable temperature magnetic susceptibility measurement was performed on a polycrystalline sample of **2** in the temperature range 2.0 to 298 K and at an applied field of 0.5 T using a Quantum Design MPMS SQUID magnetometer. The sample holder diamagnetism was measured and subtracted from the raw data. Magnetization measurements were performed at 2 and 4 K.

2.4.2 Synthesis

2.4.2.1 Synthesis of $(V_3(\mu_3-O)O_2)(\mu_2-O_2P(CH_2C_6H_5)_2)_6(H_2O)$ (**1**)

0.200 g (0.754 mmol) of VO(acac)₂ and 0.392 g (1.585 mmol) of dibenzylphosphinic acid were placed in a sealed tube with 5 mL of ethanol and heated at 120 °C for 16 hours. A light blue precipitate formed which was isolated by filtration and recrystallized from methylene chloride and hexane resulting in 0.340 g (0.200 mmol, 79.6% yield based on VO (acac)₂) of $(V_3(\mu_3-O)O_2)(\mu_2-O_2P(CH_2C_6H_5)_2)_6(H_2O)$ (**1**). Anal. Calc. for C₈₄H₈₆O₁₆P₆V₃: C, 59.69; H, 5.13. Found: C, 59.52; H, 5.36 %. IR (Fig. S3, neat, cm⁻¹) 3628 vw, 3537 vw, 3062 vw, 3029 vw, 2909 vw, 1602 w, 1496 m, 1453 m, 1400 w, 1234 w, 1189 m, 1164 m, 1103 m, 1024 vs, 995 sh, 942 m, 915 m, 840 s, 806 s, 732 m, 695 vs.

2.4.2.2 Synthesis of $(V_3(\mu_3-O)O_2)(\mu_2-O_2P(CH_2C_6H_5)_2)_6(py)$ (**2**)

$(V_3(\mu_3-O)O_2)(\mu_2-O_2P(CH_2C_6H_5)_2)_6(py)$, **2**, was produced by mixing 0.050 g (0.186 mmol) of VO(acac)₂, 0.093 g (0.376 mmol) of dibenzylphosphinic acid, and 2 drops of pyridine in 5 mL of methylene chloride. The mixture was stirred overnight at room temperature. It was then filtered, concentrated, and the subsequent addition of hexanes resulted in 0.070 g (0.040 mmol, 63.25% based on VO(acac)₂) of **2**. Anal. Calc.

for $C_{89}H_{91}O_{15}P_6V_3N$: C, 60.75; H, 5.12. Found: C, 60.44; H, 5.40%. IR (Fig. S4, neat, cm^{-1}) 3062 vw, 3028 vw, 2911 vw, 1602 w, 1496 m, 1454 m, 1400 w, 1234 m, 1189 s, 1169 s, 1116 m, 1098 m, 1067 m, 1026 vs, 989 sh, 918 s, 840 s, 805 s, 732 s, 696 vs.

2.4.2.3 Synthesis of $(VO(O_2PPh_2)_2)_\infty$ (**3**)

0.035 g (0.133 mmol) of $VO(acac)_2$ and 0.058 g (0.266 mmol) of diphenylphosphinic acid were dissolved in 10 mL of methylene chloride and stirred overnight and resulted in 0.049 g of light blue **3**. Alternately, 0.0510 g (0.1923 mmol) of $VO(acac)_2$ and 0.0837 g (0.3846 mmol) of diphenylphosphinic acid were added to 5 mL of ethanol in a sealed tube and heated to 120 °C overnight. The light blue precipitate that had formed was filtered, rinsed with ethanol and then dried under vacuum to give 0.0580 g of light blue **3**. Both of these preparations resulted in species of identical IR spectra. Anal. Calc. for $C_{24}H_{20}O_5P_2V$: C, 57.50; H, 4.02. Found: C, 57.07; H, 3.94%. IR (Fig. S5, neat, cm^{-1}): 3058 (vw), 1592 (vw), 1486 (vw), 1437 (m), 1124 (vs), 1057 (s), 1014 (s), 998 (m), 749 (m), 729 (s), 692 (s).

2.4.2.4 Synthesis of $((H_2O)VO(O_2P(o-(CH_2)_2(C_6H_4)))_\infty$ (**4**)

0.0402 g (0.1516 mmol) of $VO(acac)_2$ and 0.0510 g (0.3033 mmol) of 2-hydroxyisophosphindoline-2-oxide were dissolved in 10 mL of methylene chloride and stirred overnight. The light blue precipitate that was produced was filtered off, rinsed with methylene chloride and then dried in a vacuum to give 0.0330 g of compound **4**. Anal. Calc. for $C_{16}H_{18}O_6P_2V$: C, 45.84; H, 4.33. Found: C, 44.20; H, 3.87%. IR (Fig. S6, neat, cm^{-1}): 3636 (vw), 3024 (vw), 2911 (vw), 1621 (vw), 1576 (vw), 1483 (w), 1458 (w), 1393 (w), 1267 (w), 1215 (s), 1197 (m), 1173 (s), 1153 (s), 1133 (w), 1094 (s), 1079

(s), 1062 (s), 1040 (vs), 1003 (s), 995 (vs), 950 (s), 854 (s), 818 (s), 796 (m), 760 (m), 735 (vs).

2.4.2.5 Synthesis of $(VO(O_2P(o-(CH_2)_2(C_6H_4)))_\infty$ (**5**)

0.0420 g (0.1584 mmol) of VO(acac)₂ and 0.0533 g (0.3168 mmol) of 2-hydroxyisophosphin-doline-2-oxide acid were added to 5 mL of ethanol in a sealed tube and heated to 120 °C overnight. The light blue precipitate that had formed was filtered, rinsed with ethanol and then dried in a vacuum to give 0.0460 g of compound **5**. Anal. Calc. for C₁₆H₁₆O₅P₂V: C, 47.90; H, 4.02. Found: C, 48.54; H, 4.36%. IR (Fig. S7, neat, cm⁻¹): 3061 (vw), 2903 (vw), 1574 (vw), 1526 (vw), 1481 (w), 1455 (w), 1391 (w), 1295 (vw), 1221 (w), 1184 (s), 1178 (s), 1136 (vs), 1094 (vs), 1064 (vs), 1005 (vs), 881 (vw), 856 (s), 818 (m), 795 (m), 762 (m), 749 (s), 734 (s).

2.4.3 X-Ray Crystallography

Suitable crystals were grown by a slow diffusion of hexanes into a saturated solution of either **1** or **2** in a 1:1 mixture of hexanes and methylene chloride in an H-tube. Diffraction data for all compounds were collected using a Bruker AXS SMART APEX CCD diffractometer using monochromatic Mo K α radiation with the omega scan technique. Single crystals of compounds containing **1** and **2** were mounted on Mitegen micromesh supports using viscous oil flash-cooled to 100 K. Data were collected, unit cells determined, and the data integrated and corrected for absorption and other systematic errors using the Apex2 suite of programs.²⁵ The structures were solved by direct methods and refined by full matrix least squares against F² with all reflections using SHELXL.²⁶ Complex **1** cocrystallized with 3.5 dichloromethane molecules in the

asymmetric unit with the entire contents of the crystal labeled as **A**. The dichloromethane molecules were not orderly arranged and the different disordered arrangements were adequately accounted for using standard models, see CIF file. Complex **1** within crystal **A** contained a three-fold disorder consisting of the unique V-(OH₂) moiety occurring in three positions in unequal ratios as is illustrated in Fig. 2.1. The disorder, readily apparent from the difference

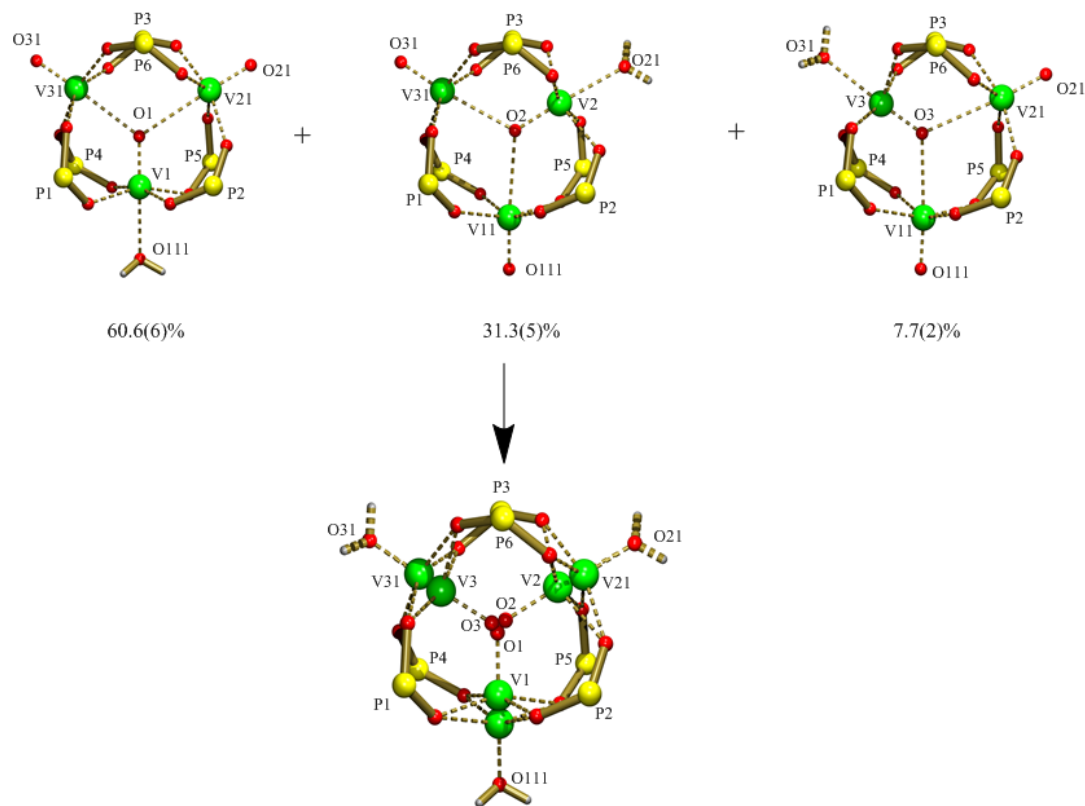


Figure 2.1. POV-Ray rendered Platon27 constructed representations of the nature of the disorder in **1**. For clarity the dibenzylphosphinate ligands are represented by "PO₂" fragments.

electron density maps during structure refinement, constitutes the only obvious way to rationalize the pattern obtained from the solution to the structure which looked like the combination figure of the three disordered patterns in Fig. 1. Crystals for the study of

complex **2**, where the entire contents of the crystal are labeled as **B**, were obtained via a different route to the one given above in the experimental details which affords analytically pure samples of **2**. This route, an exploratory reaction, consisted of reacting VO(acac)₂(py) and dibenzylphosphinic acid (without any additional py) in a sealed tube with 5 mL of ethanol and heating at 120 °C for 16 hours. In this case, the crystals **B** that were grown from this reaction (as described directly above) refined to represent a co-crystal of composition **2** and **1** in a 78.3(6):21.7(6) respective ratio. Evidence suggestive of the presence of **1** (smaller absorption at 3628 cm⁻¹, compared to the equivalent in Fig. S3 of pure **1**) was observed in the FTIR spectrum of the crystals, Fig. S8. One benzyl ligand also contained disorder. This was refined independently first to determine the occupancy ratio over the two sites and as this was similar to the composition of crystal **B**, it was then refined tied to the free variable that defined the occupancies of **2** and **1** in crystal **B**. The N atom (78.3(6)%) in the py ligand was refined with anisotropic thermal parameters and the O atom (21.7(6)%) in the ligated water molecule with isotropic parameters. The final Flack x parameter was -0.00(1) and for the inverted structure 0.96(2). We believe that the source of the water ligated in both crystal structures was the wet ethanol used in the synthesis. Pure crystals of **2** were grown by allowing slow diffusion of hexane into a dichloromethane solution of **2**. The final Flack x parameter was -0.02(1) and for the inverted structure 1.00(1). In all cases the final models consisted of non-H atoms represented by anisotropic displacement parameters and all H-atoms (including those on the aqua ligands in crystals **A** and **B**) were refined through constraints

to the atoms they were bonded to. Details of the data collection and refinement of the compounds are given in Table 2.1.

Table 2.1. Crystal data and refinement details of crystals **A** containing **1**, **B** containing **2** and **1** in a 78.3(6):21.7(6) respective ratio and pure **2**.

Identification code	A	B	2
Chemical Formula			
Sum	C ₁₇₅ H ₁₈₆ Cl ₁₄ O ₃₂ P ₁₂ V ₆	C _{87.91} H _{88.34} N _{0.78} O _{15.22} P ₆ V ₃	
Formula weight (g)	3974.72	1737.88	1751.25
Temperature (K)	100(2)	100(2)	100(2)
Wavelength (Å)	0.71069	0.71069	0.71069
Crystal system	Monoclinic	Triclinic	Triclinic
Space group	<i>P</i> 2 ₁ /c	<i>P</i> 1	<i>P</i> 1
Unit cell dimensions (Å, °)	a = 26.630(1), α = 90 b = 20.903(8), β = 90.804(9) c = 16.779(7), γ = 90	a = 13.1842(8), α = 108.063(1) b = 13.7341(9), β = 103.954(1) c = 13.9398(9), γ = 110.953(1)	a = 13.248(2), α = 108.30(1) b = 13.779(2), β = 103.97(1) c = 14.050(1), γ = 110.889(2)
Volume (Å ³)	9339(6)	2057.4(2)	2086.7(5)
Z	2	1	1
Density (calculated, mg/m ³)	1.413	1.413	1.394
Absorption coefficient (mm ⁻¹)	0.659	0.517	0.510
F(000)	4096	909	909
Crystal size (mm)	0.50 × 0.31 × 0.13 mm	0.36 × 0.36 × 0.08 mm	0.45 × 0.26 × 0.15 mm
θ range for data collection (°)	0.76 to 29.59 deg. -32 ≤ h ≤ 36, -28 ≤ k ≤ 28, -21 ≤ l ≤ 23	1.67 to 31.44 deg. -18 ≤ h ≤ 18, -20 ≤ k ≤ 20, -19 ≤ l ≤ 19	1.66 to 31.43 deg. -18 ≤ h ≤ 19, -18 ≤ k ≤ 19, -20 ≤ l ≤ 20
Index ranges			
Reflections collected	66641	25292	25844
Independent reflections	25531 [R(int) = 0.0640]	21357 [R(int) = 0.0255]	21017 [R(int) = 0.0242]
Absorption correction	multi-scan	multi-scan	multi-scan
Max. and min. transmission	0.9192 and 0.7340	0.9598 and 0.8356	0.9274 and 0.8029
Data / restraints / parameters	25531 / 46 / 1212	21357 / 279 / 1085	21017 / 3 / 1027
Goodness-of-fit on F ²	1.028	1.001	0.998
Final R indices [I > 2 σ (I)]	R ₁ = 0.0712, ^a wR ₂ = 0.1822 ^{b,c} R ₁ = 0.1268, wR ₂ = 0.2125	R ₁ = 0.0516, wR ₂ = 0.1112 ^{b,d} R ₁ = 0.0773, wR ₂ = 0.1196	R ₁ = 0.0475, wR ₂ = 0.0990 ^{b,e} R ₁ = 0.0617, wR ₂ = 0.1085
R indices (all data)			
Max diff. peak and hole (e.Å ⁻³)	1.397 and -1.555	1.118 and -0.605	0.916 and -0.492

^a $R_1 = \sum ||F_o| - |F_c|| / \sum |F_o|$. ^b $wR_2 = [\sum [w(F_o^2 - F_c^2)^2] / \sum [w(F_o^2)^2]]^{1/2}$. ^c $w = 1 / [^2(FO^2) + (0.0924P)^2 + 15.7040P]$ where $P = (FO^2 + 2(Fc)^2) / 3$. ^d $w = 1 / [^2(FO^2) + (0.0532P)^2 + 0.0000P]$. ^e $w = 1 / [^2(FO^2) + (0.0496P)^2 + 0.0000P]$.

2.5. Results and Discussion

2.5.1 Synthesis

Compounds **1** and a mixture of **1** and **2** were prepared by heating two equivalents of dibenzylphosphinic acid with one equivalent of VO(acac)₂ or VO(acac)₂(py) respectively in ethanol. The ligated water molecule in compound **1** is attributable to adventitious water in the ethanol which was not dried. The mixture of the pyridine and water adducts that was produced in the reaction employed to prepare compound **2**, as determined in crystal **B**, is also attributable to water being present in the ethanol. Here it is noteworthy that no peaks assignable to OH stretches were evident in the IR spectrum of the starting material VO(acac)₂(py) and indeed VO(acac)₂ is known to contain a five coordinated vanadium atom.²⁴ Analytically pure **2** was made by mixing VO(acac)₂ with dibenzylphosphinic acid and adding a slight excess of pyridine in methylene chloride.

The IR spectra of compounds **1** and **2** (see Figs. 2.S3 and 2.S4) contain peaks in the same regions with some notable differences. First complex **1** exhibits absorptions due to OH stretches at 3628 and 3537 cm⁻¹ which are not evident in the spectrum for pure **2**. Second, there are subtle differences in the vanadium to oxygen atom stretching region where two bands at 1024 and 995 cm⁻¹ for **1** and 1026 and 989 cm⁻¹ for **2** are obtained. Perhaps facilitating assignment of these peaks is the fact that the VO stretch in VO(acac)₂ and VO(acac)₂(py) comes at 993 and 964 cm⁻¹ respectively, see Figs. 2.S1 and 2.S2. Therefore the absorptions at 1024 and 1027 cm⁻¹ can be assigned to the two “base” vanadium atoms containing terminal oxo ligands and the absorptions at 995 and 989 cm⁻¹ in **1** and **2** respectively to the “vertex” VO bond located *trans* to the aqua and pyridine ligands.

The reactions with diphenylphosphinic acid or 2-hydroxyisophosphindoline-2-oxide used in place of dibenzylphosphinic acid using the same procedure conducted to produce **1**, resulted in blue intractable precipitates that proved to be insoluble in most common organic solvents as was detailed previously for diphenylphosphinate complexes with zirconium, vanadium and molybdenum.²⁸ Reactions consisted either of stirring at room temperature in CH₂Cl₂ or heating the reactants in EtOH at 120 °C. In the case of diphenylphosphinic acid, seemingly identical products assigned on the basis of elemental analysis as (VO(O₂PPh₂)₂)_∞, **3**, were obtained based on a comparison of the IR spectra, Fig. 2.S5. It should be noted that this IR spectrum for **3** differs substantially from that reported previously²⁸ but similar thermal stabilities were found with an 8% weight lost (Fig. S10) over the temperature range of 300-400 °C compared to the reported loss of 10.3%.²⁸

In the case of 2-hydroxyisophosphindoline-2-oxide, the complex ((H₂O)VO(O₂P*o*-(CH₂)₂C₆H₄)₂)_∞, **4**, was produced when the reactants were stirred at room temperature in CH₂Cl₂ (which was not dried), and, (VO(O₂P(*o*-(CH₂)₂(C₆H₄)))_∞, **5** was obtained when the reaction was conducted at 120 °C in EtOH. These assignments are based on elemental analyses. The IR spectra for **4** (Fig. 2.S6) contained a stretch at 3636 cm⁻¹ which is indicative of a ligated water molecule whereas that for **5** (Fig. 2.S7) did not contain absorptions in the 3600 cm⁻¹ region. Also noteworthy was the fact that the finger print regions of these FTIR spectra for complexes **3-5** were considerable different than those obtained for **1** and **2** in that strong absorptions around the 995 and 1025 cm⁻¹ region were not present. These would be indicative of a nonclassical [(V₃(μ₃-

$\text{O})\text{O}_2)]^{6+}$ moiety as described above. These insoluble products may be in the form of large clusters and/or polymers²⁹⁻³¹ but this is somewhat speculative.¹⁹ For additional identification purposes the x-ray powder diffraction pattern for these compounds is presented as Fig. 2.S9 and these revealed dramatically different patterns between compounds $((\text{H}_2\text{O})\text{VO}(\text{O}_2\text{P}o\text{-(CH}_2)_2\text{C}_6\text{H}_4)_2)_\infty$, **4** and $(\text{VO}(\text{O}_2\text{P}(o\text{-(CH}_2)_2(\text{C}_6\text{H}_4)))_\infty$, **5**. It is somewhat difficult to account for this difference in the reaction products for the different phosphinic acids, though the lower solubility and the larger steric effects of the dibenzylphosphinate ligand may be contributing factors leading to the trimers.

2.5.2 Crystallography

Crystals studied were obtained from saturated 1:1 solutions of hexanes and methylene chloride layered with more hexanes. Crystals were shaped as flat plates and colored light blue. Compound **1** crystallized as a solvate with four molecules of **1** and fourteen molecules of CH_2Cl_2 in the unit cell of crystal **A**. Complex **1** of formulation $(\text{V}_3(\mu_3\text{-O})\text{O}_2)(\mu_2\text{-O}_2\text{P}(\text{CH}_2\text{C}_6\text{H}_5)_2)_6(\text{H}_2\text{O})$, has the three vanadium atoms in the “ $(\text{VO})_3$ ” moiety forming a triangle with one oxo bond roughly in the center of the quasi-isosceles triangle (C_{2v} symmetry) and the other two oxo ligands outside with one on each vanadium atom. The outer periphery of complex **1**, namely the six bridging benzyl phosphinate ligands did not contain disorder, but the inner “ $\text{V}_3(\mu_3\text{-O})\text{O}_2)(\text{H}_2\text{O})$ ” unit was refined to occupy three non-equal sites with 60.6(6):31.3(5):7.7(2) occupancies as illustrated in Fig. 2.1. In this formation, each vanadium atom is six coordinated (distorted octahedral). Two of the three vanadium atoms are coordinated in a pseudo-octahedral fashion to an outwards pointing oxo ligand, four O atoms from the four bridging

phosphinate ligands and at long distances of 2.74(20 and 2.57(2) Å to the central oxygen atom; the third vanadium atom is coordinated to one outwards pointing aqua ligand and double bonded to the central O atom (1.60(2) Å) completing the octahedral coordination spheres as illustrated in Fig. 2.2 which shows the major orientation. Our first attempt at obtaining the crystal structure of complex **2** revealed a

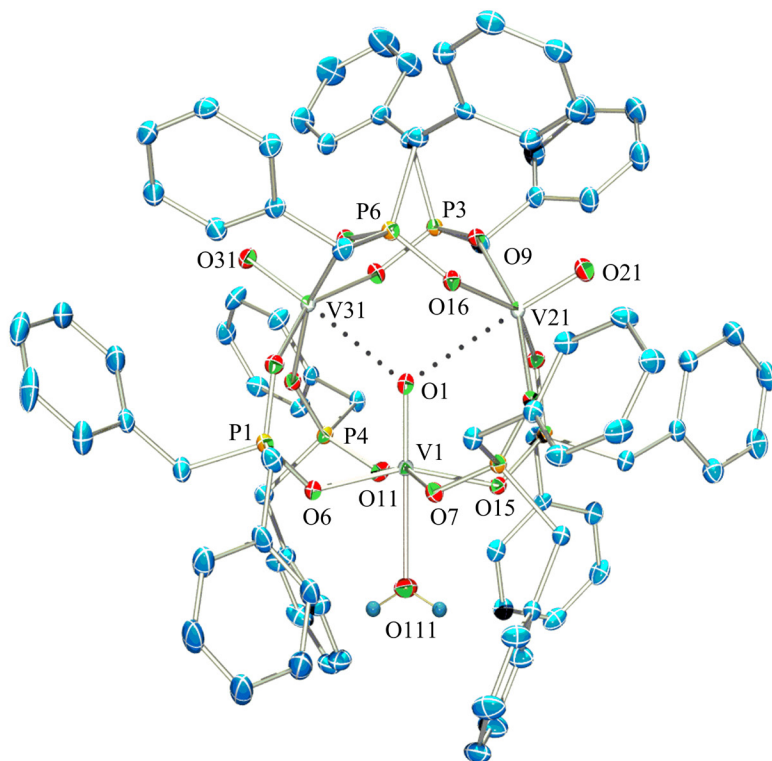


Fig. 2.2 A POV-Ray rendered drawing of an ORTEP-332 illustration of the major orientation of **1** within crystal A. Hydrogen atoms (except those on the aqua ligand, represented by spheres of arbitrary radii) have been omitted for clarity and the thermal ellipsoids are drawn at 30% probability. Dotted lines represent the long interactions between the central oxygen and the two vanadium atoms on the base.

co-crystal consisting of **2** and **1** in a 78.3(6):21.7(6) respective ratio described here as crystal **B** and **2** was then more deliberately crystallized in pure form. Drawings of the

two complexes in crystal **B** are depicted in Fig. 2.3 and that for pure **2** is given in Fig. 2.4. Table 2 and 3 list selected bond distances and angles for **1**, **2** as defined in crystal **B** and pure **2**. Table 2.4 contains a comparison of the three different refined triangular arrangements in complexes **1**, pure **2** and that for the previously reported $(V_3(\mu_3-O)O_2)(C_6H_5CO_2)_6(THF)$, **6**¹⁹ and related $[(V_3(\mu_3-O)O_2)((C_2H_5O)_2PO_2)_6 \cdot CH_3CN]$, **7**.⁵ In all cases, significantly different distances for the two long interactions between the interstitial oxygen atom to two vanadium atoms on the base were

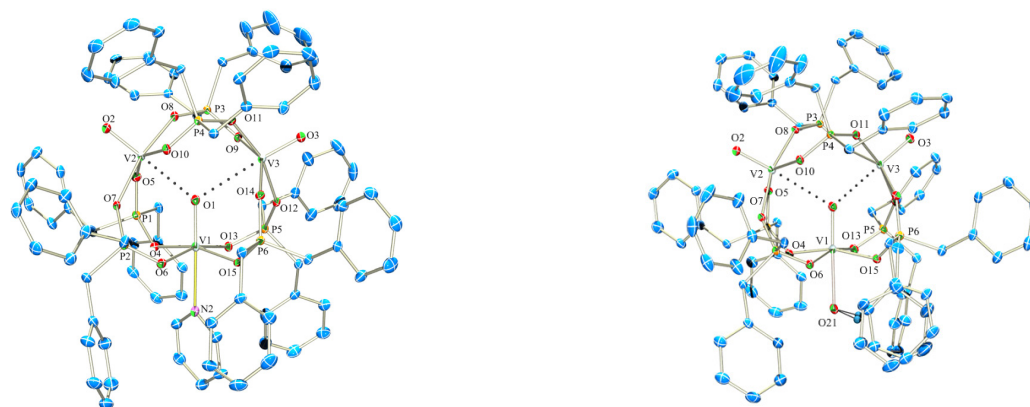


Figure 2.3. POV-Ray rendered drawings of ORTEP-332 representations of complex **2** (left, 78.3(6)%) and **1** (right, 21.7(6)%) which co-crystallized in the form of crystal **B**. Hydrogen atoms (except those on the aqua ligand, represented by spheres of arbitrary radii) have been omitted for clarity and the thermal ellipsoids are drawn at 30% probability. Dotted lines represent the long interactions between the central oxygen and the two vanadium atoms on the base.

present, see rows 3 and 4 in Table 2.2. This asymmetry was utilized in producing the overlay diagrams since this allowed for the alignment of the “ V_3 ” triangles and all the equivalent distances noted in Tables 2.2 and 2.3 were based on this alignment. The fact that an examination of the equivalent bond distances and angles for the three

arrangements of the inner core of complex **1** are not that significantly different suggests that the model is accurate and that dibenzylphosphinate ligands have great flexibility in stabilizing the inner core geometries. The flexibility is demonstrated in the fact that an overlay of the two V_3 triangular cores in **1** from crystal **A** and **2** from crystal **B** reveals different arrangements of the benzyl groups as illustrated in Fig. 2.5. Interestingly these differences in benzyl group arrangements are more pronounced in an overlay between complex **2** from crystal **B** and pure **2** as illustrated in Fig. 2.5. This suggests that the co-crystallization of 78.3(6)% of **2**:21.7(6)% of **1** resulted in a packing arrangement which differs substantially from that occurring in pure **2** which would imply that any differences in bond lengths and angles noted in Tables 2.2 and 2.3 may partly be as a result of the co-crystallization in crystal **B** but more likely the different internal ligand arrangements. As can be seen in Fig. 2.6, the py ligand plane in crystal **B** in these two structures is oriented almost parallel to the O4-V1-O15 plane in **2** from crystal **B** whereas the py plane is rotated 90° and is almost parallel to the O6-V1-O13 plane in pure **2**. While these different orientations of the py ligand in these two molecules result in the interesting fact that the overall geometries depicted in Fig. 2.6 appear as mirror images, it is the main reason why some of the equivalent bond angles listed in Table 2.6 are significantly different.

The nature of the disorder in crystal **A** reduced the accuracy with which some of the distances in the different orientations of **1** could be refined and, in particular, the nature of the interstitial oxygen atom was not determined accurately as reflected in the number of decimal places (i.e., 2 and not 3) for data associated with the atoms labeled as

O(1), O(2) and O(3) and only a listing of the two major orientations for **1** is given in Table 2.4.

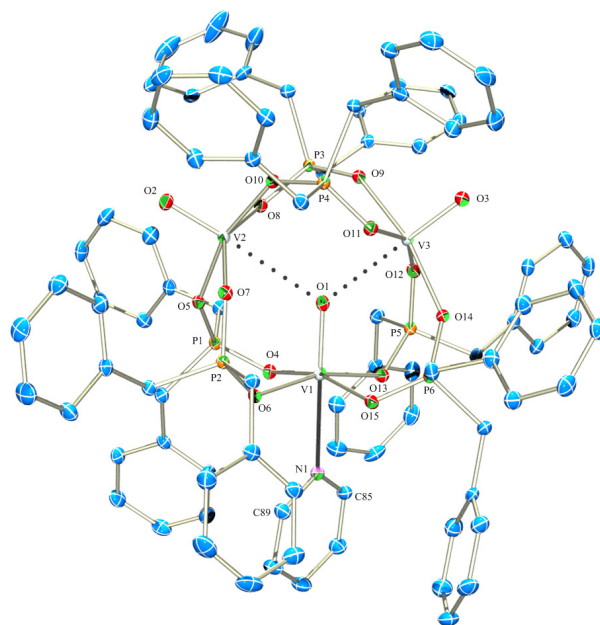


Figure 2.4. POV-Ray rendered drawings of ORTEP-332 representations of pure complex 2. Hydrogen atoms have been omitted for clarity and the thermal ellipsoids are drawn at 30% probability. Dotted lines represent the long interactions between the central O and the two vanadium atoms on the base.



Figure 2.5. POV-Ray rendered Mercury³³ produced overlay of the “(V₃)” cores of the major orientation of **1** (light or yellow) in crystal **A** and the H₂O adduct (dark or blue) in crystal **B** on the left and an overlay of **2** from crystal **B** (light or yellow) and that of pure **2** (dark or blue).

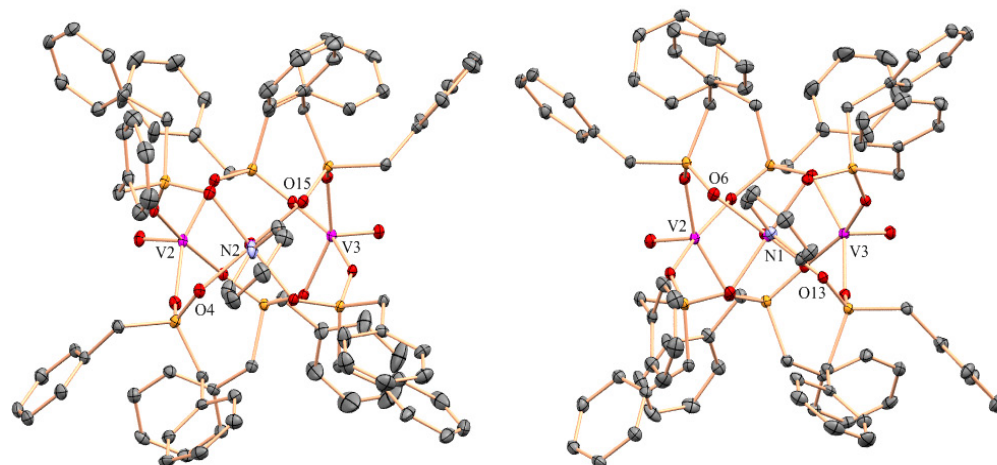


Figure 2.6. POV-Ray rendered Mercury³³ produced illustration of **2** from crystal **B** (left) and pure **2** (right) with the V2 and V3 atoms located in similar positions depicting the different orientation of the py ligands.

Table 2.2. Selected bond distances for major components, i.e., major orientation for **1**, **2** from crystal **B** and pure **2**. Equivalent distances are on the same horizontal line.

Bond Distances (Å)					
Compound 1		2 from crystal B		Pure 2	
V(1)-O(1)	1.600(17)	V(1)-O(1)	1.619(3)	V(1)-O(1)	1.625(2)
V(31)-O(1)	2.57(2)	V(2)-O(1)	2.487(3)	V(2)-O(1)	2.510(2)
V(21)-O(1)	2.74(2)	V(3)-O(1)	2.837(2)	V(3)-O(1)	2.830(3)
V(2)-O(2)	1.63(2)	V(2)-O(2)	1.581(2)	V(2)-O(2)	1.588(2)
V(3)-O(3)	1.58(9)	V(3)-O(3)	1.587(2)	V(3)-O(3)	1.584(2)
V(1)-O(7)	1.942(3)	V(1)-O(15)	2.010(2)	V(1)-O(13)	2.019(2)
V(1)-O(11)	1.962(3)	V(1)-O(4)	1.997(3)	V(1)-O(4)	1.988(2)
V(1)-O(6)	1.985(3)	V(1)-O(6)	1.981(2)	V(1)-O(6)	2.010(2)
V(1)-O(15)	2.024(3)	V(1)-O(13)	1.974(2)	V(1)-O(15)	1.984(2)
V(21)-O(21)	1.562(4)	V(3)-O(3)	1.587(2)	V(3)-O(3)	1.584(2)
V(21)-O(14)	1.979(3)	V(3)-O(14)	1.981(2)	V(3)-O(14)	1.999(2)
V(21)-O(8)	1.979(3)	V(3)-O(12)	1.986(2)	V(3)-O(12)	1.984(2)
V(21)-O(9)	1.997(3)	V(3)-O(9)	1.967(2)	V(3)-O(9)	2.003(2)
V(21)-O(16)	1.999(3)	V(3)-O(11)	1.988(2)	V(3)-O(11)	1.971(2)
V(31)-O(31)	1.572(3)	V(2)-O(2)	1.581(3)	V(2)-O(2)	1.588(2)
V(31)-O(10)	1.986(3)	V(2)-O(8)	2.010(2)	V(2)-O(8)	1.989(2)
V(31)-O(13)	1.992(3)	V(2)-O(5)	1.986(3)	V(2)-O(5)	2.024(2)
V(31)-O(5)	1.999(3)	V(2)-O(7)	2.024(2)	V(2)-O(7)	1.993(2)
V(31)-O(12)	2.003(3)	V(2)-O(10)	1.984(2)	V(2)-O(10)	2.019(2)
O(5)-P(1)	1.511(3)	P(1)-O(5)	1.505(3)	P(1)-O(5)	1.513(2)
O(6)-P(1)	1.501(3)	P(1)-O(4)	1.513(3)	P(1)-O(4)	1.518(2)
O(7)-P(2)	1.517(3)	P(2)-O(7)	1.495(3)	P(2)-O(7)	1.516(2)
O(8)-P(2)	1.511(3)	P(2)-O(6)	1.507(3)	P(2)-O(6)	1.516(2)
O(9)-P(3)	1.508(3)	P(3)-O(8)	1.502(2)	P(3)-O(8)	1.523(2)
O(10)-P(3)	1.522(3)	P(3)-O(9)	1.514(2)	P(3)-O(9)	1.516(2)
O(11)-P(4)	1.513(3)	P(4)-O(11)	1.514(2)	P(4)-O(11)	1.524(2)
O(12)-P(6)	1.507(3)	P(4)-O(10)	1.517(3)	P(4)-O(10)	1.506(2)
O(13)-P(4)	1.500(3)	P(5)-O(12)	1.510(2)	P(5)-O(12)	1.522(2)
O(14)-P(5)	1.503(3)	P(5)-O(13)	1.518(2)	P(5)-O(13)	1.515(2)
O(15)-P(5)	1.518(3)	P(6)-O(15)	1.509(3)	P(6)-O(15)	1.521(2)
O(16)-P(6)	1.516(3)	P(6)-O(14)	1.512(3)	P(6)-O(14)	1.514(2)
		V(1)-N(2)	2.331(11)	V(1)-N(1)	2.350(3)
		N(2)-C(13)	1.232(10)	N(1)-C(85)	1.339(4)
		N(2)-C(17)	1.434(12)	N(1)-C(89)	1.353(4)
V(1)-O(111)	2.307(4)	V(1)-O(21)	2.24(3)		

Table 2.3. Selected bond angles for **1** (major orientation), **2** from crystal **B** and pure **2**. Equivalent angles are on the same horizontal line.

Compound 1 (°)		2 from crystal B (°)		Pure 2 (°)	
O(1)-V(1)-O(7)	98.8(7)	O(1)-V(1)-O(15)	99.39(11)	O(1)-V(1)-O(15)	98.40(10)
O(1)-V(1)-O(11)	97.1(7)	O(1)-V(1)-O(4)	96.39(11)	O(1)-V(1)-O(4)	98.79(10)
O(7)-V(1)-O(11)	164.05(19)	O(4)-V(1)-O(15)	164.21(10)	O(4)-V(1)-O(15)	162.81(9)
O(1)-V(1)-O(6)	101.0(6)	O(1)-V(1)-O(6)	98.72(11)	O(1)-V(1)-O(6)	96.14(10)
O(7)-V(1)-O(6)	89.10(12)	O(6)-V(1)-O(15)	87.94(10)	O(6)-V(1)-O(15)	89.05(9)
O(11)-V(1)-O(6)	89.30(12)	O(6)-V(1)-O(4)	89.22(10)	O(6)-V(1)-O(4)	89.39(9)
O(1)-V(1)-O(15)	101.4(6)	O(1)-V(1)-O(13)	98.47(11)	O(1)-V(1)-O(13)	99.39(10)
O(7)-V(1)-O(15)	88.27(11)	O(13)-V(1)-O(15)	88.95(10)	O(13)-V(1)-O(15)	89.02(9)
O(11)-V(1)-O(15)	87.19(12)	O(13)-V(1)-O(4)	89.19(10)	O(13)-V(1)-O(4)	87.92(9)
O(6)-V(1)-O(15)	157.65(18)	O(13)-V(1)-O(6)	162.81(11)	O(13)-V(1)-O(6)	164.46(9)
O(1)-V(1)-O(111)	179.8(9)	O(1)-V(1)-N(2)	179.4(3)	O(1)-V(1)-N(1)	176.95(10)
O(7)-V(1)-O(111)	81.33(13)	O(15)-V(1)-N(2)	81.2(3)	O(15)-V(1)-N(1)	79.94(9)
O(11)-V(1)-O(111)	82.79(14)	O(6)-V(1)-N(2)	81.1(3)	O(6)-V(1)-N(1)	81.30(9)
O(6)-V(1)-O(111)	79.14(13)	O(4)-V(1)-N(2)	83.0(3)	O(4)-V(1)-N(1)	82.89(9)
O(15)-V(1)-O(111)	78.52(13)	O(13)-V(1)-N(2)	81.7(3)	O(13)-V(1)-N(1)	83.18(9)
O(21)-V(21)-O(14)	104.77(15)	O(3)-V(3)-O(12)	98.58(11)	O(3)-V(3)-O(12)	105.16(11)
O(21)-V(21)-O(8)	100.53(15)	O(3)-V(3)-O(14)	105.25(12)	O(3)-V(3)-O(14)	98.26(11)
O(14)-V(21)-O(8)	89.59(11)	O(14)-V(3)-O(12)	89.59(10)	O(14)-V(3)-O(12)	89.55(9)
O(21)-V(21)-O(9)	98.29(15)	O(3)-V(3)-O(9)	106.30(12)	O(3)-V(3)-O(9)	99.03(11)
O(14)-V(21)-O(9)	85.72(11)	O(9)-V(3)-O(12)	86.69(10)	O(9)-V(3)-O(12)	86.66(9)
O(8)-V(21)-O(9)	161.17(15)	O(9)-V(3)-O(14)	148.44(10)	O(9)-V(3)-O(14)	162.69(9)
O(21)-V(21)-O(16)	105.54(15)	O(3)-V(3)-O(11)	98.98(11)	O(3)-V(3)-O(11)	106.26(11)
O(14)-V(21)-O(16)	149.55(15)	O(12)-V(3)-O(11)	162.43(9)	O(12)-V(3)-O(11)	148.57(9)
O(8)-V(21)-O(16)	87.73(11)	O(14)-V(3)-O(11)	86.50(10)	O(14)-V(3)-O(11)	86.87(9)
O(9)-V(21)-O(16)	87.14(11)	O(9)-V(3)-O(11)	87.71(10)	O(9)-V(3)-O(11)	87.58(9)
O(31)-V(31)-O(10)	104.09(14)	O(2)-V(2)-O(8)	95.89(11)	O(2)-V(2)-O(8)	103.11(11)
O(31)-V(31)-O(13)	98.07(13)	O(2)-V(2)-O(5)	102.06(12)	O(2)-V(2)-O(5)	97.10(10)

O(10)-V(31)-O(13)	86.98(11)	O(5)-V(2)-O(8)	86.82(10)	O(5)-V(2)-O(8)	88.87(9)
O(31)-V(31)-O(5)	103.55(13)	O(2)-V(2)-O(7)	97.03(11)	O(2)-V(2)-O(7)	102.12(11)
O(10)-V(31)-O(5)	152.36(12)	O(8)-V(2)-O(7)	166.93(10)	O(8)-V(2)-O(7)	154.77(9)
O(13)-V(31)-O(5)	88.63(11)	O(5)-V(2)-O(7)	88.60(10)	O(5)-V(2)-O(7)	88.45(9)
O(31)-V(31)-O(12)	97.73(13)	O(2)-V(2)-O(10)	103.42(12)	O(2)-V(2)-O(10)	95.83(10)
O(10)-V(31)-O(12)	89.86(11)	O(10)-V(2)-O(8)	90.13(10)	O(10)-V(2)-O(8)	90.47(9)
O(13)-V(31)-O(12)	164.19(11)	O(10)-V(2)-O(5)	154.52(10)	O(10)-V(2)-O(5)	166.86(9)
O(5)-V(31)-O(12)	87.00(11)	O(10)-V(2)-O(7)	88.75(10)	O(10)-V(2)-O(7)	86.56(9)

Table 2.4. Comparison of core bonding distances in $(V_3(\mu_3\text{-O})O_2)(\mu_2\text{-O}_2P(\text{CH}_2\text{C}_6\text{H}_5)_2)_6\text{H}_2\text{O}$, **1**, $(V_3(\mu_3\text{-O})O_2)(\mu_2\text{-O}_2P(\text{CH}_2\text{C}_6\text{H}_5)_2)_6\text{py}$, pure **2**, $(V_3(\mu_3\text{-O})O_2)(\text{C}_6\text{H}_5\text{CO}_2)_6(\text{THF})$, **6**¹⁹ and $[(V_3(\mu_3\text{-O})O_2)((\text{C}_2\text{H}_5\text{O})_2\text{PO}_2)_6\cdot\text{CH}_3\text{CN}]$, **7**.⁵

60.6% 1 , Fig. 1	31.3% 1 , Fig. 1	Pure 2 , Fig. 4	6	7
Distances (Å)				
V(1)-O(1)	1.60(2)	V(2)-O(2)	V(1)-O(1)	1.623(4)
V(21)-O(21)	1.562(3)	V(11)-O(111)	V(2)-O(2)	1.584(3)
V(31)-O(31)	1.572(3)	V(31)-O(31)	V(3)-O(9)	
V(1)-O(111)	2.307(4)	V(2)-O(21)	V(1)-N(1)	2.352(6)
V(21)-O(1)	2.74(2)	V(11)-O(2)	V(2)-O(10)	2.765(3)
V(31)-O(1)	2.57(2)	V(31)-O(2)	V(3)-O(10)	
V(1)···V(21)	3.830(3)	V(2)···V(11)	V(1)···V(2)	3.926(2) ^a
V(1)···V(31)	3.742(2)	V(2)···V(31)		
V(21)···V(31)	4.422(2)	V(11)···V(31)	V(2)···V(2')	4.540(2) ^a

^a As indicated, some distances for **7** were obtained using Mercury³³ and the data code named NEJCUA available on the CCDC.³⁴

Table 2.5. Comparison of core bonding angles in $(V_3(\mu_3-O)O_2)(\mu_2-O_2P(CH_2C_6H_5)_2)H_2O$, **1**, $(V_3(\mu_3-O)O_2)(\mu_2-O_2P(CH_2C_6H_5)_2)6py$, pure **2**, $(V_3(\mu_3-O)O_2)(C_6H_5CO_2)_6(THF)$, **6**¹⁹ and $[(V_3(\mu_3-O)O_2)((C_2H_5O)_2PO_2)_6 \cdot CH_3CN]$, **7**.⁵

60.6% 1 , Fig. 1		31.3% 1 , Fig. 1		Pure 2 , Fig. 4		6		7
Bond Angles (°)								
O(1)-V(1)-O(111)	179.8(6)	O(2)-V(2)-O(21)	177(1)	O(1)-V(1)-N(1)	176.95(10)	O(10)-V(1)-O(7)	179.2(3)	O(1)-V(1)-N(1)
V(1)-O(1)-V(21)	121.6(8)	V(2)-O(2)-V(31)	122(1)	V(1)-O(1)-V(3)	120.7(1)	V(1)-O(10)-V(2)	123.9(3)	
V(1)-O(1)-V(31)	125.8(9)	V(2)-O(2)-V(11)	125(1)	V(1)-O(1)-V(2)	128.1(1)	V(1)-O(10)-V(3)	120.9(3)	V(1)-O(1)-V(2)
V(21)-O(1)-V(31)	112.6(6)	V(11)-O(2)-V(31)	113(1)	V(2)-O(1)-V(3)	111.15(9)	V(2)-O(10)-V(3)	115.2(2)	V(2)-O(1)-V(2')
V(21)-V(1)-V(31)	71.45(4)	V(11)-V(2)-V(31)	70.66(7)	V(2)-V(1)-V(3)	70.28(2)	V(2)-V(1)-V(3)	69.65(4)	V(2)-V(1)-V(3)
V(1)-V(31)-V(21)	55.20(3)	V(2)-V(31)-V(11)	55.61(6)	V(1)-V(3)-V(2)	52.95(1)	V(1)-V(3)-V(2)	54.57(4)	V(1)-V(2)-V(2')
V(1)-V(21)-V(31)	53.35(3)	V(2)-V(11)-V(31)	53.73(6)	V(1)-V(2)-V(3)	56.7(1)	V(1)-V(2)-V(3)	55.78(4)	V(1)-V(2)-V(3)

^a As indicated, some distances for **7** were obtained using Mercury³³ and the data code named NEJCUA available on the CCDC.³⁴

This suffices to demonstrate equivalency and merit in the refinement and we restrict a comparison in distances to 60.6 % **1** and **2** as detailed in Tables 2.4 and 2.5. Some conclusions can be drawn as follows.

1. There are no discernable significant differences in the vanadium to interstitial oxygen atom and the other two vanadium to O_{oxo} atom distances in **1**, namely V(1)-O(1) = 1.60(2) Å, V(21)-O(21) = 1.562(3) Å and V(31)-O(31) = 1.572(3) Å for **1**. The equivalent distances, i.e., V to O_{central} compared to V to O_{terminal} in **2**, **6** and **7** (situated on a crystallographic two-fold axis) are significantly different presumably as a result of the ligand *trans* to the central O atom. It is likely that the disorder in **1**, i.e., this one oxygen atom (O(1) + O(2) + O(3) = 100 % O in **1**) was refined over three different positions, prevented accurate resolution.
2. The vanadium to oxygen atom distance in the aqua ligand in **1** (2.307(4) Å) is comparable with the equivalent distance for **1** in crystal **B** at 2.24(3) Å and the vanadium to nitrogen atom in pyridine in **2** from crystal **B** (2.331(11) Å) is equivalent to that in pure **2** at 2.350(2) Å. However, the vanadium to oxygen atom distances in **1** are significantly longer than the vanadium to O_{THF} atom distance in **6** at 2.186(6) Å whereas the vanadium to N(py) distances in **2** are equivalent to the vanadium to N atom in acetonitrile in **7** at 2.352(6) Å.
3. The lengths of the sides of the “V₃” quasi-isosceles triangle in **1** (3.830(3), 3.742(2), 4.422(2) Å) and pure **2** (3.917(1), 3.738(1), 4.409(1) Å) are significantly larger than those in **6** (3.520(2), 3.572(2), 4.050(2) Å), and shorter than those in **7** (3.926(2) and 4.540(2) Å), see Table 2.4. This can be attributed to the larger chelating capabilities

of the phosphinate ligand as compared with that of the carboxylate moieties in **6** as noted previously.²

4. The interstitial O atom, O(1), is displaced more from the center of the quasi-isosceles triangle formed by the three vanadium atoms in **2** compared to **1** judging by the V(2)-O(1) and V(3)-O(1) labeled distances in **2**. The fact that the equivalent distances are shorter in **6** may be attributed to the shorter triangle. The three interstitial angles add up to exactly 360° for **1** and **2** thus proving the planarity of the core.
5. The bond distances between the vanadium and the O atom on the aqua ligand in both **1** from crystals **A** and **B** at 2.307(4) and 2.24(3) Å is suggestive of a long single bond and it is noteworthy that there are no hydrogen bonds associated with this coordinated water molecule, presumably due to steric shielding from the bulky benzyl groups. Apart from the coordination by the O atom, the environment of the two H atoms being surrounded by phenyl groups is similar to that in the recently reported H₂O@C₆₀ where a single water molecule was encapsulated by C₆₀.³⁵

In light of this analysis and that previously reported for **6**,¹⁹ the structures of related trinuclear vanadium complexes both which contained disorder and were assigned by crystallography as co-crystals consisting of [(C₂H₅)₂NH₂]₂[{V⁴⁺O(μ₂-H₂L)}₃(μ₃-O)]_{0.67}[{V⁴⁺(OH)(μ₂-HL)}₃(μ₃-O)]_{0.33}·2H₂O, where H₄L = CH₃C(OH)PO₃H₂)₂,³⁶ and, {[V₃O₃(OH)(H₂hedp)(Hhedp)₂]⁶⁻}³⁷ where H₅hedp = etidronic acid, may be in need of reassignment.

2.5.3 Magnetic susceptibility measurements

The magnetic moments of compounds **1-5** were measured at 296K in triplicate and are listed in Table 2.6 with raw data as Table 2.S1. Compounds **1** and **2** display magnetic moments for

Table 2.6. Magnetic moments of oxovanadium phosphinate compounds.

Compound	$\mu_{\text{eff}}^{\text{a}}/\mu_{\text{B}}$
1	3.02(1)
2	3.045(6)
3	1.76(2)
4	1.758(7)
5	1.77(3)

^aAll measurements conducted in triplicate at 296K.

three oxovanadium d¹ centers contained in one molecule and the variable temperature measurement on complex **2**, Fig. 2.7, suggest that this is ferromagnetically coupled. The data (susceptibility versus temperature and magnetization versus field) were simultaneously simulated with MAGPACK,³⁸ using the same set of parameters: $g = 1.98$, $J = +0.64 \text{ cm}^{-1}$ and $J' = -0.61 \text{ cm}^{-1}$ for the Hamiltonian: $H = -2J(S_1S_2 + S_2S_3) - 2J'S_1S_3$. The very weak exchange interactions are consistent with the crystal structure and the long V...V distances. This is in contrast to the data reported for the antiferromagnetically coupled vanadium(IV) dimer $[\text{V}_2\text{O}_2(\mu\text{-OH})(\mu\text{-SO}_4)([\text{9}]_{\text{aneN}_3})_2]\text{Br}_2$ of $1.2 \mu_{\text{B}}$ ³⁹ at 293K and for the anionic cluster $[(\text{VO})_2\text{BP}_2\text{O}_{10}]_6^{18-}$ of $1.59 \mu_{\text{B}}$ ⁴⁰ at 298K which both contain shorter V...V distances. The magnetic moments for polymeric

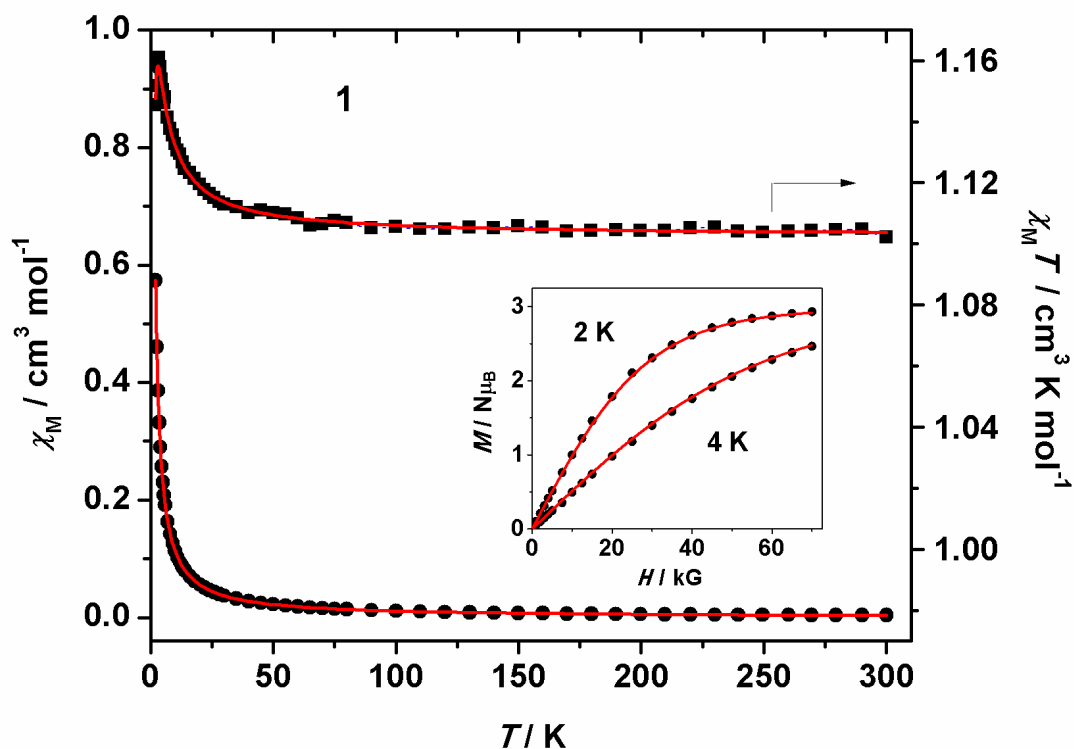


Figure 2.7. Measured and calculated χ_M and $\chi_M T$ against T for compound X. Inset: M vs H for compound X at 2 and 4 K. The lines are the best fit of the data using the parameters described in the text.

species **3-5** were similar to the spin-only moment for an unpaired d^1 electron as was noted for molecular vanadium(IV) species.^{41, 42} Previous measurements with oxovanadium dimers in which two or three diphenylphosphinate ligands bridged two vanadium centers resulted in magnetic moments at room temperature close to the spin-only moment for one unpaired electron.^{9, 11, 43} Additionally, a 2-dimensional oxovanadium phosphinate polymer was also reported to have a magnetic moment near the spin-only moment for one unpaired electron.¹² In each case, the vanadium centers are

connected to each other by bridging phosphinate ligands but show no meaningful magnetic interaction.

2.5.4 TGA and DSC Analysis

The TGA for VO(acac)₂, Fig. 2.S11, and TGA and DSC for VO(acac)₂(py), Figs. 2.S12 and 2.S13, have been previously reported^{41, 44} and we re-measured these as a check of instrumental accuracy. The results suggest (based solely upon color and weight loss) that both VO(acac)₂ and VO(acac)₂(py) decompose to V₂O₃ by 270 °C and the pathway with VO(acac)₂(py) includes the loss of pyridine (calc. 23.0%; obs. 21.6%), Fig. 2.S12. DSC suggests that the absorption of 58.0 kJ/mol is required to break the vanadium to N_{py} bond in VO(acac)₂(py), Fig. 2.S13, which is comparable to the 69.4 kJ/mol previously reported.⁴⁴ VO(acac)₂ and VO(acac)₂(py) presented 74.1% and 80.2% weight losses, which are higher than the expected values of 71.7% and 78.1% for a V₂O₃ residue possibly because of sublimation of VO(acac)₂, Figs 2.S11-2.S12. Sublimation of VO(acac)₂ was thought not to occur under these conditions⁴⁵ but more recent work suggests otherwise.⁴⁶

In order to understand the TGA data of the complexes produced we measured that for the ligand dibenzylphosphinic acid which is reproduced as Fig. 2.S14. This revealed a loss in weight of 82.0 % from 250-400 °C corresponding to the decomposition of the ligand and possib %). A bulk study where we obtained an IR spectrum of the dissociated material revealed that this was dissociated ligand. At 500 °C the complex decomposed further and, in this run, the sample was heated to 600 °C and kept at this temperature for 30 minutes, Fig. 2.S15a. The TGA of **2**, Fig. 2.S16, conducted in a similar manner to that

for **1**, revealed a weight loss corresponding to pyridine (calc. 5.2%; obs. 4.5%) and then presumably some ligand dissociation (obs. 11.7%) followed by decomposition with heating up to 600 °C for 30 minutes, Fig. 2.S16a. The FTIR spectra of the final products obtained after heating **1** and **2** up to 600 °C were identical and that for complex **1**, Fig. 2.S17, and is comparable to that reported after heating V₂O₅-P₂O₅ (in the P/V ratio = 2) which was mostly VO(PO₃)₂.⁴⁷ While the thermolysis of (VO)₃((C₂H₅O)₂PO₂)₆·CH₃CN was reported to produce VO(PO₃)₂,⁵ in our studies on **1** and **2** loss of dissociated ligand would prevent this compound from being produced in a pure state. An X-ray powder diffraction measurement on this residue product was not conclusive as the spectrum was amorphous.

The DSC of **1** contained two small absorptions at 120 and 140 °C corresponding to 3.9 and 6.8 kJ/mol and a melting transition at 240 °C of 60.7 kJ/mol, Fig. 2.S18. The DSC of **2** revealed a crystallization process at 120 °C corresponding to the release of 6.8 kJ/mol and two absorptions at 170 and 200 °C (also contains a shoulder blip) of 13.3 and 28.7 kJ/mol respectively followed by a melting transition at 240 °C of 65.2 kJ/mol, Fig. 2.S19. These two plots (without the melting transitions) are illustrated in Fig. 2.8. We believe that some sort of reorganization is taking place in these complexes that prevents the sharp rupture and dissociation of the H₂O and pyridine ligands in **1** and **2** respectively. Evidence for this is present in the crystallization of **2** in the DSC plot and the fact that the TGA only indicated weight loss for the H₂O and pyridine ligands in **1** and **2** up to 280 °C. Therefore it is reasonable to consider the absorptions of the sum of the two peaks for **1** at 120 and 140 °C of 10.7 kJ/mol and that for **2** at 170 and 200 °C

equal to 42.0 kJ/mol as corresponding to the energies required to liberate the vanadium to O_{water} bond in **1** and the vanadium to N_{py} bond in **2**. It did require 58.0 kJ/mol for the dissociation of py from $\text{VO}(\text{acac})_2(\text{py})$.

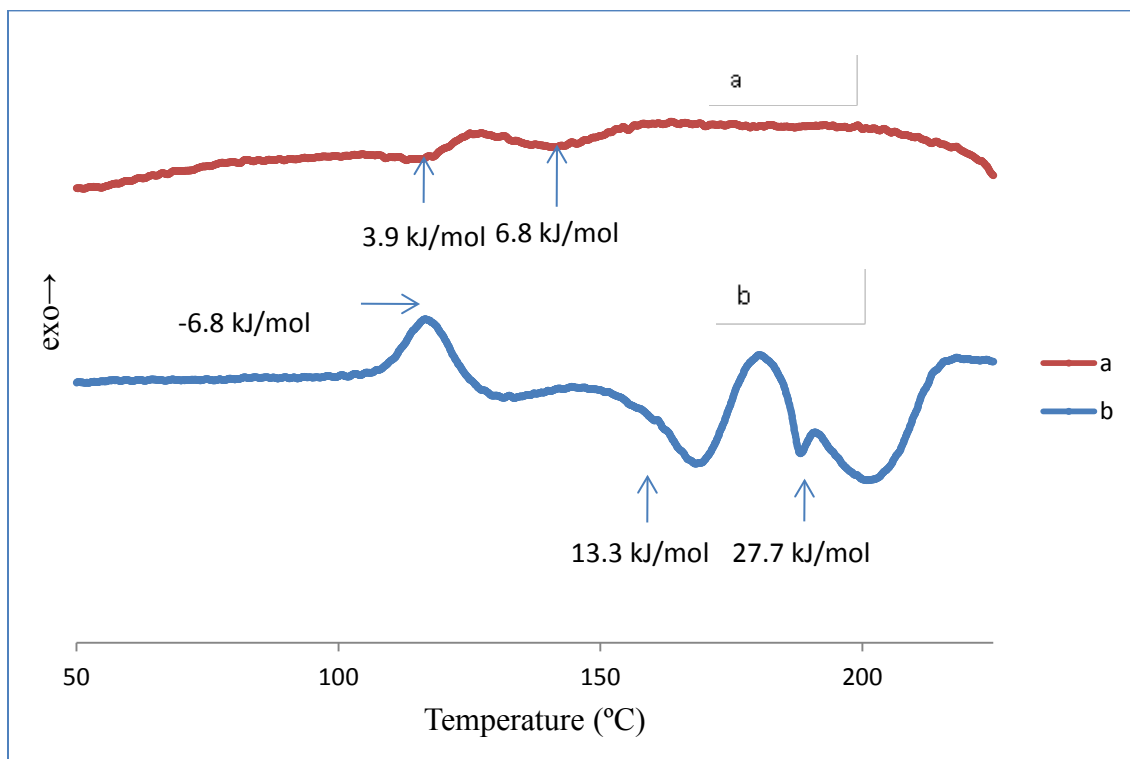


Figure 2.8. DSC thermograms ($5\text{ }^{\circ}\text{C min}^{-1}$, N_2 atmosphere) for **1** (a, top curve) and **2** (b, bottom curve).

2.6. Conclusions

The nonclassical trimers $(\text{V}_3(\mu_3\text{-O})\text{O}_2)(\mu_2\text{-O}_2\text{P}(\text{CH}_2\text{C}_6\text{H}_5)_2)_6(\text{H}_2\text{O})$, **1**, and $(\text{V}_3(\mu_3\text{-O})\text{O}_2)(\mu_2\text{-O}_2\text{P}(\text{CH}_2\text{C}_6\text{H}_5)_2)_6(\text{py})$, **2**, can be obtained either under solvothermal reaction conditions or an easier substitution route conducted at room temperature. The presence of absorptions in the IR spectra in the 995 and 1025 cm^{-1} region of intensity 1:2 may signify the nonclassical arrangement. Reactions using diphenylphosphinic acid and 2-

hydroxyisophosphindoline-2-oxide resulted in polymeric species. The structural characterization of compounds **1** and **2** was based upon the collection and refinement of data collected from material labeled as crystals **A** and **B**. Crystal **A** consisted entirely of **1** but contained disorder whereby the outer periphery of the ligand structure was maintained but the inner core “(V₃(μ₃-O)O₂)(H₂O)” was oriented in three different arrangements for **1**. Crystal **B** consisted of a co-crystallization of **1** and **2** in a 21.7(6):78.3(6)% ratio. The structure of pure **2** was also detailed. Different arrangements of the coordinated py ligand were observed. Magnetic susceptibility measurements revealed values close to the spin only value for one unpaired electron for **1-5** and this was confirmed by variable temperature magnetic susceptibility and magnetization measurements on complex **2** suggesting that this complex was ferromagnetically coupled. Thermal analysis assessed the bond strengths of the ligated water in **1** and the pyridine molecule in **2** at 10.7 and 42.0 kJ/mol respectively, and upon heating to 600 °C the complexes decomposed. Experiments are currently being conducted to see if the aforementioned polymers can be broken into smaller complexes with suitable binding ligands.⁴⁸

Acknowledgements

The diffractometer used to collect structural data was funded by NSF Grant 0087210, by Ohio Board of Regents Grant CAP-491, and by YSU. Helpful comments from reviewers and Professor L. K. Thompson of Memorial University, Newfoundland, Canada and support by Michigan Technological University is acknowledged.

Supplementary material

Table 2.S1 featuring the magnetic data, FTIR spectra of complexes VO(acac)₂, VO(acac)₂(py), complexes **1-5**, and, crystal **B** Figs. 2.S1-2.S8. X-ray powder pattern for complexes **3-5**, Fig. 2.S9. TGA plots on (VO(O₂PPh₂)₂)_∞ (**3**), VO(acac)₂ and VO(acac)₂(py), Figs. 2.S10, 2.S11 and 2.S12, and DSC thermogram of VO(acac)₂(py), Fig. 2.S13. TGA on diphenylphosphinic acid, complexes **1** and **2**, Figs. 2.S14-2.S16; FTIR spectrum of the residue from **1**, Fig 2.S17; DSC thermograms of **1** and **2**, Figs. S18-S19. CCDC's 827865, 827866 and 842909 contain the supplementary crystallographic data for complexes **A**, **B** and **2** respectively. These data can be obtained free of charge from The Cambridge Crystallographic Data Centre via www.ccdc.cam.ac.uk/data_request/cif. This material is also available free of charge via the Internet at <http://pubs.acs.org>.

References

1. Feng, L.; Luck, R. L.; Maass, J. S. In *Syntheses, properties and olefin epoxidation reactivities of "Mo-4O8" clusters stabilized by phosphinate ligands*, 2010; 239th ACS National Meeting: 2010; pp INOR-910.
2. Jimtaisong, A.; Feng, L.; Sreehari, S.; Bayse, C. A.; Luck, R. L. *J. Cluster Sci.* **2008**, *19*, 181-195.
3. Jimtaisong, A.; Luck, R. L. *J. Cluster Sci.* **2005**, *16*, 167-184.
4. Maass, J. S.; Chen, Z.; Zeller, M.; Luck, R. L. *Dalton Transactions* **2011**, *40* (43), 11356-11358.
5. Herron, N.; Thorn, D. L.; Harlow, R. L.; Coulston, G. W. *J. Am. Chem. Soc.* **1997**, *119*, 7149-7150.
6. Butler, A.; Sandy, M. *Nature (London, U. K.)* **2009**, *460*, 848-854.

7. Willsky, G. R.; Goldfine, A. B.; Kostyniak, P. J.; McNeill, J. H.; Yang, L. Q.; Khan, H. R.; Crans, D. C. *J. Inorg. Biochem.* **2001**, *85*, 33-42.
8. Khan, M. I.; Zubieta, J. *Prog. Inorg. Chem.* **1995**, *43*, 1-149.
9. Dean, N. S.; Bond, M. R.; O'Connor, C. J.; Carrano, C. J. *Inorg. Chem.* **1996**, *35*, 7643-7648.
10. Kawasaki, S.; Koikawa, M.; Tokii, T. *Mol. Cryst. Liq. Cryst. Sci. Technol., Sect. A* **2002**, *376*, 365-370.
11. Koga, K.; Ueno, M.; Koikawa, M.; Tokii, T. *Inorg. Chem. Commun.* **2003**, *6*, 374-376.
12. Costantino, F.; Midollini, S.; Orlandini, A.; Sorace, L. *Inorg. Chem. Commun.* **2006**, *9*, 591-594.
13. Norman, R. E.; Holz, R. C.; Menage, S.; Que, L., Jr.; Zhang, J. H.; O'Connor, C. J. *Inorg. Chem.* **1990**, *29*, 4629-37.
14. Turowski, P. N.; Armstrong, W. H.; Roth, M. E.; Lippard, S. J. *J. Am. Chem. Soc.* **1990**, *112*, 681-90.
15. Liu, S.-J.; Staples, R. J.; Fackler, J. P. *Polyhedron* **1992**, *11*, 2427-2430.
16. Cotton, F. A.; Extine, M. W.; Falvello, L. R.; Lewis, D. B.; Lewis, G. E.; Murillo, C. A.; Schwotzer, W.; Tomas, M.; Troup, J. M. *Inorg. Chem.* **1986**, *25*, 3505-12.
17. Castro, S. L.; Streib, W. E.; Sun, J.-S.; Christou, G. *Inorg. Chem.* **1996**, *35*, 4462-4468.
18. Chaudhuri, P.; Hess, M.; Weyhermüller, T.; Bill, E.; Haupt, H.-J.; Flörke, U. *Inorg. Chem. Commun.* **1998**, *1*, 39-42.
19. Cotton, F. A.; Lewis, G. E.; Mott, G. N. *Inorg. Chem.* **1982**, *21*, 3127-30.
20. Kickelbick, G.; Holzinger, D.; Brick, C.; Trimmel, G.; Moons, E. *Chem. Mater.* **2002**, *14*, 4382-4389.
21. Boyd, E. A.; Boyd, M. E. K.; Kerrigan, F. *Tetrahedron Lett.* **1996**, *37*, 5425-5426.
22. Venezky, D. L.; Poranski, C. F., Jr. *J. Org. Chem.* **1967**, *32*, 838-40.
23. Rowe, R. A.; Jones, M. M. *Inorg. Synth.* **1957**, *5*, 113-116.

24. Jones, M. M. *J. Am. Chem. Soc.* **1954**, 76, 5995-5997.
25. Bruker *Apex2 v2.1-4*, Bruker AXS Inc.: Madison (WI), USA, 2007.
26. Sheldrick, G. *Acta Cryst.* **2008**, A64, 112-122.
27. Spek, A. L. *Acta Cryst.* **2009**, D65, 148-155.
28. Pitts, J. J.; Robinson, M. A.; Trotz, S. I. *J. Inorg. Nucl. Chem.* **1969**, 31, 3685-90.
29. La, G. A.; Marucci, G.; Monaci, A. *Gazz. Chim. Ital.* **1964**, 94, 1459-63.
30. Podall, H. E.; Iapalucci, T. L. *J. Polym. Sci., Part B: Polym. Lett.* **1963**, 1, 457-9.
31. Rosca, I. *Bul. Inst. Politeh. Iasi* **1970**, 16, 15-24.
32. Farrugia, L. J. *J. Appl. Crystallogr.* **1997**, 30, 565.
33. Macrae, C. F.; Bruno, I. J.; Chisholm, J. A.; Edgington, P. R.; McCabe, P.; Pidcock, E.; Rodriguez-Monge, L.; Taylor, R.; van de Streek, J.; Wood, P. A. *J. Appl. Crystallogr.* **2008**, 41, 466-470.
34. Allen, F. H. *Acta Cryst.* **2002**, B58, 380-388.
35. Kurotobi, K.; Murata, Y. *Science* **2011**, 333, 613-616.
36. Aleksandrov, G. G.; Sergienko, V. S.; Afonin, E. G. *Crystallogr. Rep.* **2001**, 46, 46-50.
37. Rocha, J.; Almeida Paz, F. A.; Shi, F.-N.; Ferreira, R. A. S.; Trindade, T.; Carlos, L. D. *Eur. J. Inorg. Chem.* **2009**, 2009, 4931-4945.
38. Borrás-Almenar, J. J.; Clemente-Juan, J. M.; Coronado, E.; Tsukerblat, B. S. *J. Comput. Chem.* **2001**, 22, 985-991.
39. Wieghardt, K.; Bossek, U.; Volckmar, K.; Swiridoff, W.; Weiss, J. *Inorg. Chem.* **1984**, 23, 1387-9.
40. Do, J.; Zheng, L.-M.; Bontchev, R. P.; Jacobson, A. J. *Solid State Sci.* **2000**, 2, 343-351.
41. Ahmed, M. A. K.; Fjellvåg, H.; Kjekshus, A.; Klewe, B. Z. *Anorg. Allg. Chem.* **2004**, 630, 2311-2318.

42. Le Bail, A.; Marcos, M. D.; Amoros, P. *Inorg. Chem.* **1994**, 33, 2607-2613.
43. Bircsak, Z.; Hall, A. K.; Harrison, W. T. A. *J. Solid State Chem.* **1999**, 142, 168-173.
44. Shibutani, Y.; Shinra, K. *Bull. Chem. Soc. Jpn.* **1989**, 62, 1477-81.
45. Dilli, S.; Patsalides, E. *Aust. J. Chem.* **1976**, 29, 2369-79.
46. Van Der Voort, P.; White, M. G.; Vansant, E. F. *Langmuir* **1998**, 14, 106-112.
47. Satsuma, A.; Hattori, A.; Furuta, A.; Miyamoto, A.; Hattori, T.; Murakami, Y. *J. Phys. Chem.* **1988**, 92, 2275-2282.
48. Siqueira, M. R.; Tonetto, T. C.; Rizzatti, M. R.; Lang, E. S.; Ellena, J.; Burrow, R. A. *Inorg. Chem. Commun.* **2006**, 9, 537-540.

Supplemental Data

Syntheses, x-ray structural characterizations and thermal stabilities of two nonclassical trinuclear vanadium (IV) complexes; $(V_3(\mu_3-O)O_2)(\mu_2-O_2P(CH_2C_6H_5)_2)_6(H_2O)$ and $(V_3(\mu_3-O)O_2)(\mu_2-O_2P(CH_2C_6H_5)_2)_6(py)$

John S. Maass,^b Zhichao Chen,^b Matthias Zeller,^c Rudy L. Luck^{b,*}

^b*Department of Chemistry, Michigan Technological University, 1400 Townsend Drive, Houghton, MI 49931, USA*

^c*Department of Chemistry, Youngstown State University, 1 University Plaza, Youngstown, OH 44555, USA*

Supplementary material:

Table 2.S1. Raw Data for the Magnetic Susceptibilities for 1-5 and VO(acac)₂.

Figure 2.S1. FTIR spectrum (neat) of VO(acac)₂.

Figure 2.S2. FTIR spectrum (neat) of VO(acac)₂(py).

Figure 2.S3. FTIR spectrum (neat) of $(V_3(\mu_3-O)O_2)(\mu_2-O_2P(CH_2C_6H_5)_2)_6(H_2O)$ (**1**).

Figure 2.S4. FTIR spectrum (neat) of $(V_3(\mu_3-O)O_2)(\mu_2-O_2P(CH_2C_6H_5)_2)_6(py)$ (**2**).

Figure 2.S5. FTIR spectrum (neat) of $(VO(O_2PPh_2)_2)_\infty$ (**3**).

Figure 2.S6. FTIR spectrum (neat) of $((H_2O)VO(O_2P(o-(CH_2)_2C_6H_4)_2)_\infty$ (**4**).

Figure 2.S7. FTIR spectrum (neat) of $(VO(O_2P(o-(CH_2)_2(C_6H_4)))_\infty$ (**5**).

Figure 2.S8. FTIR spectrum (neat) of crystal B.

Figure 2.S9. X-ray powder diffraction patterns for complexes **3** – **5** at 295 °C.

Figure 2.S10. TGA curve of $(VO(O_2PPh_2)_2)_\infty$ (**3**) at a heating rate of 10 °C/min

Figure 2.S11. TGA curve of VO(acac)₂ at a heating rate of 5 °C min⁻¹.

Figure 2.S12. TGA curve of VO(acac)₂(py) at a heating rate of 5 °C min⁻¹.

Figure 2.S13. DSC thermogram of VO(acac)₂(py) at a heating rate of 5 °C min⁻¹.

Figure 2.S14. TGA curve of diphenylphosphinic acid at a heating rate of 10 °C min⁻¹.

Figure 2.S15. TGA curve of $(V_3(\mu_3-O)O_2)(\mu_2-O_2P(CH_2C_6H_5)_2)_6(H_2O)$, **1**, at a heating rate of 10 °C min⁻¹.

Figure 2.S15a. TGA curve of $(V_3(\mu_3-O)O_2)(\mu_2-O_2P(CH_2C_6H_5)_2)_6(H_2O)$, **1**, at a heating rate of 10 °C min⁻¹.

Figure 2.S16. TGA curve of $(V_3(\mu_3-O)O_2)(\mu_2-O_2P(CH_2C_6H_5)_2)_6(py)$, **2**, at a heating rate of $10\text{ }^{\circ}\text{C min}^{-1}$.

Figure 2.S16a. TGA curve of $(V_3(\mu_3-O)O_2)(\mu_2-O_2P(CH_2C_6H_5)_2)_6(py)$, **2**, at a heating rate of $10\text{ }^{\circ}\text{C min}^{-1}$.

Figure 2.S17. FTIR spectrum of the residue obtained after heating **1** at $600\text{ }^{\circ}\text{C}$.

Figure 2.S18. DSC thermogram of $(V_3(\mu_3-O)O_2)(\mu_2-O_2P(CH_2C_6H_5)_2)_6(H_2O)$, **1**, at a heating rate of $5\text{ }^{\circ}\text{C min}^{-1}$.

Figure 2.S19. DSC thermogram of $(V_3(\mu_3-O)O_2)(\mu_2-O_2P(CH_2C_6H_5)_2)_6(py)$, **2**, at a heating rate of $5\text{ }^{\circ}\text{C min}^{-1}$.

Table 2.S1. Raw Data for the Magnetic Susceptibilities for 1-5 and $VO(acac)_2$.

The magnetic susceptibility measurements for compounds **1-5** and $VO(acac)_2$ were conducted at $296\text{ }^{\circ}\text{K}$. The diamagnetic correction calculated for bis(benzyl)phosphinic acid was $-163.4 \times 10^{-6}\text{ emu mol}^{-1}$, diphenylphosphinic acid was $-139.6 \times 10^{-6}\text{ emu mol}^{-1}$, and 2-hydroxyisophosphindoline-2-oxide was $-108.3 \times 10^{-6}\text{ emu mol}^{-1}$.¹ The magnetic moment of $VO(acac)_2$ was also measured to ensure that the machine was operating properly and was found to be $1.71 \pm 0.012\text{ }^{\circ}\text{B}$.

X_m emu mol^{-1}	Compound 1	Compound 2	Compound 3	Compound 4	Compound 5	$VO(acac)_2$
Run 1	0.002701	0.002798	0.0009778	0.001052	0.001042	0.001073
Run 2	0.002757	0.002784	0.001031	0.001060	0.001115	0.001080
Run 3	0.002743	0.002826	0.0009858	0.001039	0.001049	0.001108

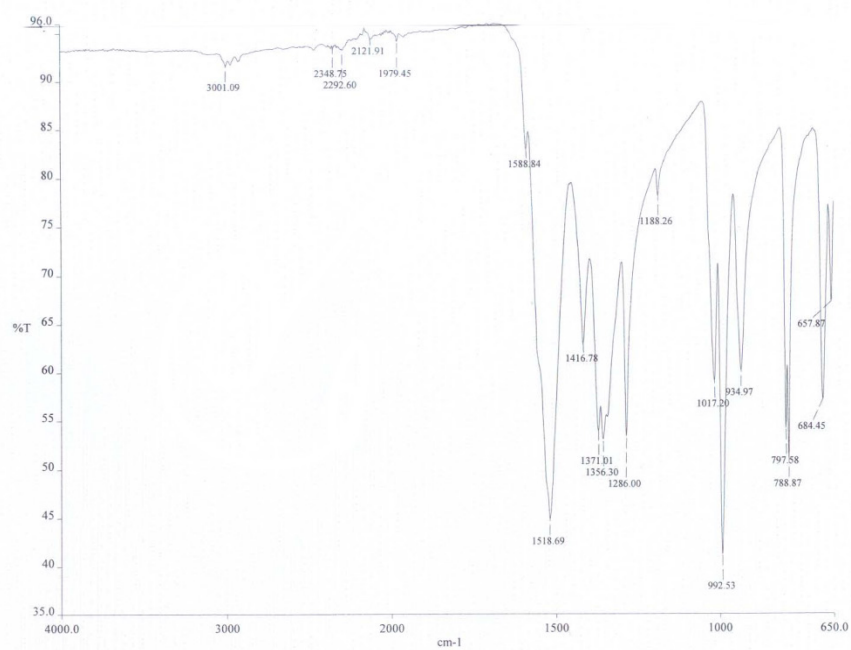


Figure 2.S1. FTIR spectrum (neat) of VO(acac)₂.

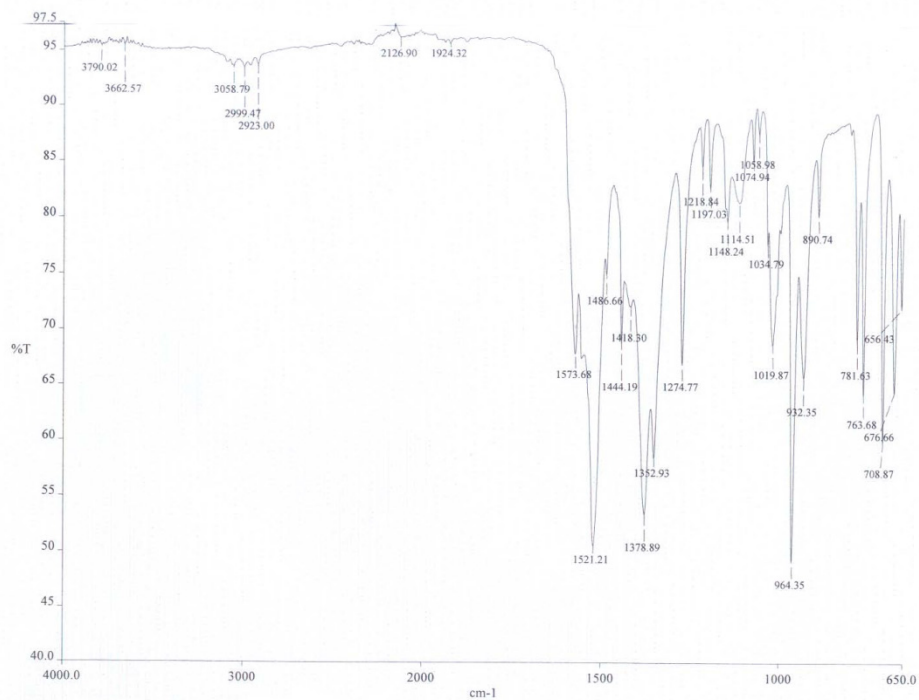


Figure 2.S2. FTIR spectrum (neat) of VO(acac)₂(py).

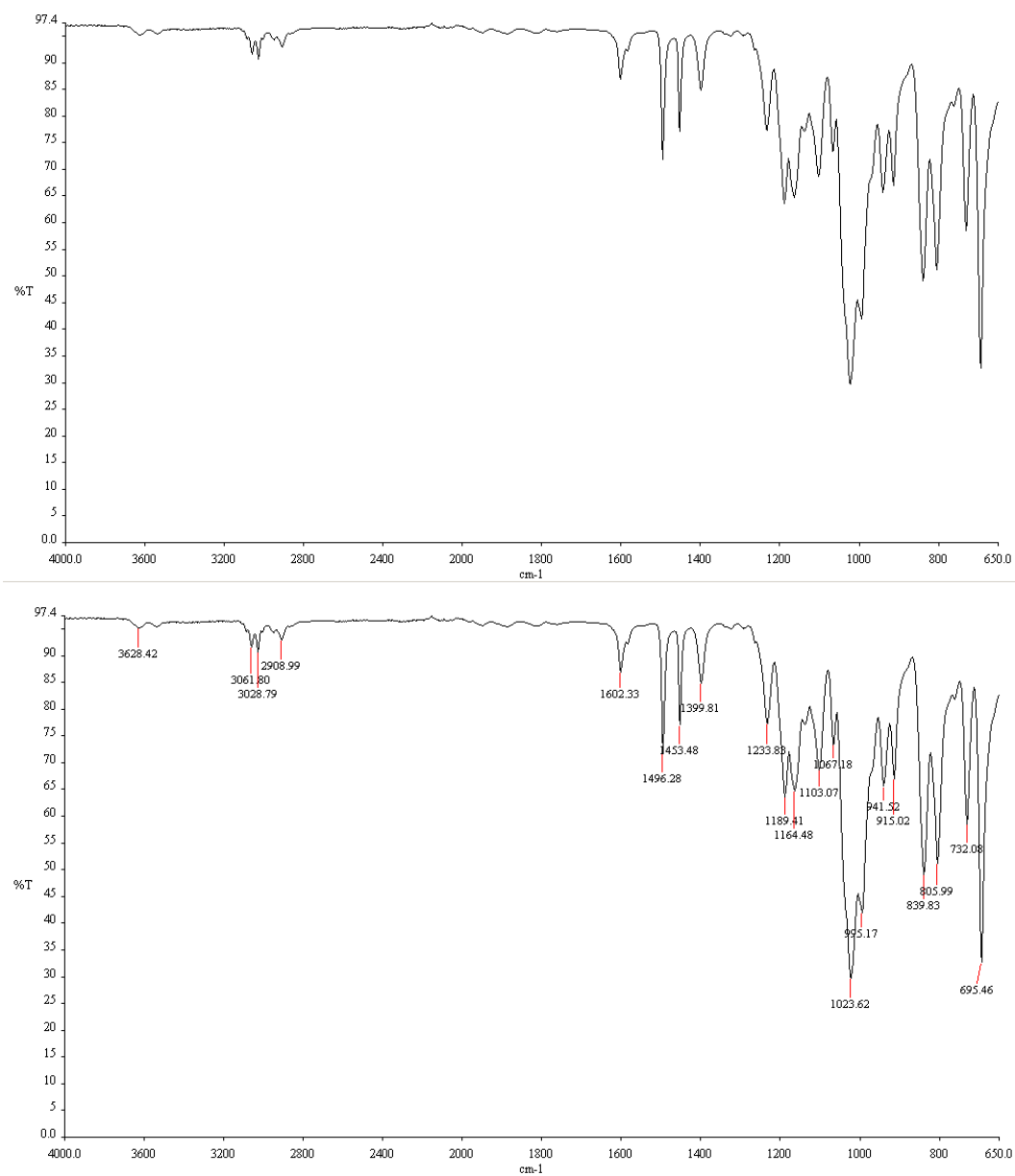


Figure 2.S3. FTIR spectrum (neat) of $(V_3(\mu_3-O)O_2)(\mu_2-O_2P(CH_2C_6H_5)_2)_6(H_2O)$ (1).

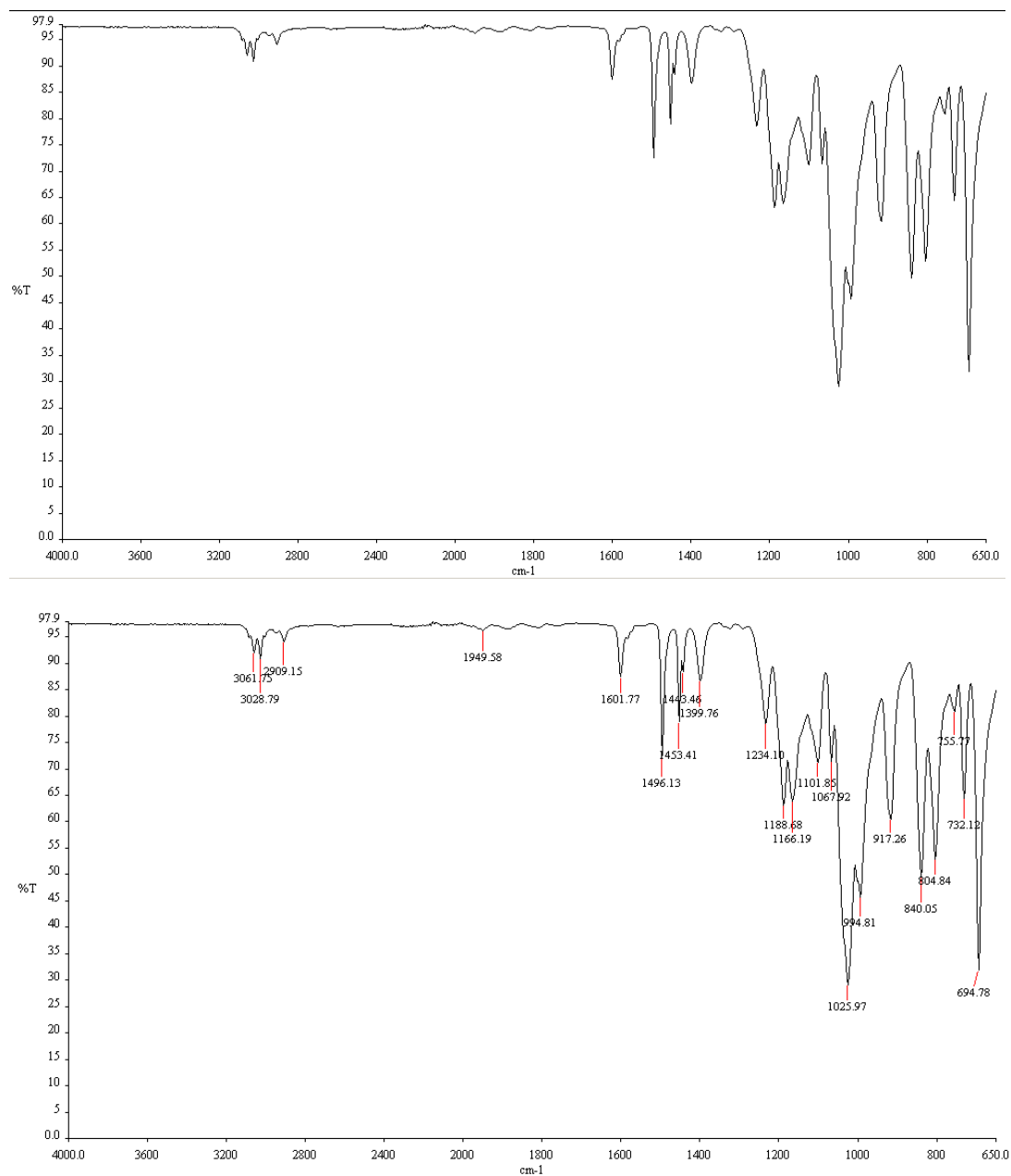


Figure 2.S4. FTIR spectrum (neat) of $(V_3(\mu_3-O)O_2)(\mu_2-O_2P(CH_2C_6H_5)_2)_6(py)$ (2).

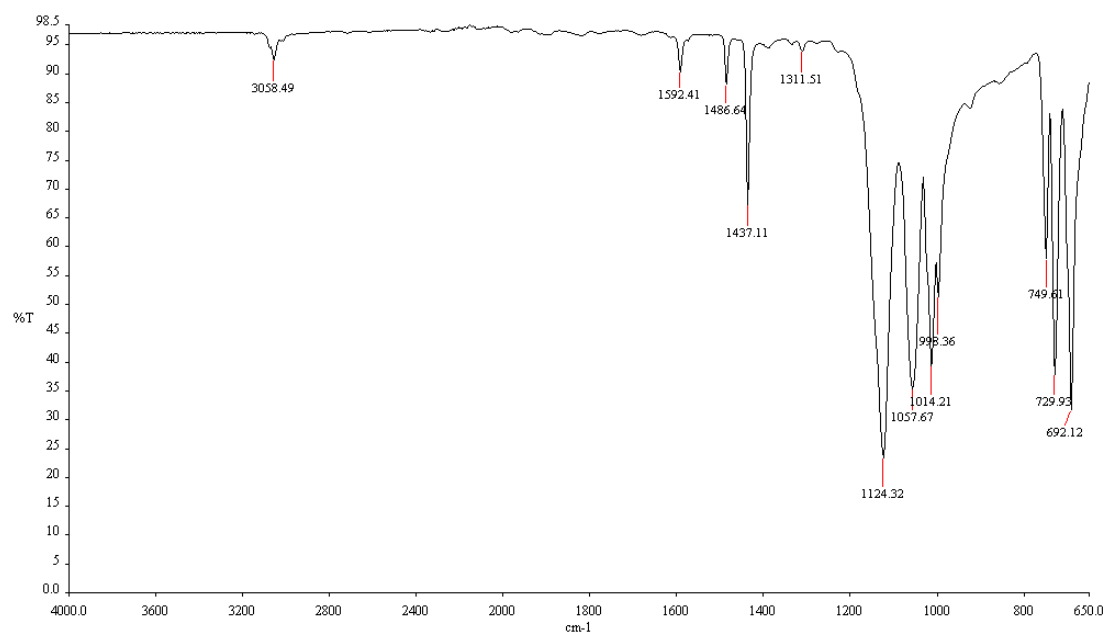
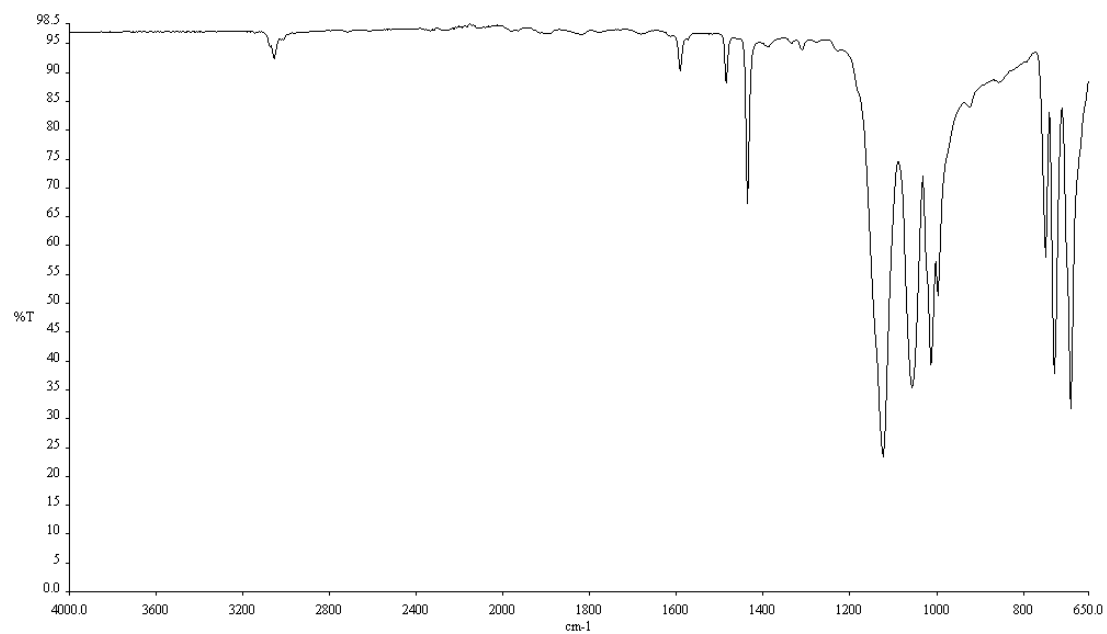


Figure 2.S5. FTIR spectrum (neat) of $(\text{VO}(\text{O}_2\text{PPh}_2)_2)_\infty$ (3).

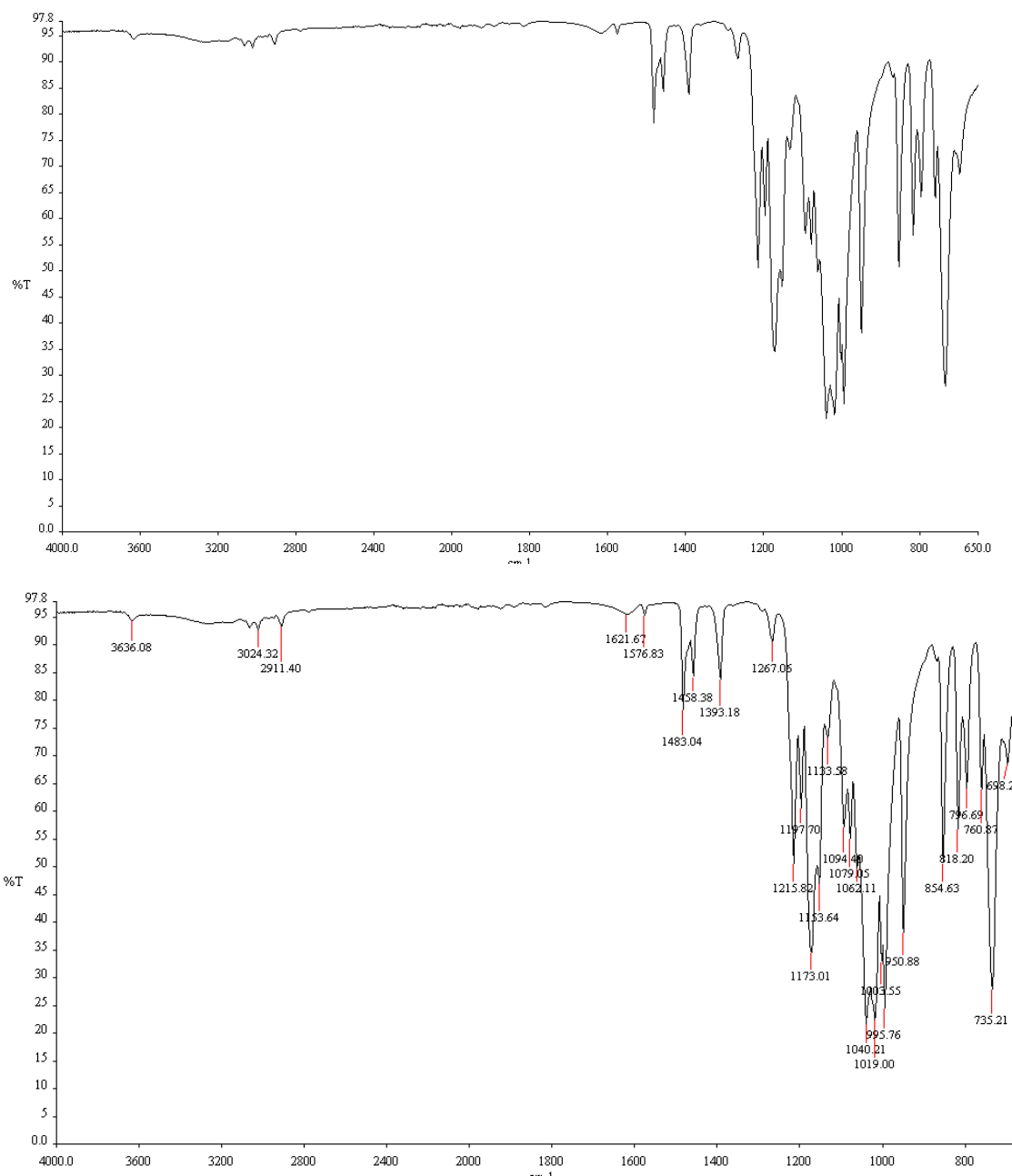


Figure 2.S6. FTIR spectrum (neat) of $((\text{H}_2\text{O})\text{VO}(\text{O}_2\text{Po}-(\text{CH}_2)_2\text{C}_6\text{H}_4)_2)_\infty$ (4).

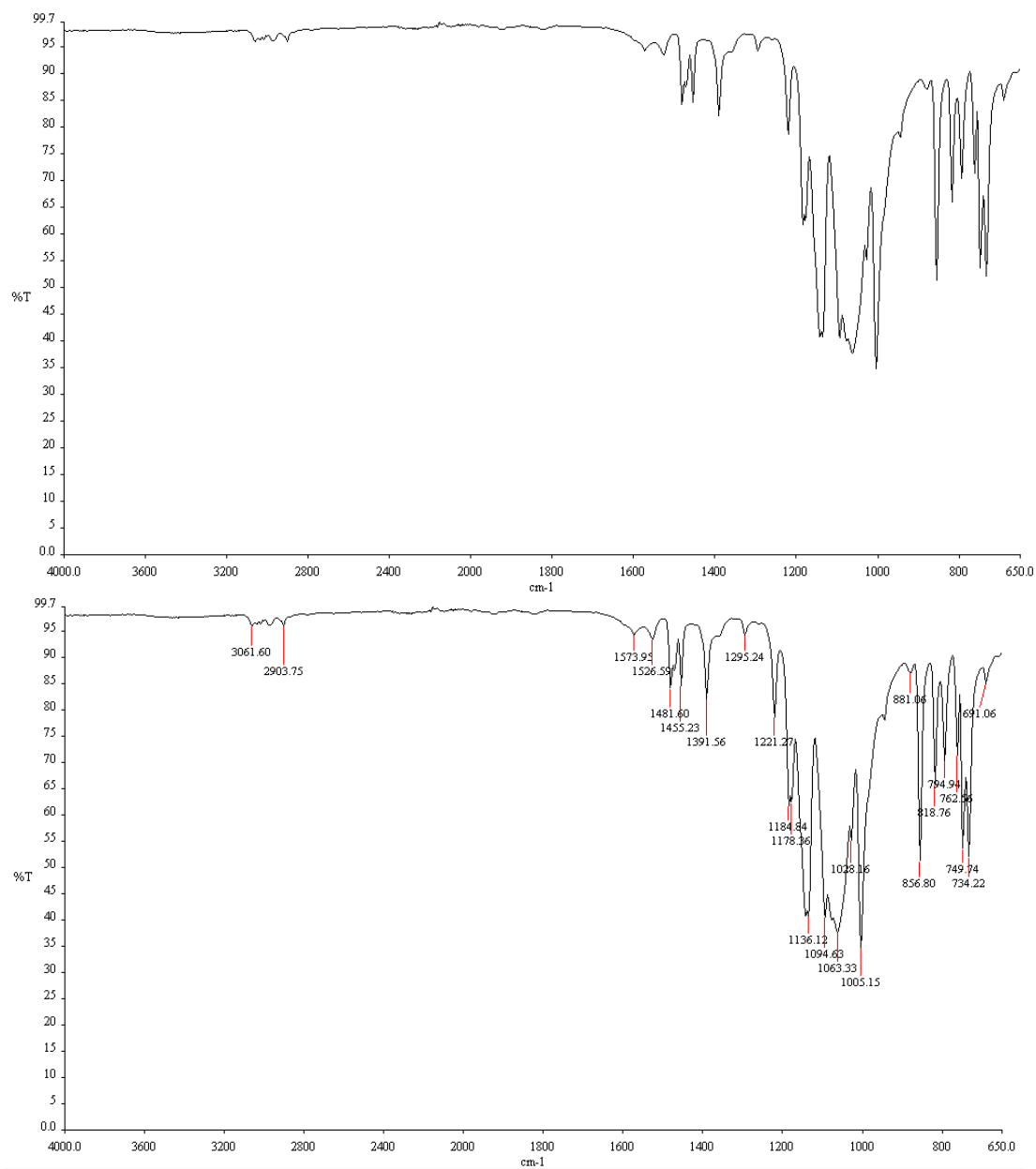


Figure 2.S7. FTIR spectrum (neat) of $(VO(O_2P(o-(CH_2)_2(C_6H_4)))_\infty$ (5).

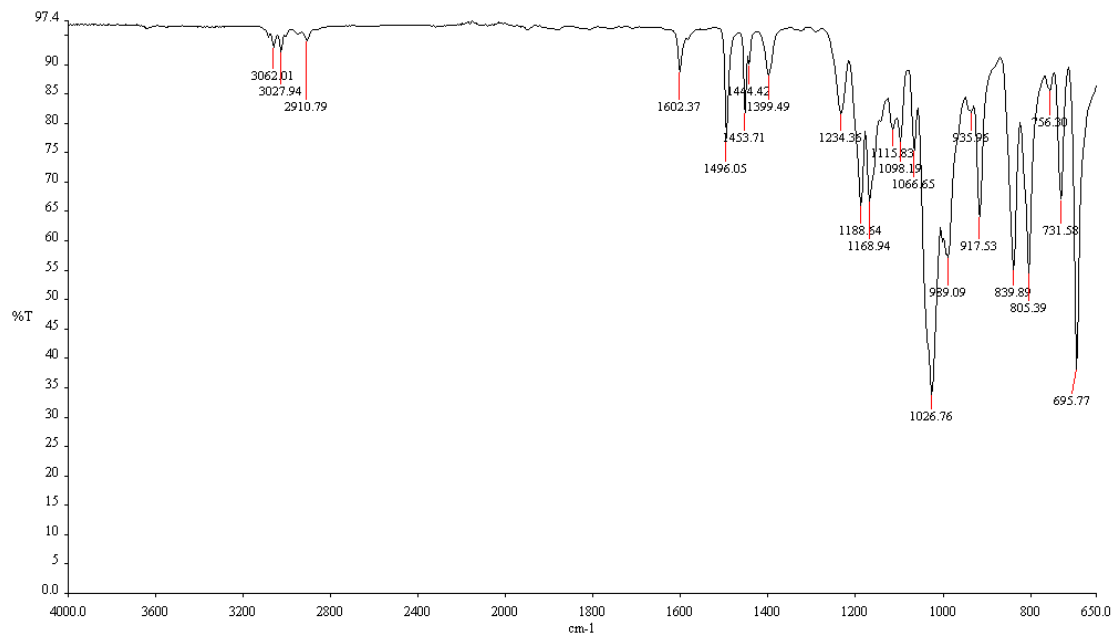


Figure 2.S8. FTIR spectrum (neat) of crystal **B**.

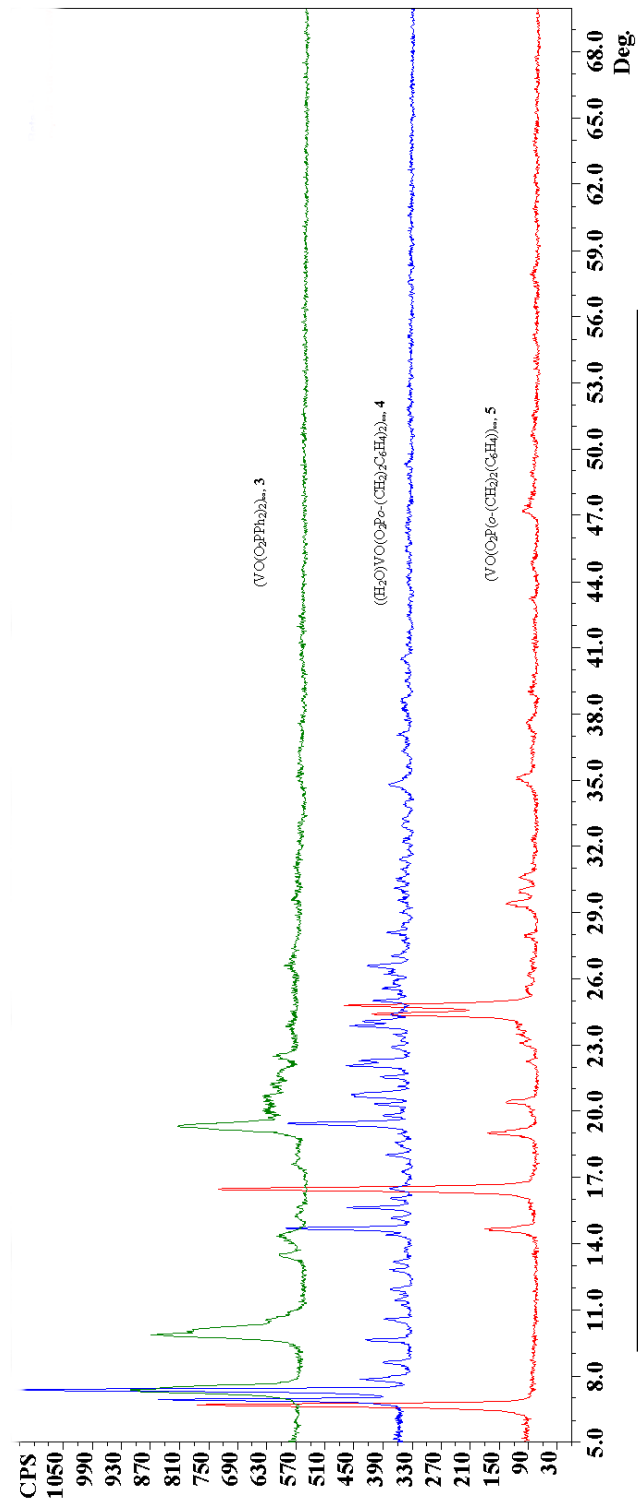


Figure 2.S9. X-ray powder diffraction patterns for complexes **3** – **5** at 295 °C.

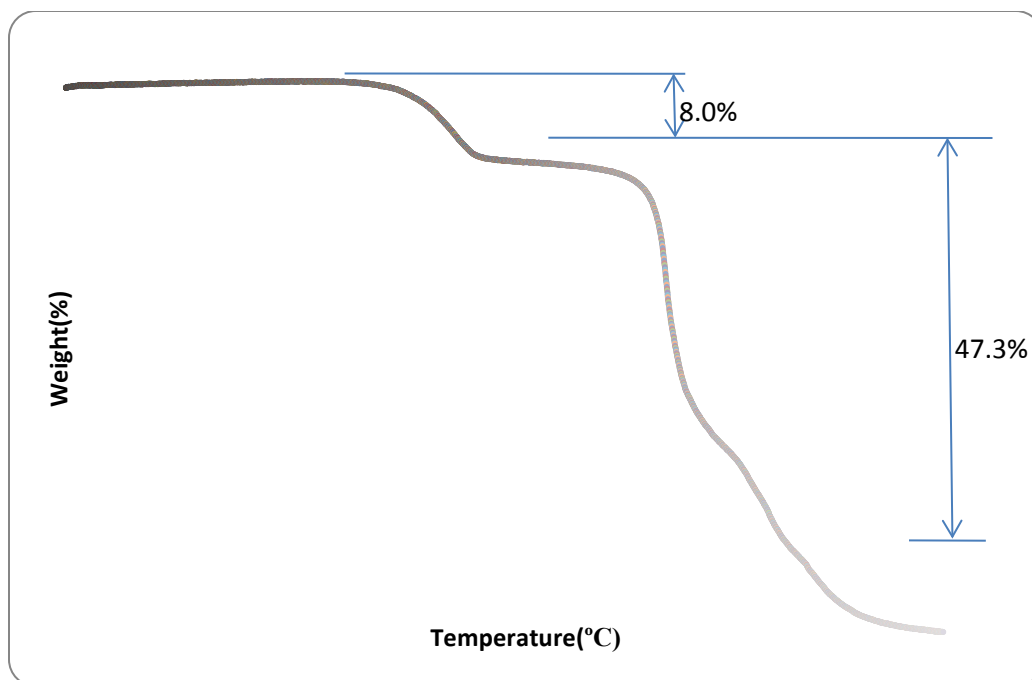


Figure 2.S10. TGA curve of $(VO(O_2PPh_2)_2)_\infty$ (**3**) at a heating rate of 10°C/min.

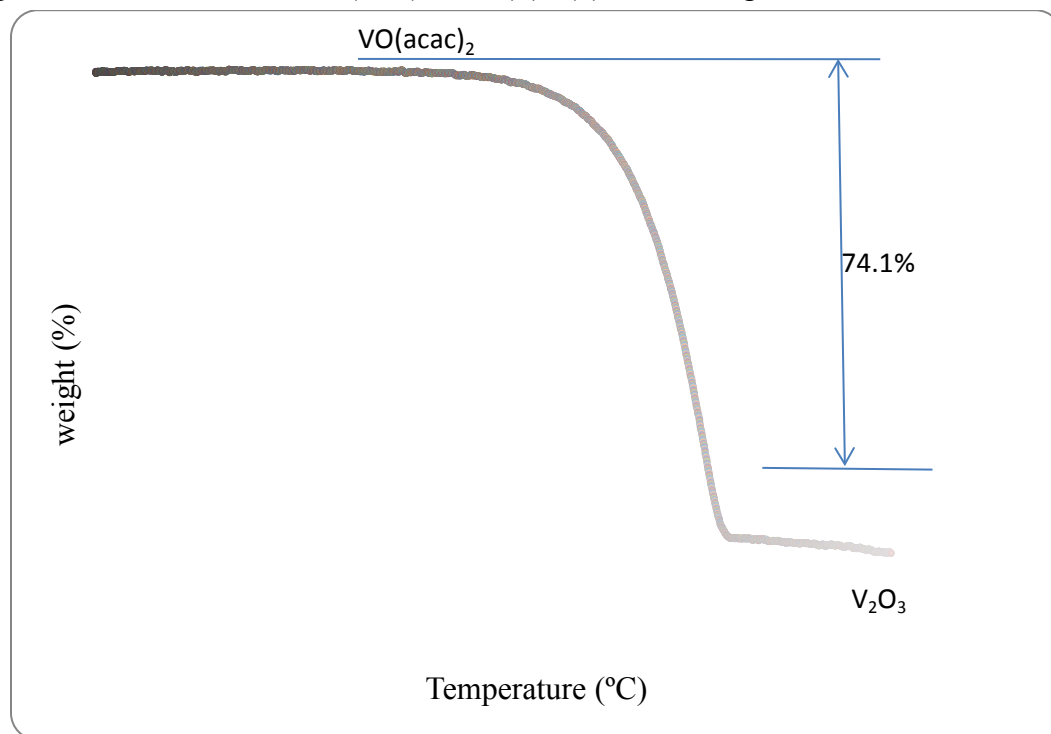


Figure 2.S11. TGA curve of $VO(acac)_2$ at a heating rate of 5 °C min⁻¹.

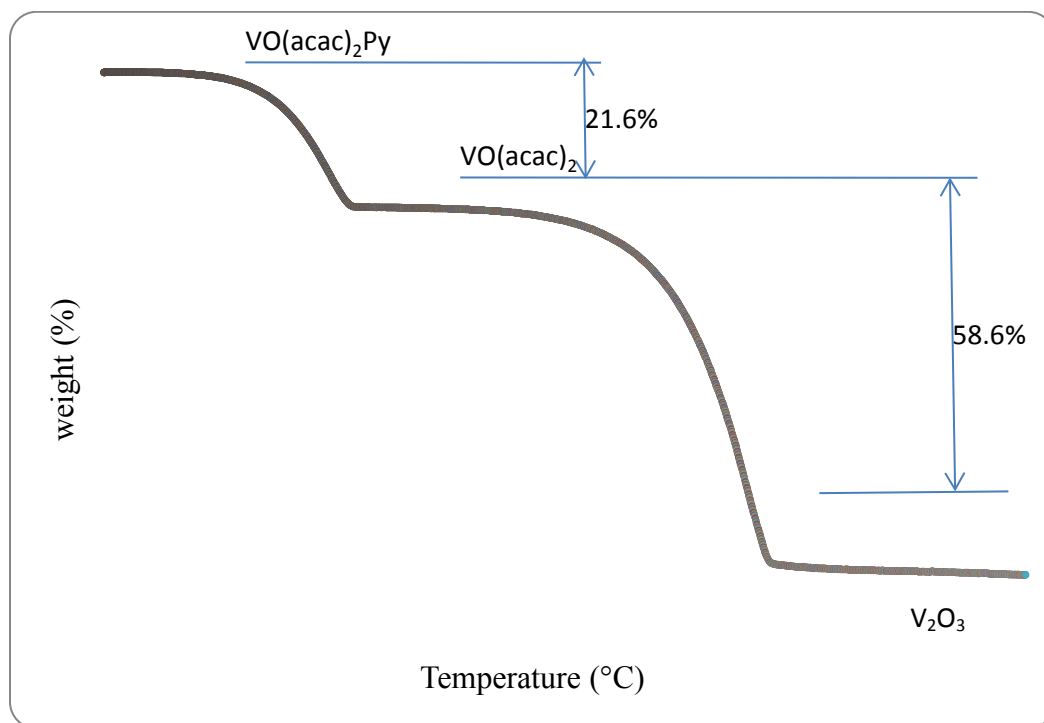


Figure 2.S12. TGA curve of $\text{VO}(\text{acac})_2(\text{py})$ at a heating rate of $5\text{ }^{\circ}\text{C min}^{-1}$.

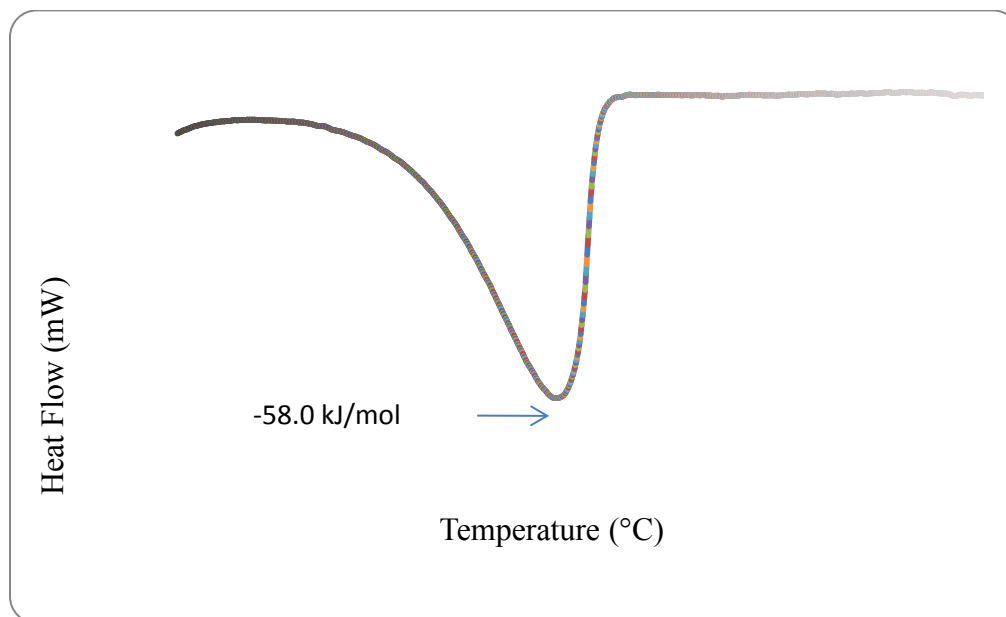


Figure 2.S13. DSC thermogram of $\text{VO}(\text{acac})_2(\text{py})$ at a heating rate of $5\text{ }^{\circ}\text{C min}^{-1}$.

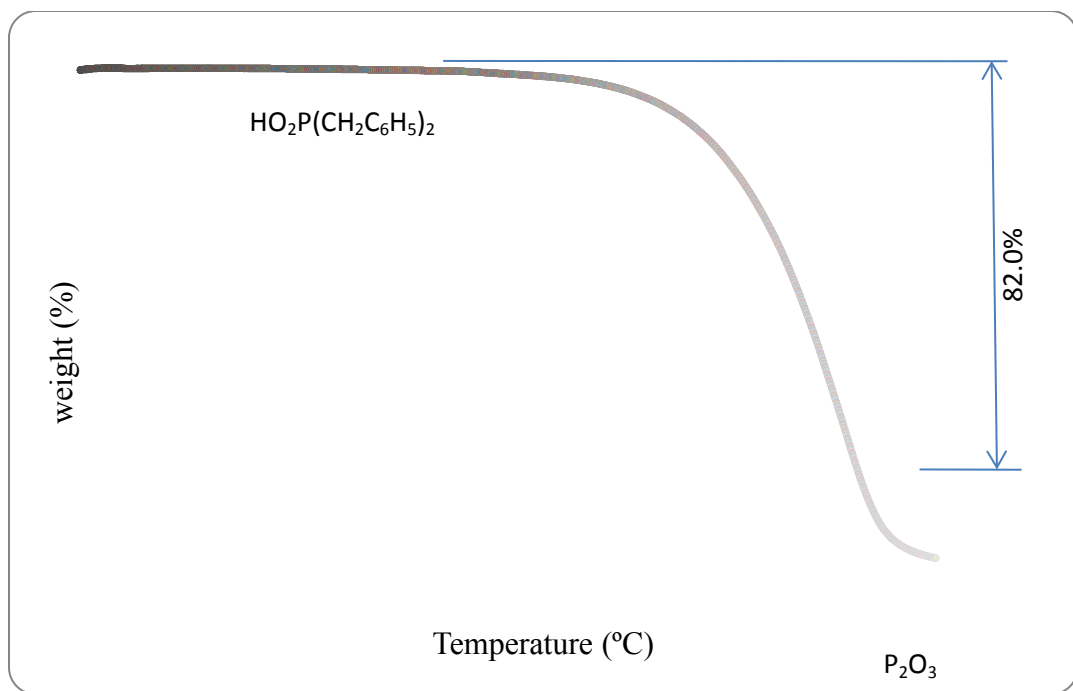


Figure 2.S14. TGA curve of diphenylphosphinic acid at a heating rate of $10\text{ }^{\circ}\text{C min}^{-1}$.

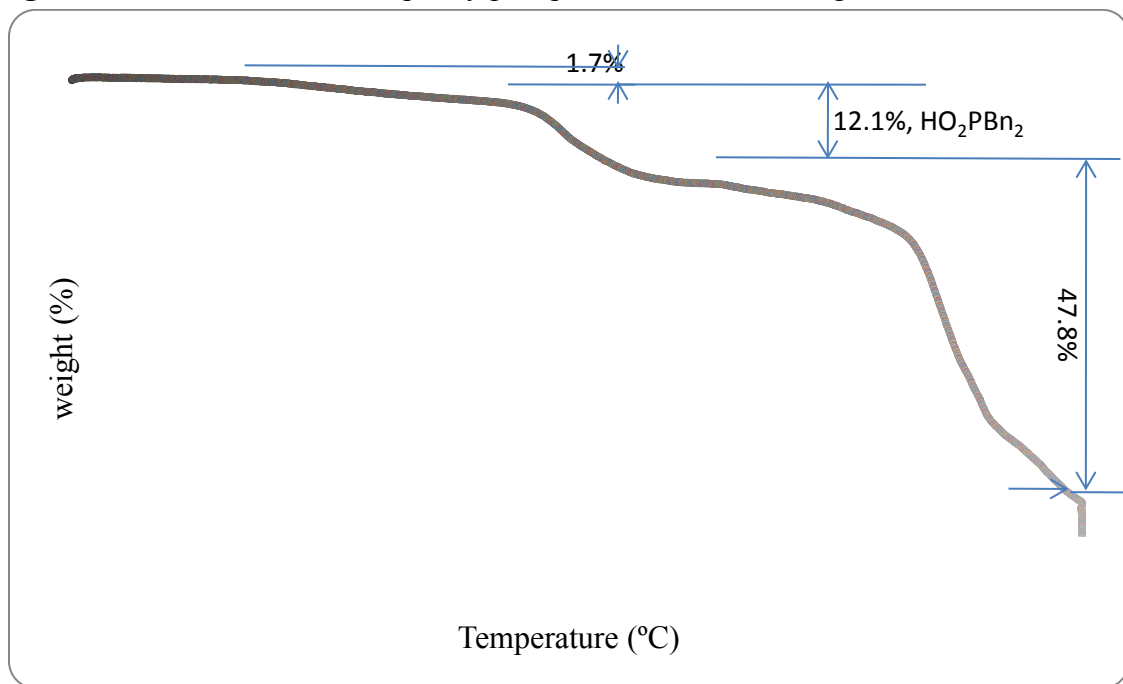


Figure 2.S15. TGA curve of $(\text{V}_3(\mu_3\text{-O})\text{O}_2)(\mu_2\text{-O}_2\text{P}(\text{CH}_2\text{C}_6\text{H}_5)_2)_6(\text{H}_2\text{O})$, 1, at a heating rate of $10\text{ }^{\circ}\text{C min}^{-1}$.

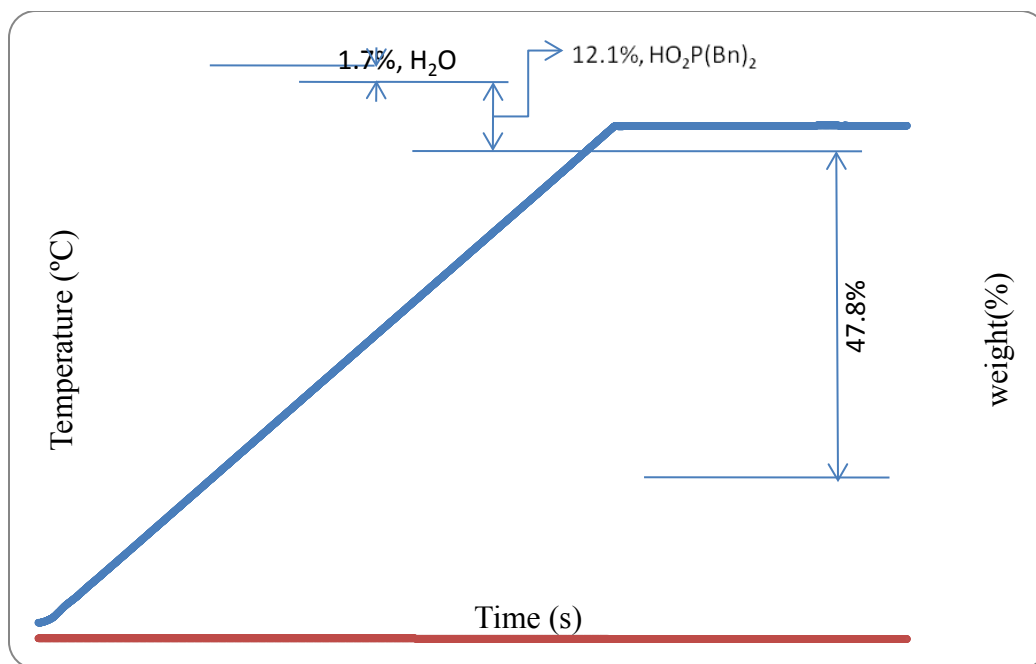
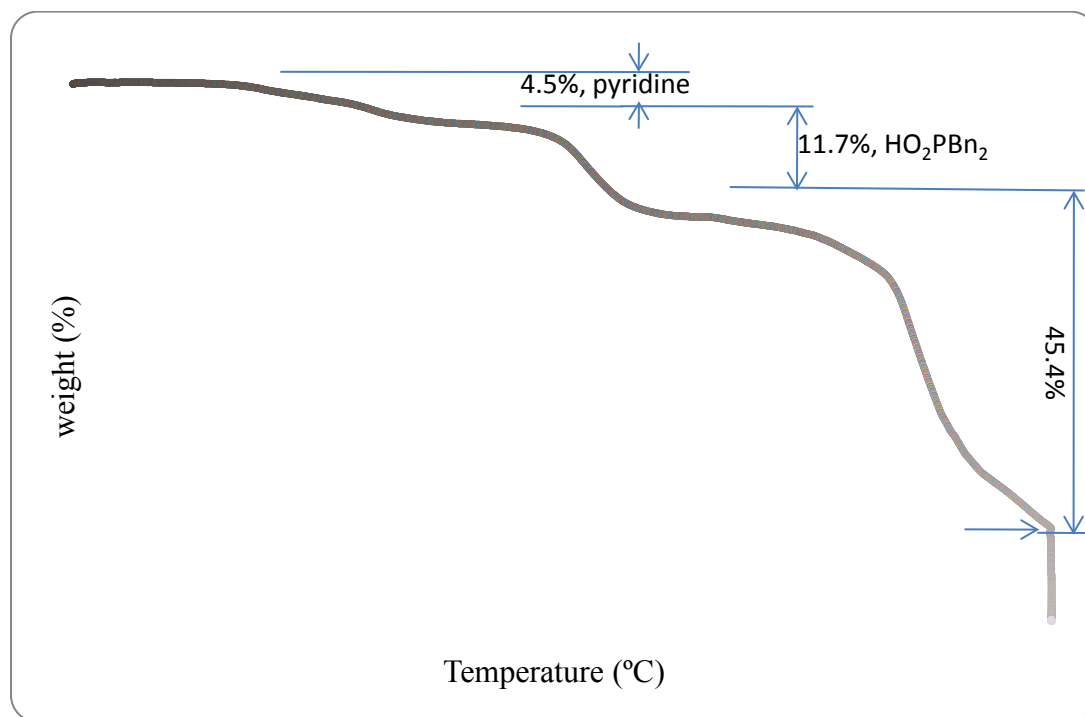


Figure 2.S15a. TGA curve of $(V_3(\mu_3-O)O_2)(\mu_2-O_2P(CH_2C_6H_5)_2)_6(H_2O)$, **1**, at a heating rate of $10\text{ }^\circ\text{C min}^{-1}$.



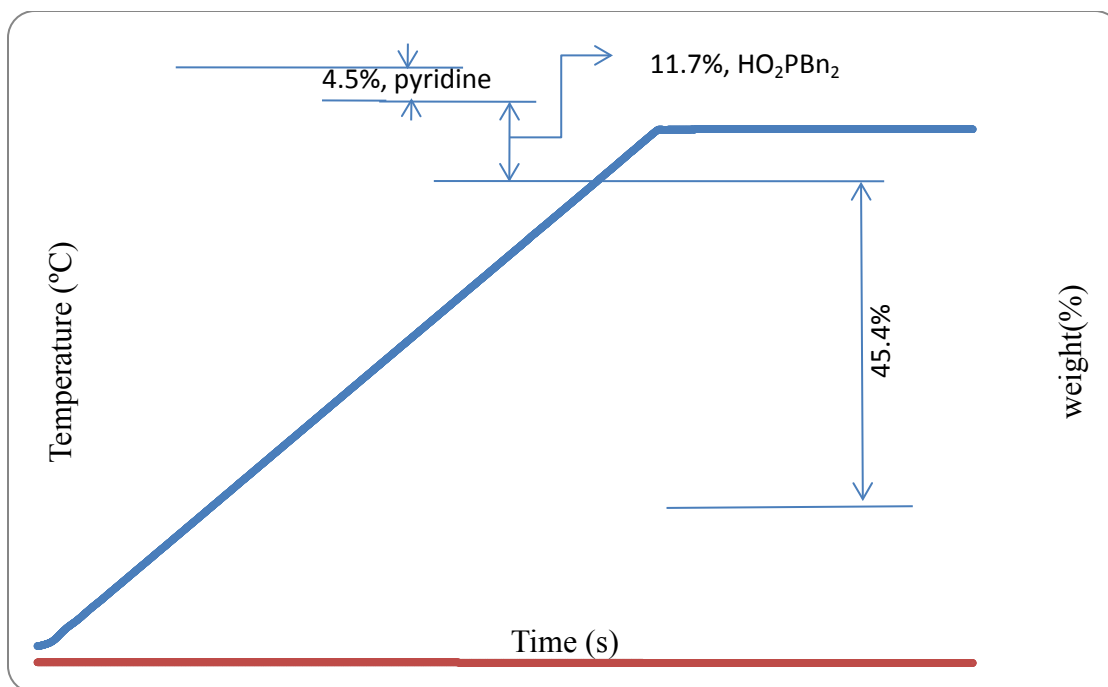


Figure 2.S16a. TGA curve of $(V_3(\mu_3-O)O_2)(\mu_2-O_2P(CH_2C_6H_5)_2)_6(py)$, **2**, at a heating rate of $10\text{ }^{\circ}\text{C min}^{-1}$.

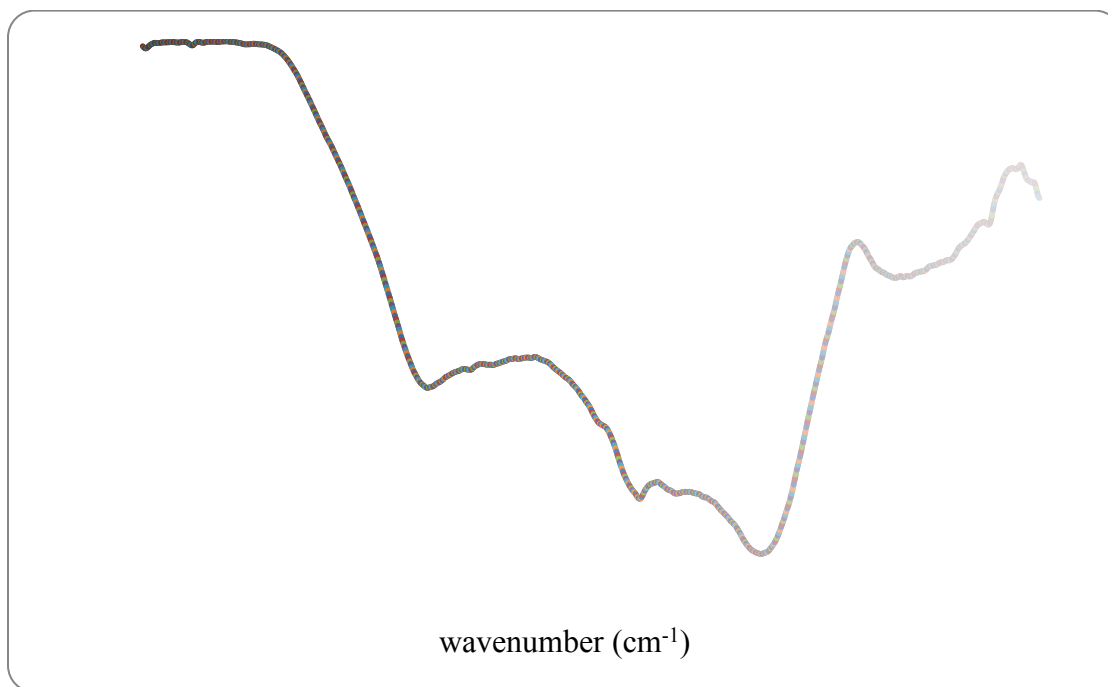


Figure 2.S17. FTIR spectrum of the residue obtained after heating **1** at $600\text{ }^{\circ}\text{C}$.

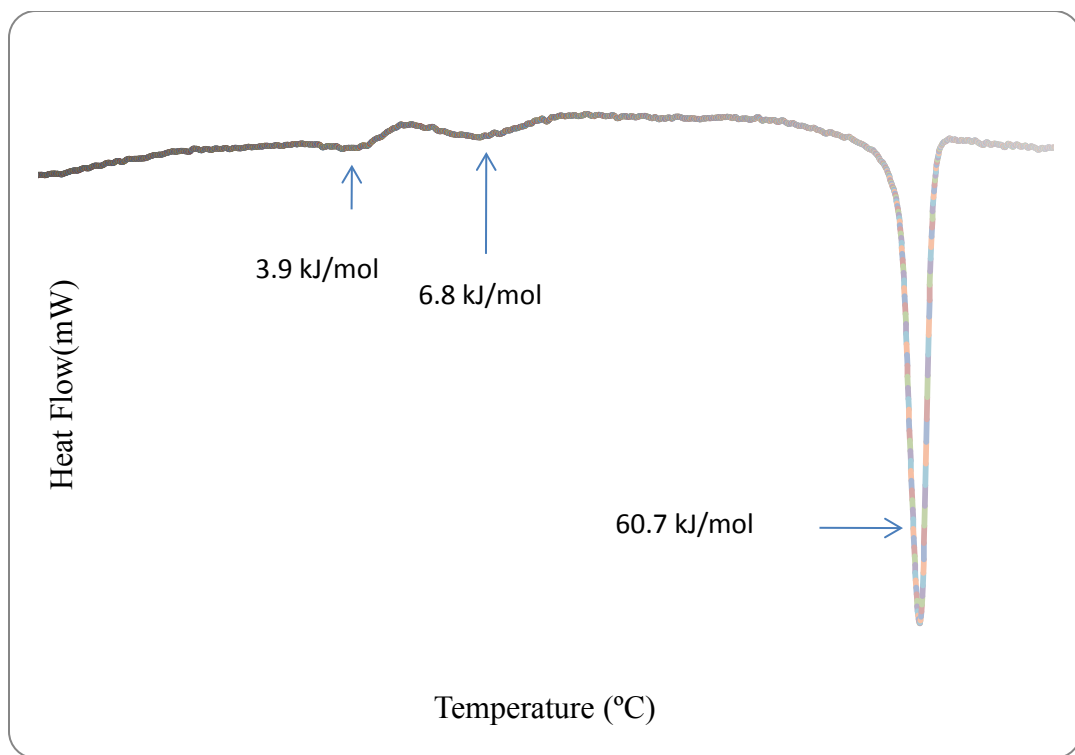


Figure 2.S18. DSC thermogram of $(V_3(\mu_3-O)O_2)(\mu_2-O_2P(CH_2C_6H_5)_2)_6(H_2O)$, **1**, at a heating rate of $5\text{ }^\circ\text{C min}^{-1}$.

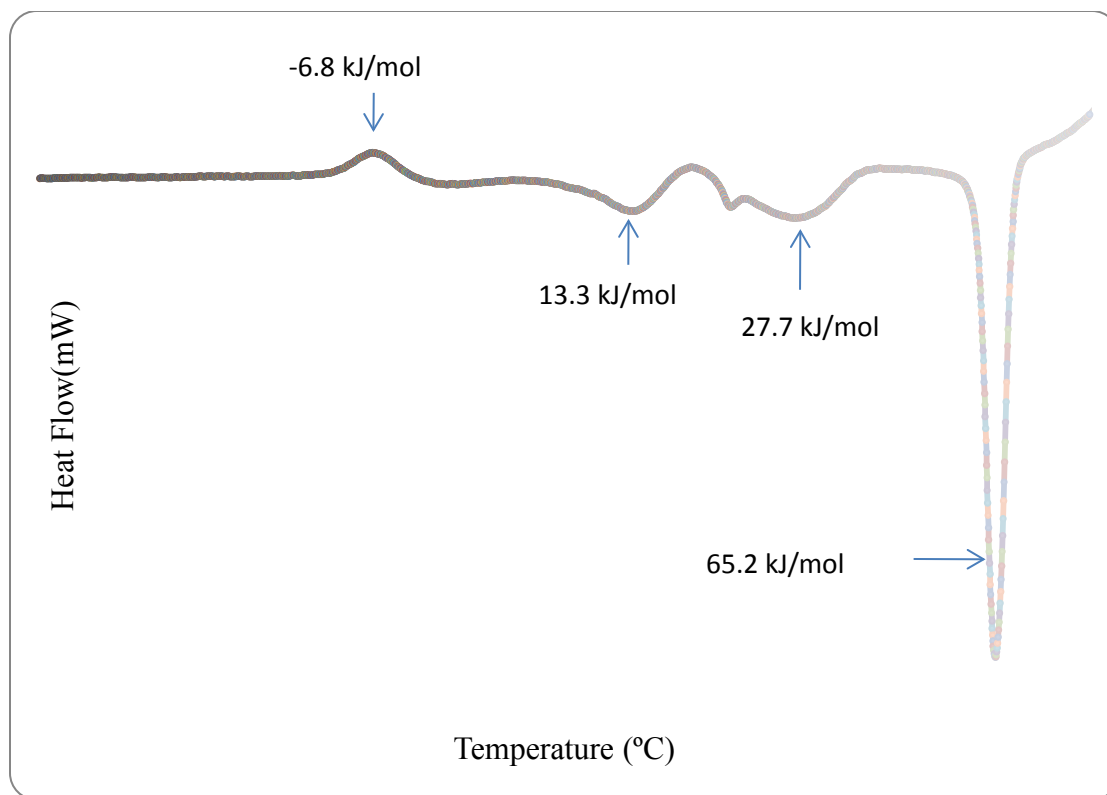


Figure 2.S19. DSC thermogram of $(V_3(\mu_3-O)O_2)(\mu_2-O_2P(CH_2C_6H_5)_2)_6(py)$, **2**, at a heating rate of $5\text{ }^\circ\text{C min}^{-1}$.

References:

1. Bain, G. A.; Berry, J. F. *J. Chem. Educ.* **2008**, *85*, 532.

Chapter 3 Tungsten and Vanadium Cubanes

3.1 Expanding molecular transition metal cubane clusters of the form $[M_4(\mu_3-O)_4]^{12+}$: Syntheses, spectroscopic and structural characterizations of molecules $M_4(\mu_3-O)_4(O_2P(Bn)_2)_4(O_4)$, $M = V^V$ and $W^{V\ddagger 1,2}$

*John S. Maass,^a Zhichao Chen,^a Matthias Zeller,^b Rudy L. Luck^{*a}*

^aDepartment of Chemistry, Michigan Technological University, 1400 Townsend Drive,
Houghton, MI 49931, USA. E-mail: rluck@mtu.edu

^bDepartment of Chemistry, Youngstown State University, 1 University Plaza,
Youngstown, Ohio 44555, USA. E-mail: mzeller@ysu.edu

¹ “The material contained in chapter 3 was previously published in [Dalton Transactions](#).
Reproduced by permission of The Royal Society of Chemistry”

² License agreement for reproduction is provided in the Appendix.

3.2 Abstract

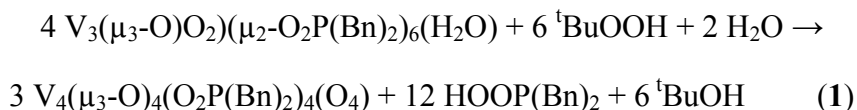
Oxidizing the trimer $V_3(\mu_3-O)(O_2)(\mu_2-O_2P(Bn)_2)_6(H_2O)$ in the presence of excess $tBuOOH$ results in $V_4(\mu_3-O)_4(\mu_2-O_2P(Bn)_2)_4(O_4)$ and heating $W(CO)_6$ and bis(benzyl)phosphinic acid in 1:1 EtOH/THF at 120 °C produces $W_4(\mu_3-O)_4(\mu_2-O_2P(Bn)_2)_4(O_4)$.

3.3 Results and Discussion

In contrast to the large number of sulfur-containing clusters known for a wide range of transition metals of the form $[M_4(\mu_3-S)_4]^{n+}$,¹ which also extends to heterometallic formulations,² there has not been an equivalent number of reports of molecular oxygen-containing clusters of the type $[M_4(\mu_3-O)_4]^{n+}$. Notable exceptions are tin³ (i.e., $[Sn_4O_4]^{8+}$), titanium⁴ $[Ti_4O_4]^{8+}$ and manganese $[Mn_4O_4]^{6+}$ clusters⁵ due to their relevance to the oxygen-evolving complex in photosystem II.⁶ There are several reports of vanadium(IV)-sulfite polyoxometalates,⁷ and, extended arrays of vanadium(V) in $[V_4O_{16}]^{8-}$ in the mineral phosphovanadylite⁸ and in two other related layered phosphovanadate structures.⁹ For tungsten, reports of planar aggregates, e.g., $[WO_2Cl_2(THF)]_4$,¹⁰ and of cubane-like clusters with tetrameric tungstate(VI) units have been detailed. The $[W_4O_{16}]^{8-}$ cores were stabilized by metal-containing units such as $[(1,5-COD)Ir]^+$,¹¹ $[Cp^*Rh]^{2+}$,¹² $[Ru(\eta^6-C_6Me_6)]^{2+}$,¹³ and $[Cr(cyclam)]^{3+}$.¹⁴ So far, dimeric

complexes featuring a $[\text{W}_2\text{O}_4]^{2+}$ core have been produced only with tungsten(V)¹⁵ exhibiting $\text{W}^{\text{V}}\text{-W}^{\text{V}}$ single bond distances in the range 2.537(1)^{15b} – 2.568(1)Å.^{15e} Our report¹⁶ of a readily available route to the previously reported $\text{Mo}_4(\mu_3\text{-O})_4(\mu_2\text{-O}_2\text{P}(\text{C}_6\text{H}_5)_2)_4(\text{O}_4)$ ¹⁷ followed by the syntheses of this molybdenum tetrameric core stabilized by other phosphinate ligands, including dibenzylphosphinate,¹⁸ raised the obvious question as to whether phosphinate ligands (also utilized in many of the complexes referred to above) would be capable of extending the number of transition metals that can exhibit this type of bonding in molecular form. This paper details our success at producing vanadium and the first reported tungsten(V) tetrameric cubane clusters of the form $\text{M}_4(\mu_3\text{-O})_4(\text{O}_2\text{P}(\text{Bn})_2)_4(\text{O}_4)$.

The synthesis of these compounds turned out to be much more difficult than one would have predicted given the various ways in which the analogous molybdenum tetramers were produced.¹⁶ Essentially, the only reliable way we have discovered to produce the vanadium tetramer, $\text{V}_4(\mu_3\text{-O})_4(\text{O}_2\text{P}(\text{Bn})_2)_4(\text{O}_4)$, **1**, consists of the oxidation of the trimer $\text{V}_3(\mu_3\text{-O})(\text{O}_2)(\mu_2\text{-O}_2\text{P}(\text{Bn})_2)_6(\text{H}_2\text{O})$ ¹⁹ in the presence of excess ^tBuOOH followed by self assembly of the desired compound, possibly as outlined in Scheme 1.[‡]



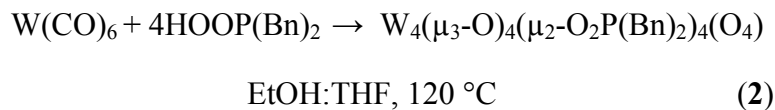
The production of $\text{HOOP}(\text{Bn})_2$ was verified by IR spectroscopy and the reaction requires water to be successful. The synthesis of complex **1** via this procedure is based on elemental analysis, IR, ¹H and ³¹P NMR spectra (see supp. Mat.) and the fact that the

spectra are similar to those for tungsten (see below) and the molybdenum¹⁶ analogs.

Routes involving the reaction of starting vanadium complexes such as V₂O₅ or [Bu₄N]₃[H₃V₁₀O₂₈] and HOOP(Bn)₂ in CH₃CN with or without [Bu₄N][OH] either resulted in intractable products or the trimer V₃(μ₃-O)(O₂)(μ₂-O₂P(Bn)₂)₆(H₂O).

Reactions with VO(acac)₂ in EtOH under solvothermal conditions or in THF at room temperature in the presence of HOOP(Bn)₂ and either ^tBuOOH or H₂O₂ were not successful as the EtOH reduces V(V) to V(IV); these reactions also resulted in the aforementioned trimer. However, oxidizing a solution of VO(acac)₂ in EtOH with ^tBuOOH and then adding HOOP(Bn)₂ in CH₂Cl₂ (followed by stirring for 5 hrs at room temperature) leads to mixtures (38.5% yield) of the desired tetramer, the aforementioned trimer and/or some other complex. The desired orange tetramer may be obtained pure by selective crystallization consisting of the diffusion of hexane into CH₂Cl₂ solutions of the crude mixture.

The tungsten tetramer, W₄(μ₃-O)₄(μ₂-O₂P(Bn)₂)₄(O₄), **2**, was obtained using W(CO)₆ but was not obtained using a high oxidation state compound, e.g., Na₂WO₄.[§] As shown in Scheme 2, this reaction was conducted under solvothermal conditions



in a solvent mixture consisting of equal amounts EtOH and THF. W(CO)₆ is known to oxidize in solution under O₂.²⁰ In pure EtOH, **2** was obtained on occasion but this is not as reproducible compared to using the mixture of solvents. Complexes **1** and **2** have very

characteristic IR patterns in the range $1012 - 978\text{ cm}^{-1}$. This takes the form of two sharp outer peaks with a shoulder peak in the middle (1012 , 1000 and 990 cm^{-1} for **1**; 1012 , 1000 and 979 cm^{-1} for **2**) and this pattern was also observed for the molybdenum analogue

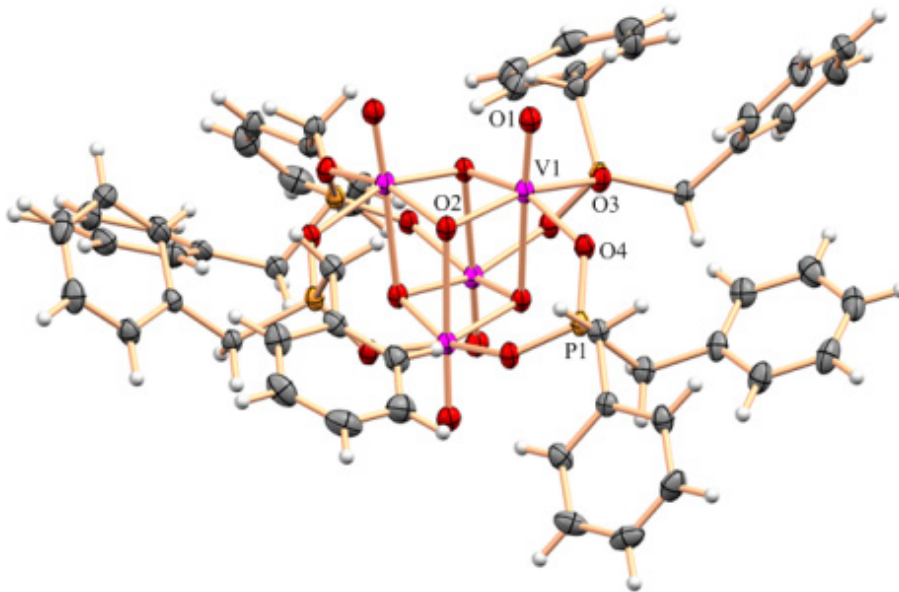


Fig. 3.1 Mercury²¹ drawing of **1** with 50% probability ellipsoids.

(1011 , 998 and 980 cm^{-1}).^{18a} The complexes yielded distinctive peaks in their ^1H NMR spectra consisting of AB patterns for the diastereotopic CH_2 protons of the benzylic ligand at δ 2.86 and 2.90 for **1** and δ 2.93 and 3.06 for **2**. The $^{31}\text{P}\{^1\text{H}\}$ NMR spectra consist of single resonances at δ 60.6 and 68.4 for **1** and **2** respectively.

We initially observed crystals of **1** growing in a tube consisting of a mixture of the trimers $\text{V}_3(\mu_3\text{-O})(\text{O}_2)(\mu_2\text{-O}_2\text{P}(\text{Bn})_2)_6(\text{H}_2\text{O})$ and $\text{V}_3(\mu_3\text{-O})(\text{O}_2)(\mu_2\text{-O}_2\text{P}(\text{Bn})_2)_6(\text{py})$ ¹⁹ in wet CH_2Cl_2 and hexane.[†] The observation of orange crystals prompted a single crystal

X-ray study which revealed that **1** was produced and crystallized as a tetrahydrate with one crystallographically independent water molecule of solvation per asymmetric unit disordered over three positions; this was refined with the sum of the occupancies constrained to one. Crystals of **2**·3(THF) were obtained by layering a solution of **2** in THF with hexane. For both **1** and **2**, single crystal X-ray diffraction studies^{**} reveal cubane core structures consisting of four diagonally arranged metal atoms and four triply bridging oxygen atoms at the vertices with terminal oxygen atoms on each metal atom (arranged so that the four metal to oxygen atom bonds are all parallel) and dibenzylphosphinate ligands bridging the four faces of the cube; see Figs. 1 and 2. We have previously described these structures as consisting of “two $[\text{M}_2\text{O}_4]^{2+}$ halves held together by the bridging phosphinate ligands.”^{18a} With these electron deficient materials, we have distortions from perfect cubane core geometries resulting in elongations along the axes formed by the bridging phosphinate groups in contrast to the almost perfect geometries exhibited by more electron rich clusters.²²

Table 1 lists selected distances and bond angles for **1** and **2** and for the complex $\text{Mo}_4(\mu_3\text{-O})_4(\mu_2\text{-O}_2\text{P}(\text{Bn})_2)_4(\text{O}_4)$, **3**.^{18a} Complex **3** did crystallize in the form of two different solvates, namely **3**·2.75C₇H₈ and **3**·2CH₂Cl₂ and the latter solvate crystallized in a monoclinic *I4*₁/*a* setting equivalent to that of **1**·4(H₂O) and **2**·3(THF) and thus the data listed in Table 1 are for isomorphous compounds, as an examination of the arrangement in the benzyl groups depicted in Figs 1 and 2 (and that **3**·2CH₂Cl₂^{18a}) would attest. The data in Table 1 show that while the metal to metal distance ($\text{M}_1\cdots\text{M}_2$) is short for **1**, that for **2** at 2.6354(5) Å represents a long W-W bond in contrast to those in dimeric W(V)

species (e.g., anti-[L₂W₂O₄]²⁺) where shorter distances of 2.565(1) Å were noted.^{15e} This distance is much shorter than that for the tungsten(VI) cubane clusters¹¹⁻¹⁴ mentioned above, where distances averaging 3.29(4) Å (indicative of no interaction between the metal atoms) were observed. Evidence of this interaction is also present in the UV-vis absorption. In this regard complex **3** displays two absorptions in CH₂Cl₂ at 314 and 450 nm where the second transition can be assigned to a Mo-Mo

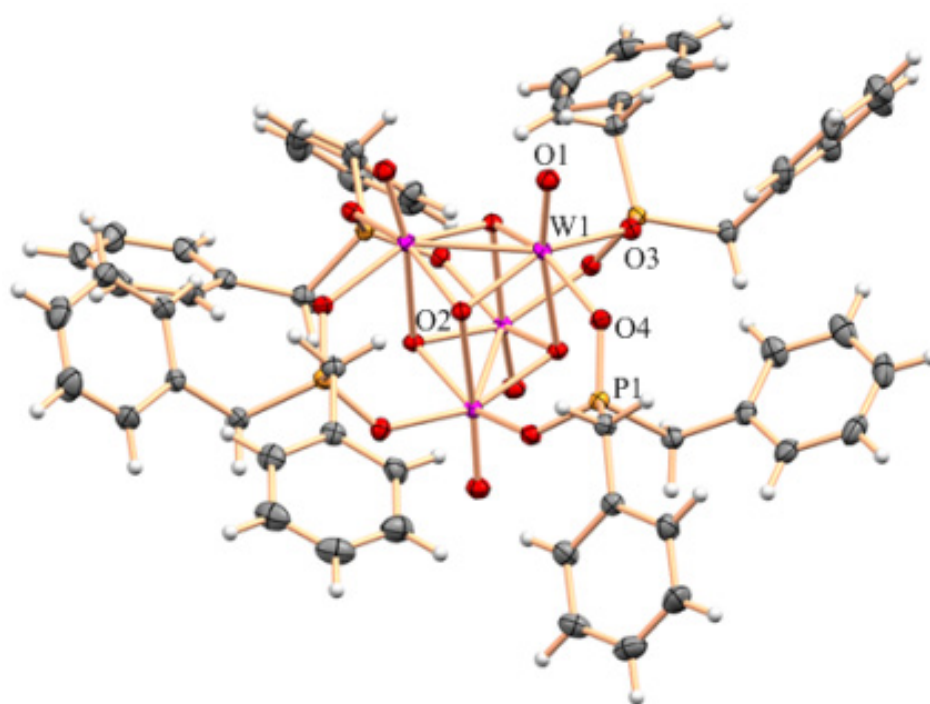
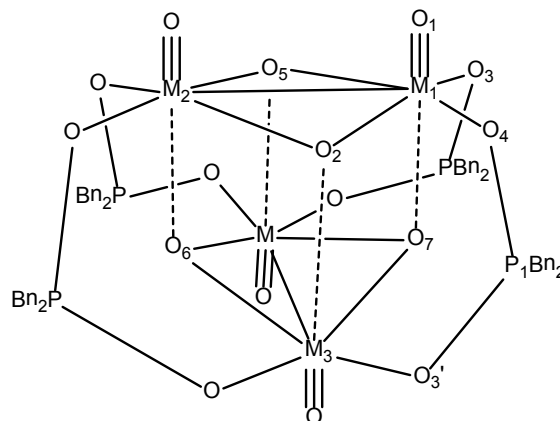


Fig. 3.2 Mercury²¹ drawing of **2** with 50% probability ellipsoids.

$\sigma \rightarrow \sigma^*$ transition. Notably complex **1** only displays one intense absorption at 340 nm which is presumably a ligand to metal charge transfer band. That for **2** is at 374 nm with the $\sigma \rightarrow \sigma^*$ transition appearing as a nondescript buried peak on this large absorption.

Table 3.1 Selected distances and bond angles for **1**, **3** and **2**.



	1 (V)	3 (Mo)	2 (W)
Distances (Å)			
M₁···M₂	2.7610(8)	2.6261(5)	2.6354(5)
O₂···O₅	2.419(2)	2.7560(2)	2.7970(4)
M₁···M₃	3.3300(6)	3.4091(2)	3.4019(4)
O₂···O₆	2.761(2)	2.7482(2)	2.7262(3)
M₁-O₁	1.5786(16)	1.668(2)	1.6964(19)
M₁-O₂	1.8161(13)	1.9555(19)	1.9809(16)
M₁-O₅	1.8919(13)	1.9612(19)	1.9825(16)
M₁-O₇	2.4392(15)	2.399(2)	2.3626(19)
M₁-O₃	1.9697(13)	2.0793(19)	2.0521(17)
M₁-O₄	1.9427(13)	2.0586(19)	2.0742(17)
O₃'···O₄	2.561(2)	2.5823(2)	2.5871(3)
Bond Angles (°)			
O₁-M₁-O₇	177.40(6)	170.36(8)	168.99(7)
M₁-O₂-M₂	96.23(6)	84.21(7)	83.35(6)
O₂-M₁-O₅	81.41(6)	89.44(8)	89.77(7)
O₁-M₁-O₂	103.16(7)	109.09(9)	110.23(8)
O₁-M₁-O₃	99.44(7)	97.61(9)	97.66(8)
O₁-M₁-O₄	99.74(7)	98.92(9)	96.55(8)
O₁-M₁-O₅	102.31(7)	109.10(9)	110.29(8)

As expected, the M₁-O₁ distance in **1** at 1.5786(16) Å and the corresponding trans M₁-O₇ at 2.4392(15) Å are the shortest and the longest respectively out of the three complexes in Table 1. The distortion from perfect cubane cores is evident in that there are much larger distances observed for M₁···M₃ compared to the M₁···M₂ interactions; see Table 1. The distance labelled as O₂···O₅ also varies among the three cubes with that for **1** being the shortest at 2.419(2) Å to that in **3** and **2** at 2.7560(2) and 2.7970(4) Å respectively. Somewhat related is the fact that the O₁-M₁-O₇ angle for **1** at 177.40(6)° is very nearly linear whereas that for **2** and **3** at 168.99(7) and 170.36(8)°, respectively, deviate more. These effects may be attributed to the repulsive effects of the metal to metal atom interaction or more simply the fact that as the metal atoms form bonds, the oxygen atoms move apart as a consequence. This also results in the M₁-O₂-M₂ and O₂-M₁-O₅ angles being the largest and smallest respectively for **1** compared to **2** and **3**; see Table 1. The last four rows of data in Table 1 illustrate the fact that the geometry at each metal center can be considered as distorted square pyramidal with the metal centers being raised out of the plane defined by the four pseudo-equatorial oxygen atoms. The listings for the corresponding distances reveal that those for the oxygen to metal atoms are significantly shorter in **1** compared to **2** and **3** with the exception of the bond trans to the multiply bonded oxo ligand. The O₃'···O₄ listing in Table 1 illustrates the accommodating nature of the phosphinate bridge ranging from 2.561(2) Å in **1** to 2.5871(3) Å in **3**.

In summary, we detail synthetic routes leading to vanadium and tungsten tetrameric complexes of the stoichiometry [M₄(μ₃-O)₄]¹²⁺. While complexes containing

this core were previously reported for vanadium albeit in the form of extended clusters, this is the first report for a tungsten(V) cluster of this core geometry.

3.4 Notes and references

[†]Electronic supplementary information (ESI) available: Elemental analyses, IR, ¹H and ³¹P NMR spectra, TGA plots for **1-3** and X-ray data for **1** and **2**. CCDC 834511 and 834512. For ESI and crystallographic data in CIF or other electronic format see DOI: 10.10XX/c1cc10XXXc

[‡]Synthesis of **1**: V₃(μ₃-O)O₂(μ₂-O₂P(Bn)₂)₆(H₂O)¹⁸ (0.0500 g, 0.0295 mmol) was dissolved in 10 mL of CH₂Cl₂ at 20 °C. To this light blue-green solution was added ^tBuOOH (0.016 mL of 5.5 M) in decane upon which the solution turned dark purple. About 5 drops of de-ionized H₂O were then added. After 3 hours of stirring, the solution had turned reddish-orange in color. The solvent was reduced to about 1 mL, kept at -20 °C overnight and then filtered. To the filtrate was added 30 mL of hexanes and this mixture was kept at -20 °C for 2 days resulting in an orange crystalline precipitate which was then filtered off, rinsed with hexanes and then dried under a vacuum to give 0.0050 g of **1** (0.0038 mmol, 17.2 % yield with respect to V₃(μ₃-O)O₂(μ₂-O₂P(Bn)₂)₆(H₂O)).

Anal. (Galbraith Laboratories, Knoxville, TN) Calc. for C₅₆H₅₆V₄O₁₆P₄: C, 51.24; H, 4.30. Found: C, 50.84; H, 4.58 %. ¹H NMR (400 MHz, CDCl₃): δ (ppm) = 2.86 (dd, 8, ²J_{HP} = 23.3, ²J_{HaHb} = 14.7 Hz, CH_aP), 2.90 (dd, 8, ²J_{HP} = 27.7, ²J_{HaHb} = 14.7 Hz, CH_bP), 7.05-7.36 (m, 40, (C₆H₅CH₂)). ³¹P{¹H} NMR (162 MHz, CDCl₃, relative to H₃PO₄): δ (ppm) = 60.6 (s, 1P). UV-vis spectrum (CH₂Cl₂) 340 nm. IR (neat, cm⁻¹): 3062(vw),

3029(vw), 1602(vw), 1496(m), 1454(m), 1398(vw), 1245(vw), 1190(vw), 1145(vw), 1101(m), 1070(m), 1012(s), 1000(s), 990(s), 914(vw), 847(br), 779(w), 698(s).

[§]Synthesis of **2**: W(CO)₆ (0.100 g, 0.284 mmol) and bis(benzyl)phosphinic acid (0.070 g, 0.283 mmol) were placed in a sealed tube with 6 mL of a 1:1 mixture of ethanol and THF and heated at 120 °C for 36 hrs. The resulting dark black-blue solution was then cooled to 20 °C. After 1 day the yellow crystals that had formed were filtered off, rinsed with ethanol and then dried under vacuum to yield **2** (0.018 g, 0.010 mmol, 13.75% yield based on W(CO)₆). Anal. (Galbraith Laboratories, Knoxville, TN) Calc. for C₅₆H₅₆W₄O₁₆P₄: C, 36.47; H, 3.06. Found: C, 36.63; H, 3.23 %. ¹H NMR (400 MHz, CDCl₃): δ (ppm) = 2.93 (dd, 8, ²J_{HP} = 19.5, ²J_{HaHb} = 14.8 Hz, CH_aP), 3.06 (dd, 8, ²J_{HP} = 14.9, ²J_{HaHb} = 14.8 Hz, CH_bP), 7.04-7.22 (m, 40, (C₆H₅CH₂)). ³¹P{¹H} NMR (162 MHz, CH₂Cl₂, relative to H₃PO₄): δ (ppm) = 68.4 (s, 1P). UV-vis spectrum (CH₂Cl₂) 374 nm. IR (neat, cm⁻¹): 3062(vw), 3030(vw), 1602(vw), 1496(m), 1454(m), 1398(vw), 1248(w), 1194(vw), 1143(vw), 1087(m), 1071(m), 1043(w), 1012(s), 1000(s), 979(s), 916(m), 854(m,br), 779(m), 694(s).

^{**}Crystal data for **1**: C₅₆H₅₆O₁₆P₄V₄•4(H₂O), M = 1376.65, tetragonal, a = 22.306(4) Å, b = 22.306(4) Å, c = 12.824(2) Å, V = 6380.7(19) Å³, T = 100(2) K, space group I4₁/a, Z = 4, μ = 0.738 mm⁻¹, 22239 reflections measured, 4828 independent reflections (R_{int} = 0.0504). R₁ = 0.0397 (I > 2σ(I)). wR(F²) = 0.0899 (I > 2σ(I)). R₁ = 0.0691 (all data). wR(F²) = 0.102 (all data). Crystal data for **2**: C₅₆H₅₆O₁₆P₄W₄•3(C₄H₈O), M = 2060.56, tetragonal, a = 22.771(4) Å, b = 22.771(4) Å, c = 13.107(2) Å, V = 6796(2) Å³, T = 100(2) K, space group I4₁/a, Z = 4, μ = 6.915 mm⁻¹, 17299 reflections measured, 5083

independent reflections ($R_{\text{int}} = 0.0225$). $R_1 = 0.0189$ ($I > 2\sigma(I)$). $wR(F^2) = 0.0425$ ($I > 2\sigma(I)$). $R_1 = 0.0241$ (all data). $wR(F^2) = 0.0457$ (all data).

1. R. Hernandez-Molina and A. G. Sykes, *J. Chem. Soc., Dalton Trans.*, 1999, 3137-3148.
2. (a) R. Hernandez-Molina and A. G. Sykes, *Coord. Chem. Rev.*, 1999, **187**, 291-302; (b) R. H. Holm, *Adv. Inorg. Chem.*, 1992, **38**, 1-71; (c) R. Llusar and S. Uriel, *Eur. J. Inorg. Chem.*, 2003, 1271-1290.
3. K. C. K. Swamy, R. O. Day and R. R. Holmes, *J. Am. Chem. Soc.*, 1987, **109**, 5546-5548.
4. (a) G. Guerrero, M. Mehring, P. Hubert Mutin, F. Dahan and A. Vioux, *J. Chem. Soc., Dalton Trans.*, 1999, 1537-1538; (b) D. L. Thorn and R. L. Harlow, *Inorg. Chem.*, 1992, **31**, 3917-3923.
5. G. C. Dismukes, R. Brimblecombe, G. A. N. Felton, R. S. Pryadun, J. E. Sheats, L. Spiccia and G. F. Swiegers, *Acc. Chem. Res.*, 2009, **42**, 1935-1943.
6. J. Barber, *Inorg. Chem.*, 2008, **47**, 1700-1710.
7. (a) G. I. Chilas, H. N. Miras, M. J. Manos, J. D. Woollins, A. M. Z. Slawin, M. Stylianou, A. D. Keramidas and T. A. Kabanos, *Pure Appl. Chem.*, 2005, **77**, 1529-1538; (b) M. J. Manos, H. N. Miras, V. Tangoulis, J. D. Woollins, A. M. Z. Slawin and T. A. Kabanos, *Angew. Chem. Int. Ed.*, 2003, **42**, 425-427; (c) H. N. Miras, R. Raptis, P. Baran, N. Lalioti, A. Harrison and T. A. Kabanos, *C. R.*

- Chimie*, 2005, **8**, 957-962; (d) H. N. Miras, R. G. Raptis, N. Lalioti, M. P. Sigalas, P. Baran and T. A. Kabanos, *Chem. Eur. J.*, 2005, **11**, 2295-2306.
8. M. D. Medrano, H. T. Evans, Jr., H.-R. Wenk and D. Z. Piper, *Am. Mineral.*, 1998, **83**, 889-895.
 9. (a) G. A. Farnum and R. L. LaDuca, *Acta Crystallogr. Sect. E.*, 2008, **64**, m1602;
(b) F.-N. Shi, Filipe A. A. Paz, J. Rocha, J. Klinowski and T. Trindade, *Eur. J. Inorg. Chem.*, 2004, **2004**, 3031-3037.
 10. X. Ma, Z. Yang, C. Schulzke, M. Noltemeyer and H.-G. Schmidt, *Inorg. Chim. Acta*, 2009, **362**, 5275-5277.
 11. Y. Hayashi, F. Müller, Y. Lin, S. M. Miller, O. P. Anderson and R. G. Finke, *J. Am. Chem. Soc.*, 1997, **119**, 11401-11407.
 12. K. Nishikawa, K. Kido, J. i. Yoshida, T. Nishioka, I. Kinoshita, B. K. Breedlove, Y. Hayashi, A. Uehara and K. Isobe, *Appl. Organomet. Chem.*, 2003, **17**, 446-448.
 13. V. Artero, A. Proust, P. Herson and P. Gouzerh, *Chem. Eur. J.*, 2001, **7**, 3901.
 14. J. Glerup, A. Hazell, K. Michelsen and H. Weihe, *Acta Chem. Scand.*, 1994, **48**, 618-627.
 15. (a) R. Hazama, K. Umakoshi, A. Ichimura, S. Ikari, Y. Sasaki and T. Ito, *Bull. Chem. Soc. Jpn.*, 1995, **68**, 456-468; (b) T. A. Budzichowski, M. H. Chisholm, K. Folting, M. G. Fromhold and W. E. Streib, *Inorg. Chim. Acta*, 1995, **235**, 339-

- 347; (c) S. Ikari, Y. Sasaki and T. Ito, *Inorg. Chem.*, 1990, **29**, 53-56; (d) S. Khalil and B. Sheldrick, *Acta Crystallogr. Sect. B*., 1978, **34**, 3751-3753; (e) P. Schreiber, K. Wieghardt, U. Floerke and H. J. Haupt, *Inorg. Chem.*, 1988, **27**, 2111-2115.
16. A. Jimtaisong, L. Feng, S. Sreehari, C. A. Bayse and R. L. Luck, *J. Cluster Sci.*, 2008, **19**, 181-195.
 17. W. Schirmer, U. Floerke and H. J. Haupt, *Z. Anorg. Allg. Chem.*, 1989, **574**, 239-255.
 18. (a) J. S. Maass, M. Zeller, D. Holmes, C. A. Bayse and R. L. Luck, *J. Cluster Sci.*, 2011, **22**, 193-210; (b) L. Feng, J. S. Maass and R. L. Luck, *Inorg. Chim. Acta*, 2011, **373**, 85-92.
 19. J. S. Maass, Z. Chen, M. Zeller and R. L. Luck, *Inorg. Chem.*, 2011, submitted.
 20. R. B. Silverman and R. A. Olofson, *Chem. Commun.*, 1968, 1313-1313.
 21. C. F. Macrae, I. J. Bruno, J. A. Chisholm, P. R. Edgington, P. McCabe, E. Pidcock, L. Rodriguez-Monge, R. Taylor, J. van de Streek and P. A. Wood, *J. Appl. Crystallogr.*, 2008, **41**, 466-470.
 22. J. E. McGrady, *J. Chem. Soc., Dalton Trans.*, 1999, 1393-1400.

Supplemental Data

Expanding molecular transition metal cubane clusters of the form $[\text{M}_4(\mu^3\text{-O})_4]^{12+}$: Syntheses, thermal analyses, spectroscopic and structural characterizations of molecules of the form $\text{M}_4(\mu^3\text{-O})_4(\text{O}_2\text{P}(\text{CH}_2\text{C}_6\text{H}_5)_2)_4(\text{O}_4)$, $\text{M} = \text{V}^{\text{V}}$ and W^{V}

John S. Maass,^a Zhichao Chen,^a Matthias Zeller,^b Rudy L. Luck^{a,*}

Supplementary Material

Elemental analyses, ¹H and ³¹P NMR spectra for 1 and 2, and, IR and TGA plots for 1, 2 and the Mo analogue, 3.

Figure 3.S1. Elemental analyses on 1 and 2.

Figure 3.S2. ¹H NMR spectrum of $\text{V}_4(\mu_3\text{-O})_4(\text{O}_2\text{P}(\text{Bn})_2)_4(\text{O}_4)$, 1, in CDCl_3 .

Figure 3.S3. ¹H NMR spectrum of $\text{W}_4(\mu_3\text{-O})_4(\text{O}_2\text{P}(\text{Bn})_2)_4(\text{O}_4)$, 2, in CDCl_3 .

Figure 3.S4. ³¹P{¹H} NMR spectrum of $\text{V}_4(\mu_3\text{-O})_4(\text{O}_2\text{P}(\text{Bn})_2)_4(\text{O}_4)$, 1, in CDCl_3 .

Figure 3.S5. ³¹P{¹H} NMR spectrum of $\text{W}_4(\mu_3\text{-O})_4(\text{O}_2\text{P}(\text{Bn})_2)_4(\text{O}_4)$, 2, in CH_2Cl_2 .

Figure 3.S6. IR spectrum of $\text{V}_4(\mu_3\text{-O})_4(\text{O}_2\text{P}(\text{Bn})_2)_4(\text{O}_4)$, 1.

Figure 3.S7. IR spectrum of $\text{W}_4(\mu_3\text{-O})_4(\text{O}_2\text{P}(\text{Bn})_2)_4(\text{O}_4)$, 2.

Figure 3.S8. IR spectrum of $\text{Mo}_4(\mu_3\text{-O})_4(\text{O}_2\text{P}(\text{Bn})_2)_4(\text{O}_4)$, 3.

Figure 3.S9a. TGA curve of $\text{V}_4(\mu^4\text{-O})_4(\mu^2\text{-O}_2\text{P}(\text{CH}_2\text{C}_6\text{H}_5)_2)_4(\text{O}_4)$, 1, at a heating rate of $10\text{ }^\circ\text{C min}^{-1}$.

Figure 3.S9b. TGA curve of $\text{V}_4(\mu^4\text{-O})_4(\mu^2\text{-O}_2\text{P}(\text{CH}_2\text{C}_6\text{H}_5)_2)_4(\text{O}_4)$, 1, at a heating rate of $10\text{ }^\circ\text{C min}^{-1}$.

Figure 3.S10a. TGA curve of $\text{W}_4(\mu^4\text{-O})_4(\mu^2\text{-O}_2\text{P}(\text{CH}_2\text{C}_6\text{H}_5)_2)_4(\text{O}_4)$, 2, at a heating rate of $10\text{ }^\circ\text{C min}^{-1}$.

Figure 3.S10b. TGA curve of $\text{W}_4(\mu^4\text{-O})_4(\mu^2\text{-O}_2\text{P}(\text{CH}_2\text{C}_6\text{H}_5)_2)_4(\text{O}_4)$, 2, at a heating rate of $10\text{ }^\circ\text{C min}^{-1}$.

Figure 3.S11a. TGA curve of $\text{Mo}_4(\mu^4\text{-O})_4(\mu^2\text{-O}_2\text{P}(\text{CH}_2\text{C}_6\text{H}_5)_2)_4(\text{O}_4)$, 3, at a heating rate of $10\text{ }^\circ\text{C min}^{-1}$.

Figure 3.S11b. TGA curve of $\text{Mo}_4(\mu^4\text{-O})_4(\mu^2\text{-O}_2\text{P}(\text{CH}_2\text{C}_6\text{H}_5)_2)_4(\text{O}_4)$, 3, at a heating rate of $10\text{ }^\circ\text{C min}^{-1}$.

Figure 3.S12. IR spectrum of the final product from the decomposition of $\text{V}_4(\mu_3\text{-O})_4(\text{O}_2\text{P}(\text{Bn})_2)_4(\text{O}_4)$, 1 at $600\text{ }^\circ\text{C}$.

Figure 3.S13. IR spectrum of the final product from the decomposition of $\text{W}_4(\mu_3\text{-O})_4(\text{O}_2\text{P}(\text{Bn})_2)_4(\text{O}_4)$, 2 at $600\text{ }^\circ\text{C}$.

Figure 3.S14. IR spectrum of the final product from the decomposition of $\text{Mo}_4(\mu_3\text{-O})_4(\text{O}_2\text{P}(\text{Bn})_2)_4(\text{O}_4)$, 3 at $600\text{ }^\circ\text{C}$.

Laboratory Report

Report prepared for:

Dr. Rudy Luck
Michigan Tech Univ
Dept of Chem
1400 Townsend Dr
Houghton, MI 49931
Phone: 906-487-2309
Email: rluck@mtu.edu

Report prepared by:

Pat B Delozier

Purchase Order:

BL506879

For further assistance, contact:

Pat B Delozier
Report Production Coordinator
PO Box 51610
Knoxville, TN 37950-1610
(865) 546-1335
patdelozier@galbraith.com

Sample: C58H56W4O18P4		Received: 2011-05-02			
Lab ID: 2011-N-9848					
Analyte	Method	Result	Base	Amount	Date (Time)
C : Carbon	GLI Procedure ME-12	36.63 %	As Received	1.153 mg	2011-05-11
H : Hydrogen	GLI Procedure ME-12	3.23 %	As Received	1.153 mg	2011-05-11

Sample: C58H56V4O18P4		Received: 2011-05-02			
Lab ID: 2011-N-9849					
Analyte	Method	Result	Base	Amount	Date (Time)
C : Carbon	GLI Procedure ME-12	50.84 %	As Received	1.033 mg	2011-05-11
H : Hydrogen	GLI Procedure ME-12	4.58 %	As Received	1.033 mg	2011-05-11

Signatures:

Modified By: [pat.b.delozier](#)
Published By: [pat.b.delozier](#)

2011-05-12T16:25:36.683-04:00
2011-05-12T16:25:50.403-04:00

Figure 3.S1. Elemental analyses on 1 and 2.

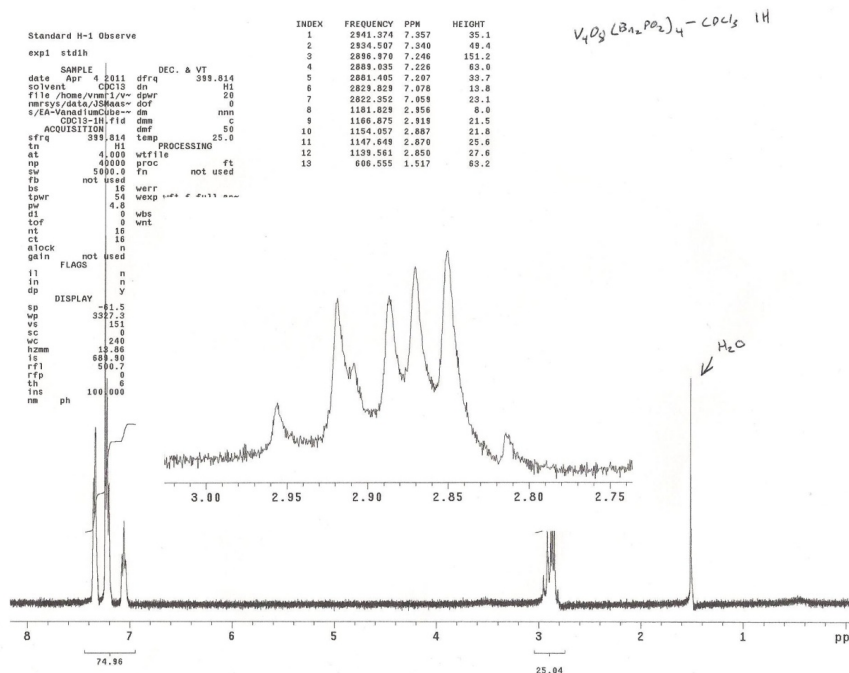


Figure 3.S2. ¹H NMR spectrum of V₄(μ₃-O)₄(O₂P(Bn)₂)₄(O₄), 1, in CDCl₃.

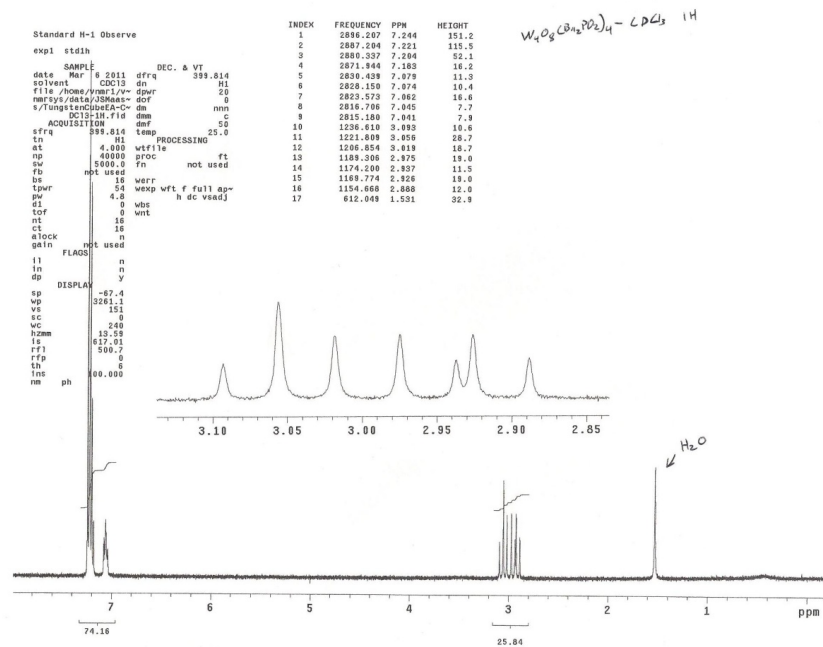
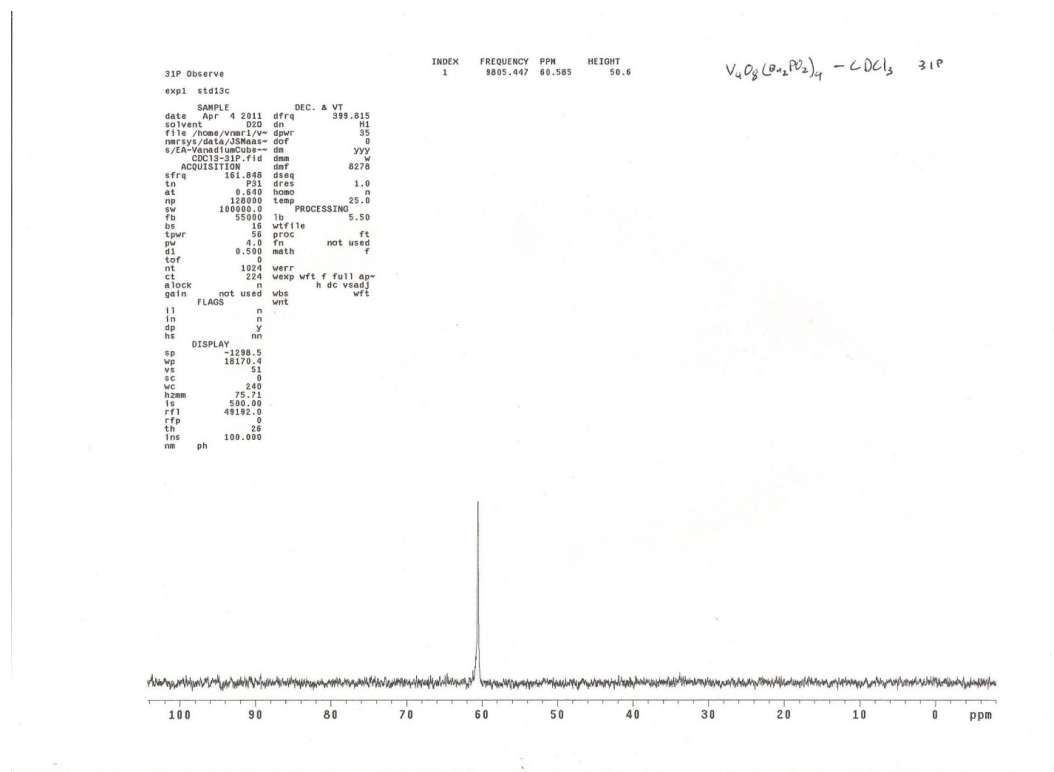


Figure 3.S3. ¹H NMR spectrum of W₄(μ₃-O)₄(O₂P(Bn)₂)₄(O₄), 2, in CDCl₃.



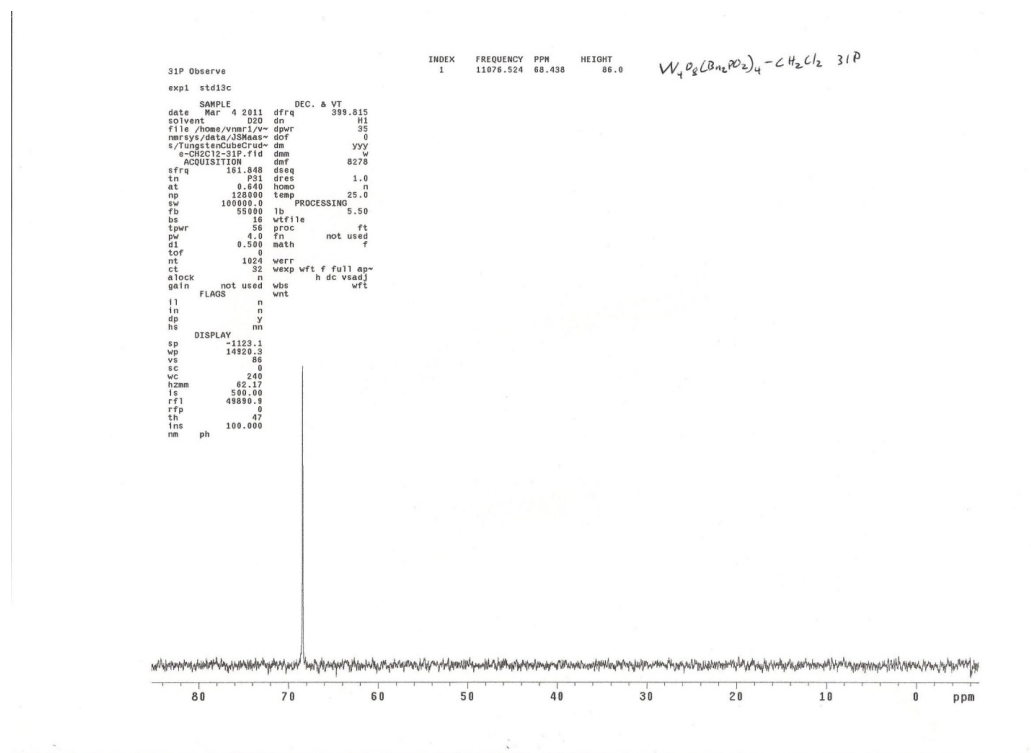


Figure 3.S5. $^{31}\text{P}\{^1\text{H}\}$ NMR spectrum of $W_4(\mu_3\text{-O})_4(\text{O}_2\text{P}(\text{Bn})_2)_4(\text{O}_4)$, 2, in CH_2Cl_2 .

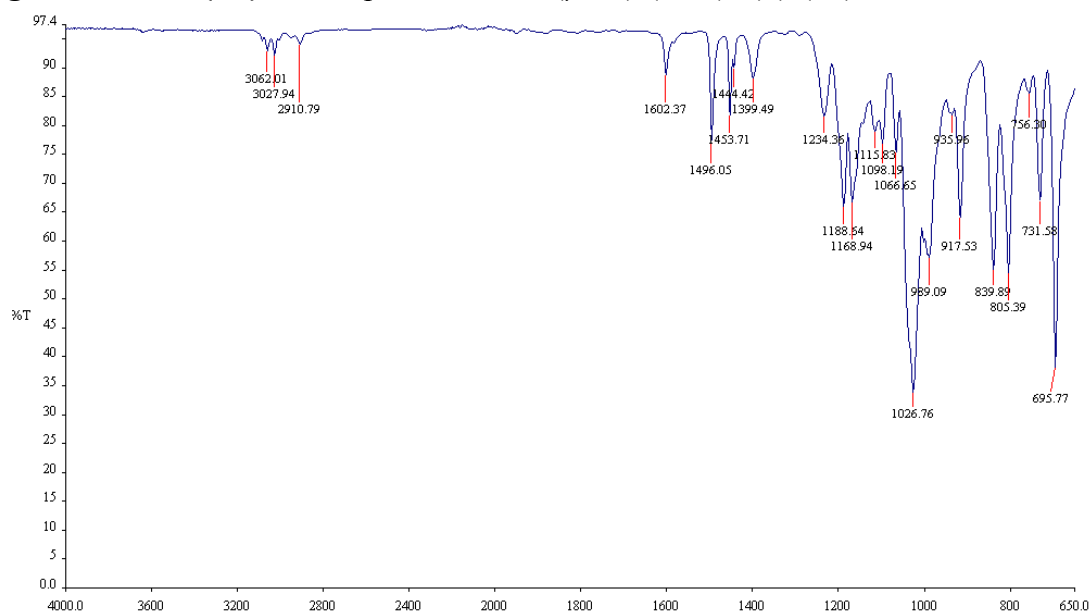


Figure 3.S6. IR spectrum of $V_4(\mu_3\text{-O})_4(\text{O}_2\text{P}(\text{Bn})_2)_4(\text{O}_4)$, 1.

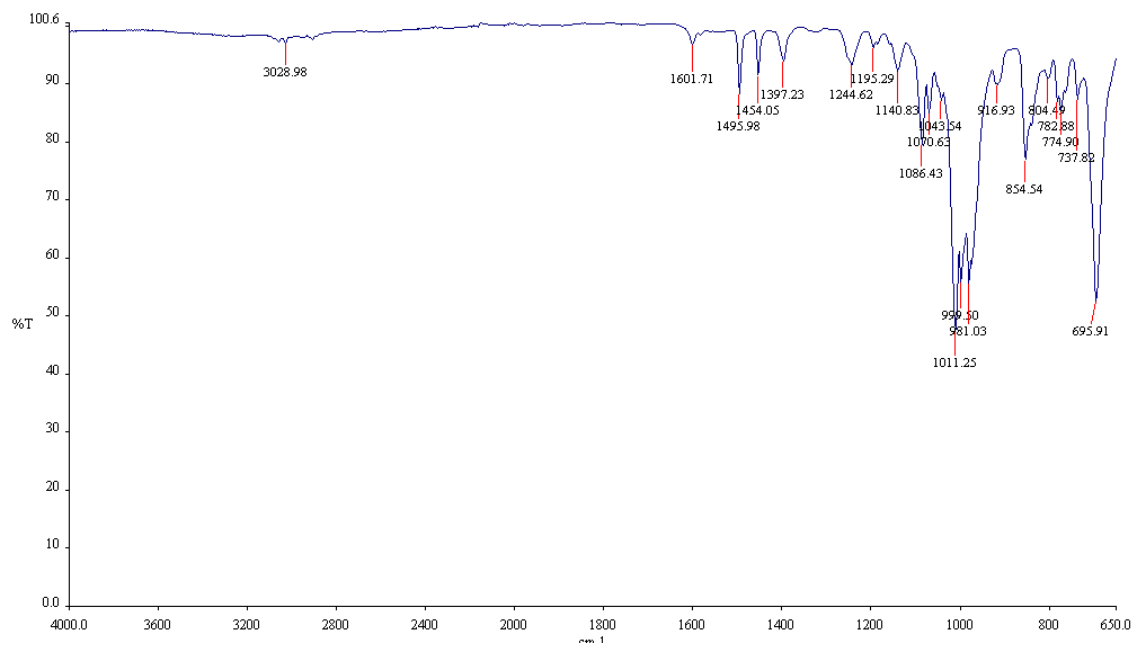


Figure 3.S7. IR spectrum of $W_4(\mu_3-O)_4(O_2P(Bn)_2)_4(O_4)$, 2.

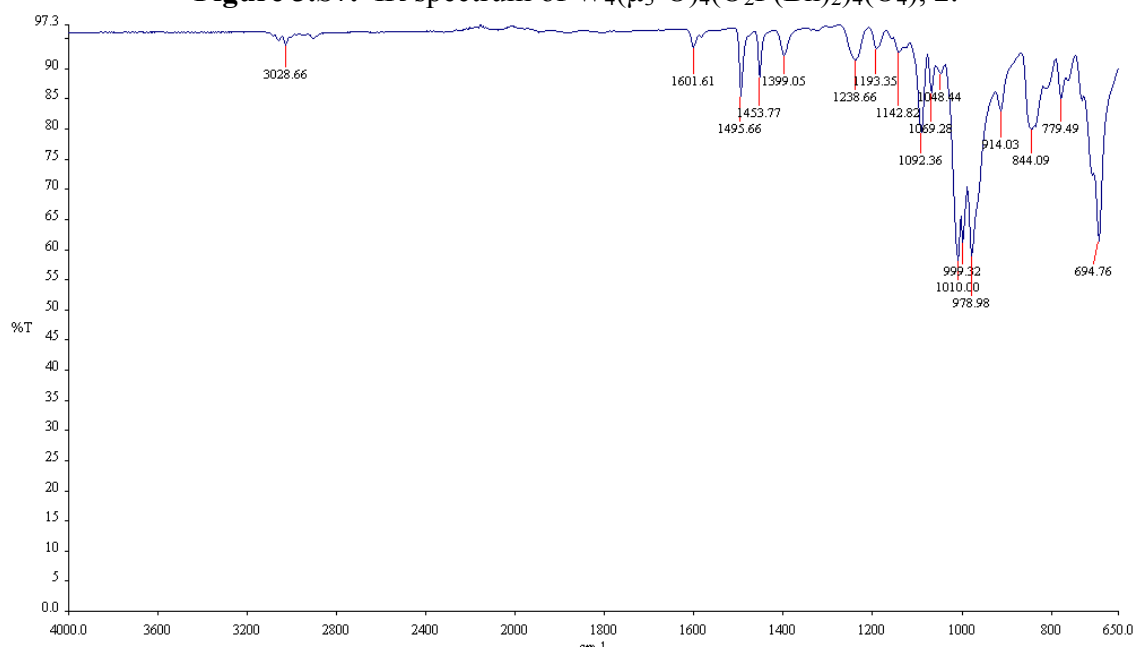


Figure 3.S8. IR spectrum of $Mo_4(\mu_3-O)_4(O_2P(Bn)_2)_4(O_4)$, 3.

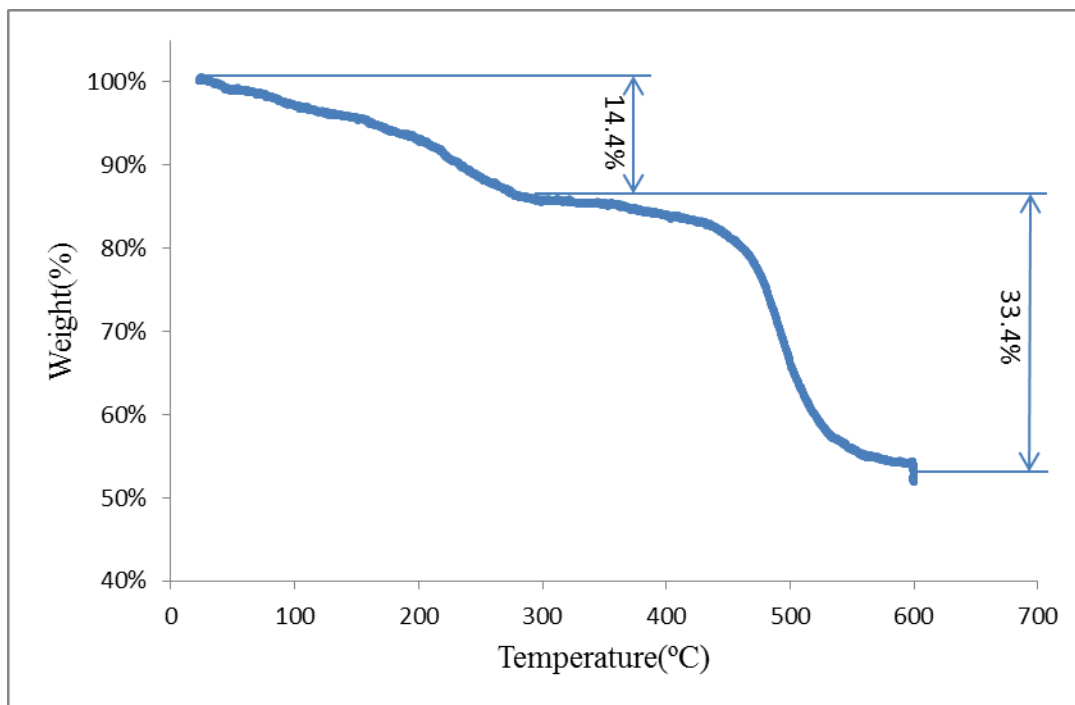


Figure 3.S9a. TGA curve of $V_4(\mu^4-O)_4(\mu^2-O_2P(CH_2C_6H_5)_2)_4(O_4)$, 1, at a heating rate of $10\text{ }^\circ\text{C min}^{-1}$.

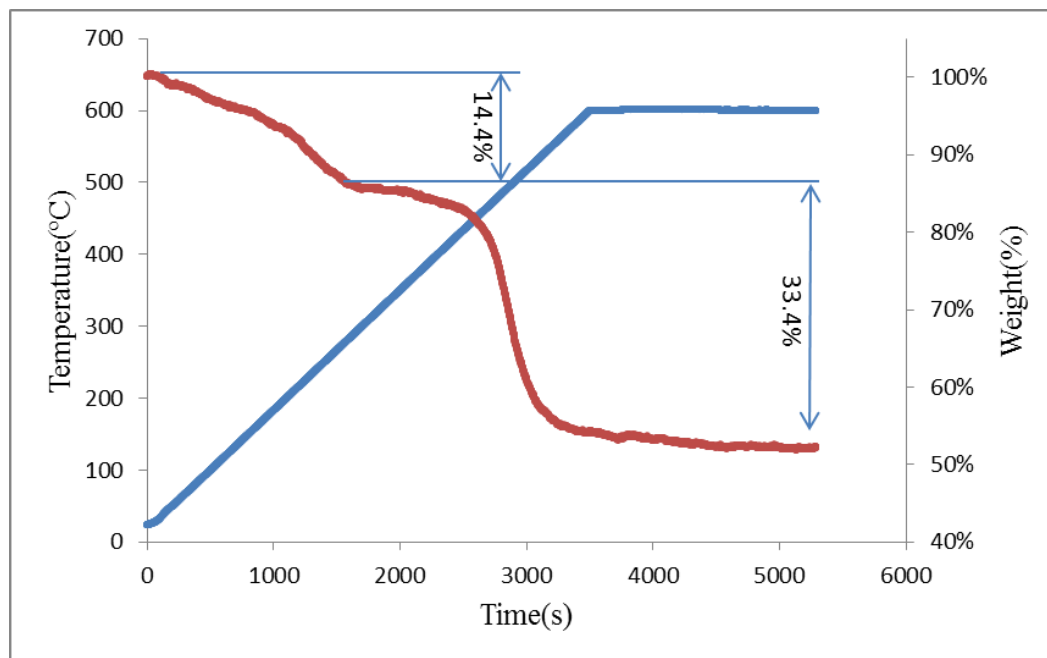


Figure 3.S9b. TGA curve of $V_4(\mu_4-O)_4(\mu_2-O_2P(CH_2C_6H_5)_2)_4(O_4)$, 1, at a heating rate of $10\text{ }^\circ\text{C min}^{-1}$.

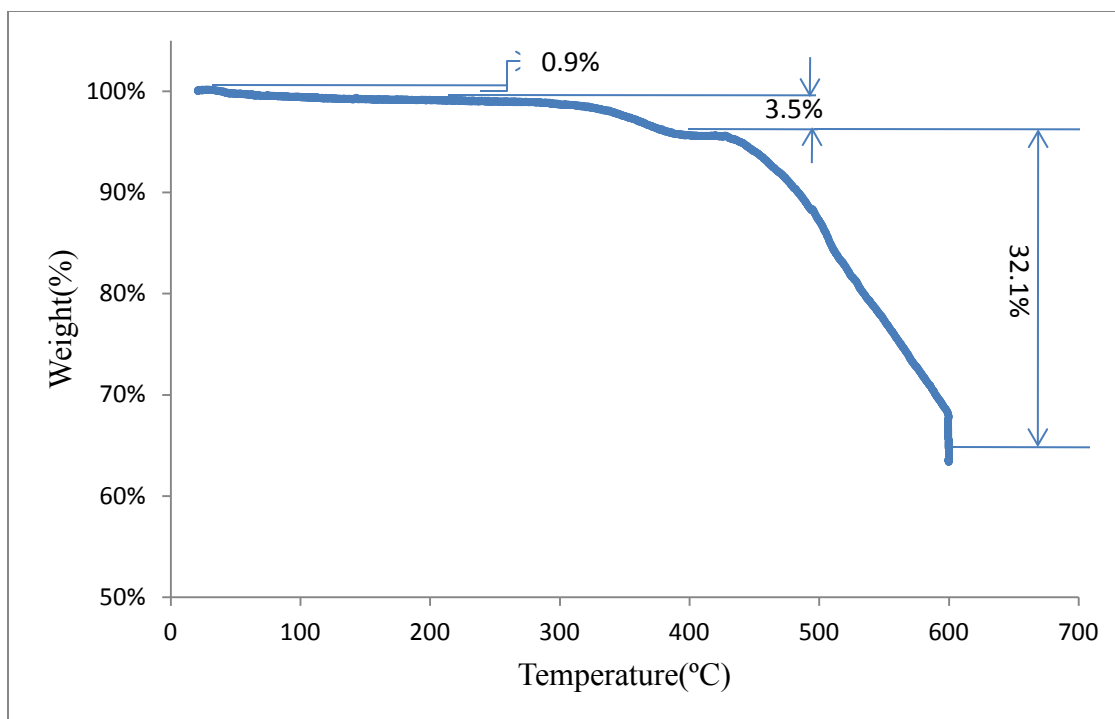


Figure 3.S10a. TGA curve of $W_4(\mu_3-O)_4(\mu^2-O_2P(CH_2C_6H_5)_2)_4(O_4)$, 2, at a heating rate of $10\text{ }^\circ\text{C min}^{-1}$.

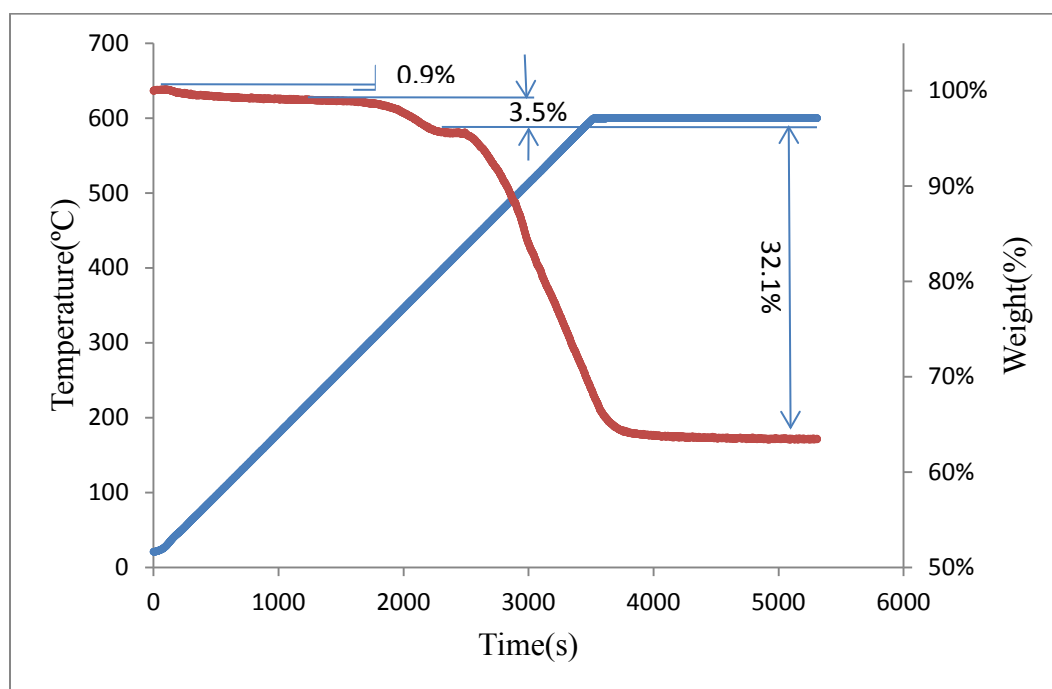


Figure 3.S10b. TGA curve of $W_4(\mu_3-O)_4(\mu_2-O_2P(CH_2C_6H_5)_2)_4(O_4)$, 2, at a heating rate of $10\text{ }^\circ\text{C min}^{-1}$.

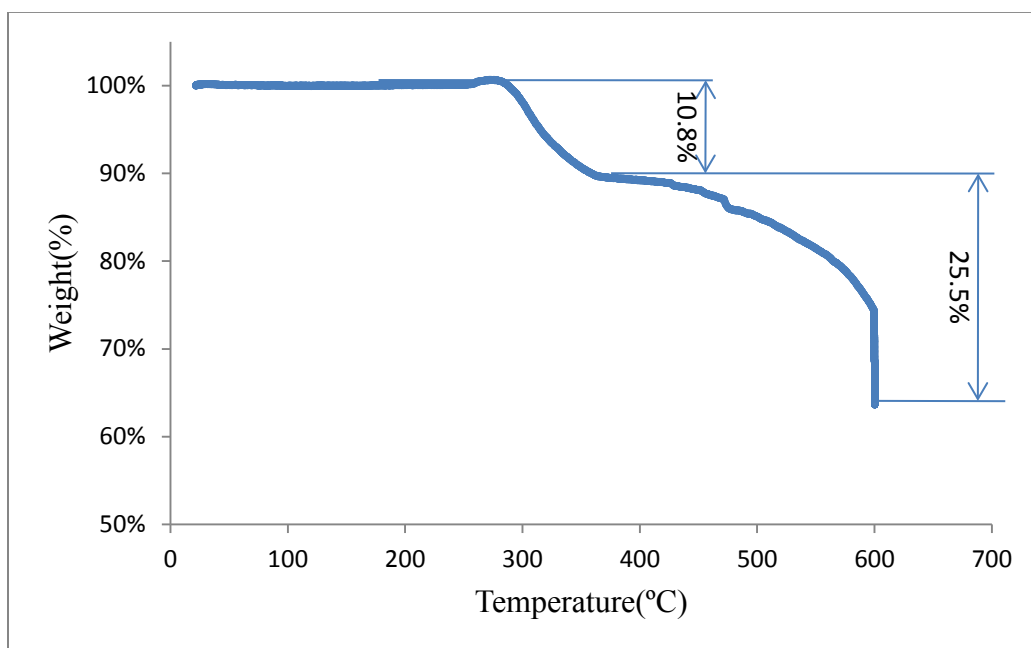


Figure 3.S11a. TGA curve of $\text{Mo}_4(\mu_3\text{-O})_4(\mu^2\text{-O}_2\text{P}(\text{CH}_2\text{C}_6\text{H}_5)_2)_4(\text{O}_4)$, 3, at a heating rate of $10^\circ\text{C min}^{-1}$.

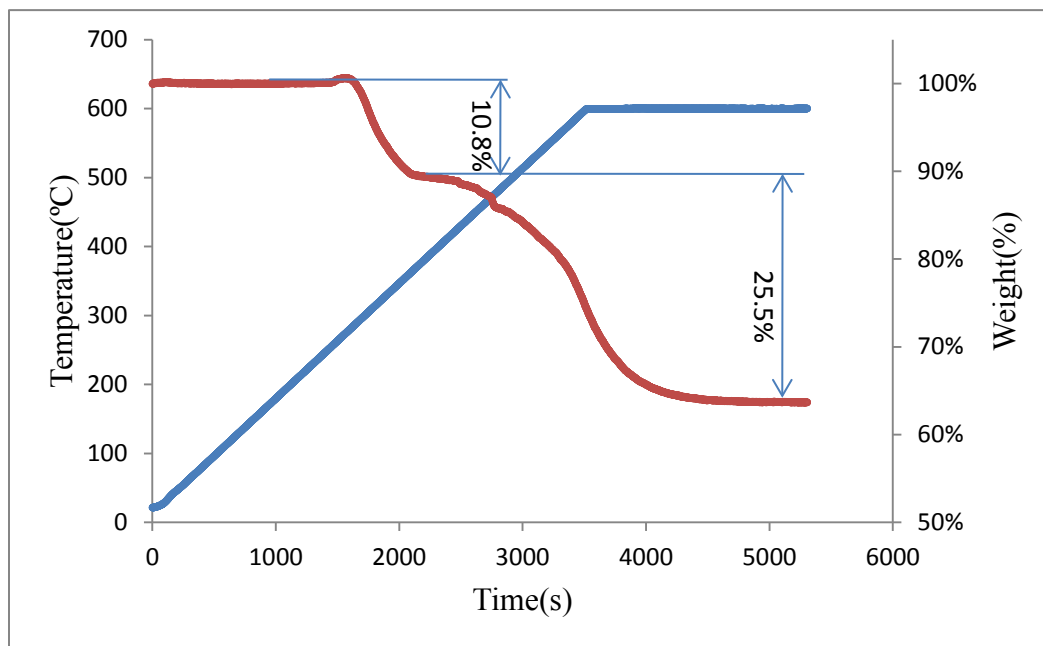


Figure 3.S11b. TGA curve of $\text{Mo}_4(\mu_3\text{-O})_4(\mu^2\text{-O}_2\text{P}(\text{CH}_2\text{C}_6\text{H}_5)_2)_4(\text{O}_4)$, 3, at a heating rate of $10^\circ\text{C min}^{-1}$.

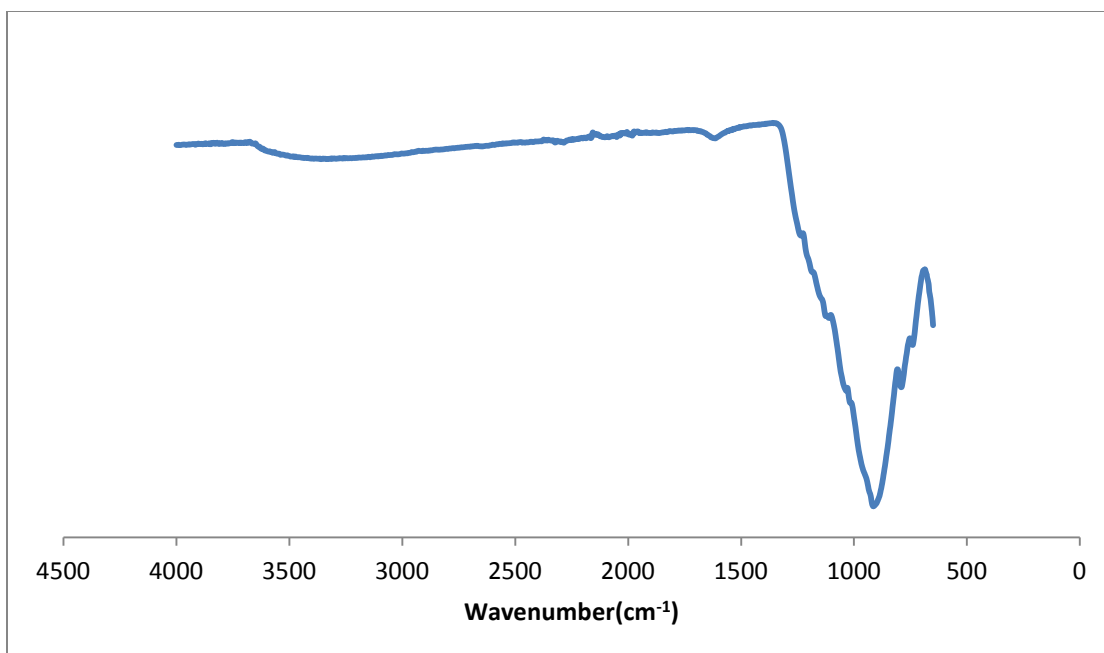


Figure 3.S12. IR spectrum of the final product from the decomposition of $V_4(\mu_3-O)_4(O_2P(Bn)_2)_4(O_4)$, 1 at 600 °C.

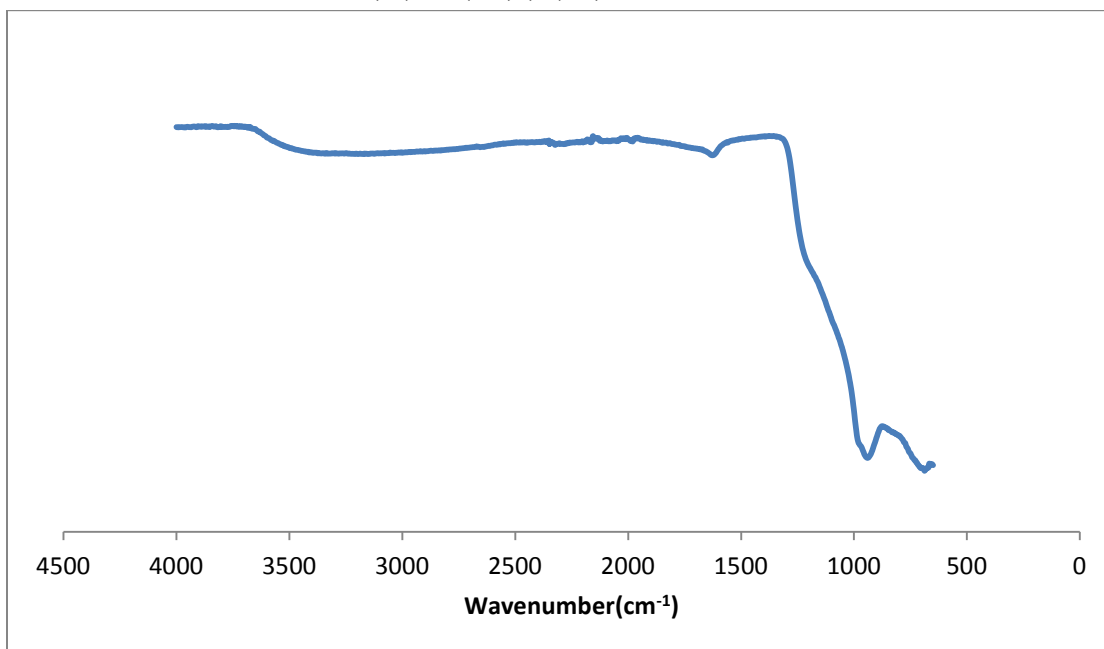


Figure 3.S13. IR spectrum of the final product from the decomposition of $W_4(\mu_3-O)_4(O_2P(Bn)_2)_4(O_4)$, 2 at 600 °C.

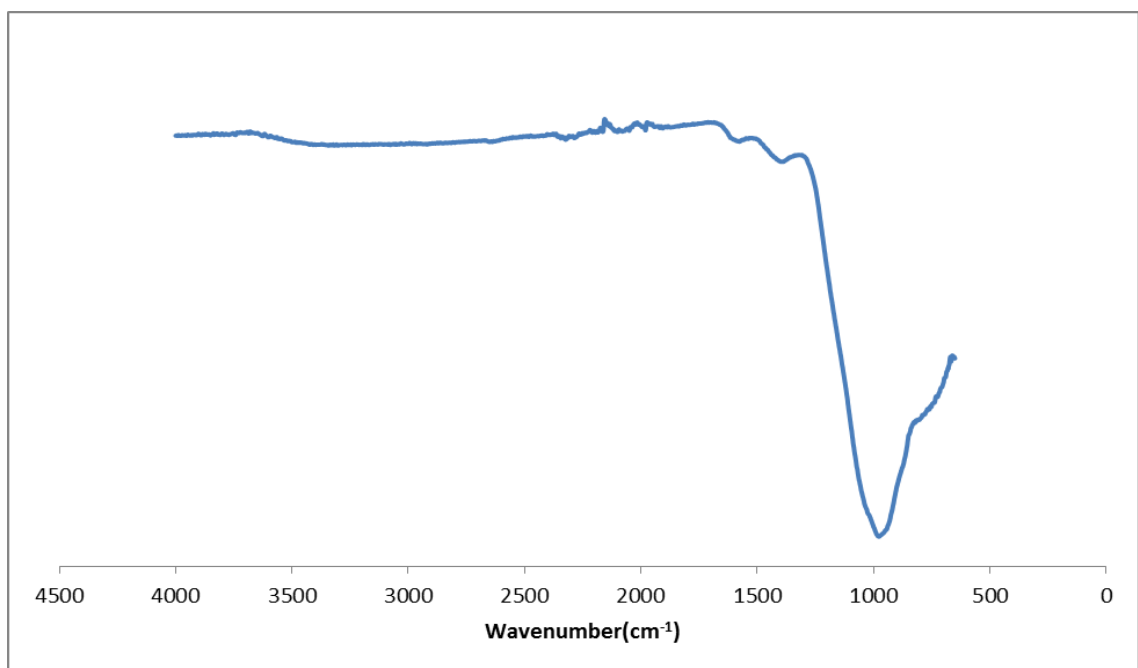


Figure 3.S14. IR spectrum of the final product from the decomposition of $\text{Mo}_4(\mu_3\text{-O})_4(\text{O}_2\text{P}(\text{Bn})_2)_4(\text{O}_4)$, **3** at 600 °C.

Chapter 4 Cobalt Dimers

4.1 Syntheses and structures of three complexes of formulae $[L_3Co(\mu_2-O_2P(Bn)_2)_3CoL']/[L']]$, featuring octahedral and tetrahedral cobalt(II) geometries; variable temperature magnetic susceptibility measurement and analysis on $[(py)_3Co(\mu_2-O_2P(Bn)_2)_3Co(py)]/[ClO_4]^{1,2}$

John S. Maass,^a Matthias Zeller,^b Tanya M. Breault,^c Bart M. Bartlett,^c Hiroshi Sakiyama,^d and Rudy L. Luck^{a,*}

^a*Department of Chemistry, Michigan Technological University, 1400 Townsend Drive, Houghton, MI 49931, USA*

^b*Department of Chemistry, Youngstown State University, 1 University Plaza, Youngstown, OH 44555, USA*

^c*Department of Chemistry, University of Michigan, 930 N. University Avenue, Ann Arbor, MI 48109-1055 USA.*

^d*Department of Material and Biological Chemistry, Faculty of Science, Yamagata University, 1-4-12 Kojirakawa, Yamagata 990-8560, Japan*

¹ “Reprinted with permission from Maass, J. S.; Zeller, M.; Breault, T. M.; Bartlett, B. M.; Sakiyama, H.; Luck, R. L. *Inorganic Chemistry* **2012**, 51, 4903. Copyright 2012 American Chemical Society.”

² License agreement for reproduction is provided in the Appendix.

4.2 Abstract

The syntheses and structural properties of three dinuclear complexes $[L_3Co(\mu_2-O_2P(Bn)_2)_3CoL']][L'']$; one ionic $L_3 = py_3$, $L' = py$, $L'' = ClO_4^-$, **1**, and two molecular $L_3 = py_3$, $L' = Cl$, **2**, $L_3 = py$, $\mu_2-NO_3^-$, $L' = py$, **3** are reported. Complexes feature octahedral Co(II) sites bridged by three dibenzylphosphinate ligands to a tetrahedrally ligated Co(II) site with the remaining coordination sites occupied by py, nitrate and chloride ligands. The Co to Co distances are 4.248 Å at 291 K and 4.265 Å at 100 K for **1** and 4.278 and 4.0313(7) Å for **2** and **3** respectively. A fit of the low temperature magnetic susceptibility data was derived for complex **1** with $g = 2.25$, $TIP = 700 \times 10^{-6} \text{ cm}^3 \text{ mol}^{-1}$, $\lambda = -173 \text{ cm}^{-1}$, $\kappa = 0.93$, $\nu = -3.9$, $\Delta = 630 \text{ cm}^{-1}$, $J = 0.15 \text{ cm}^{-1}$, and $\theta = -1.8$ resulting in $R(\chi_M) = 2.5 \times 10^{-5}$ and $R(\chi_M T) = 5.8 \times 10^{-5}$.

4.3 Results and Discussion

Dinuclear cobalt complexes featuring octahedral and tetrahedral geometries with Co(III)-Co(II)^{1,2} and Co(II)-Co(II)³⁻⁵ centers have been reported. Magnetic studies have been reported for three of the Co(II)-Co(II) compounds which have very different bridging ligands. First, for the compound [(H₂O)(dppm)₂Co(μ-CN)CoCl₃], high spin isolated ($S = 3/2$) pertained but the linear nature of the data obtained (i.e., $\chi_M^* T$ vs T was linear) could not be satisfactorily analyzed.³ Second, for the complex [Co₂L₂Cl₃]Cl, L = 2,6-diamino-3-[(2-carboxymethyl) phenylazo]-pyridine, the analysis of the magnetic data resulted in the conclusion that “two low spin (1s) Co²⁺ ions pertained.”⁴ Third for the compound [(MeCN)₅Co(NCS)Co(NCS)₃], the magnetic analysis suggested that the data can be best fit with the Curie-Weiss expression with $g_{\text{avg}} = 2.5$ and $\theta = -15.5$ K.⁵ The Co to Co distance in these compounds was 5.007, 4.800 and 5.732 Å for the first to third respectively.

Our interest in the complexes reported herein stems from our discovery that the dibenzylphosphinate ligand stabilizes tetrameric clusters such as [V₄O₈]⁴⁺, [Mo₄O₈]⁴⁺ and [W₄O₈]⁴⁺.⁶⁻⁹ Previous research reacting phosphinate ligands and cobalt have resulted in polymeric species.¹⁰⁻¹⁷ In an extension of this work to prepare clusters of Co^{III} oxides or hydroxides¹⁸ we find that this ligand affords dinuclear clusters of the form [L₃Co(μ₂-O₂P(CH₂C₆H₅)₂)₃CoL’][L’’]. Dark blue crystals of [(py)₃Co(μ₂-O₂PBn₂)₃Co(py)][ClO₄] **1** were isolated first from an ethanol solution consisting of a mixture of Bn₂PO₂K, Co(ClO₄)₂·6H₂O, pyridine and H₂O₂.¹⁹ It was later discovered that **1** can be made in good yield by reacting three equivalents of the potassium salt of the ligand with two equivalents of cobalt perchloride along with excess pyridine in ethanol. The compound

$[(\text{py})_3\text{Co}(\mu_2\text{-O}_2\text{P}(\text{Bn}_2)_3\text{Co}(\text{Cl}))]$, **2**, was also first prepared unintentionally from the reaction of $\text{Co}(\text{NO}_3)_2 \cdot 6\text{H}_2\text{O}$ with pyridine and $\text{Bn}_2\text{PO}_2\text{H}$ in methylene chloride. The addition of hexanes resulted in the formation of light pink crystals which were found to be the known compound $\text{Co}(\text{NO}_3)_2(\text{H}_2\text{O})_2(\text{py})_2$. The solution was filtered and the addition of more hexanes produced dark blue crystals of **2**. It is not clear how the chloride ion formed in this reaction but we have discovered that compound **2** can be produced starting with $\text{CoCl}_2 \cdot 6\text{H}_2\text{O}$. The complex $[(\text{py})(\mu_2\text{-NO}_3)\text{Co}(\mu_2\text{-O}_2\text{PBn}_2)_3\text{Co}(\text{py})]$, **3**, was obtained serendipitously in a reaction of $\text{Co}^{\text{III}}(\text{acac})_2\text{PyNO}_2$ and $\text{Bn}_2\text{PO}_2\text{H}$ under reflux conditions in CHCl_3 . The addition of pentane followed by keeping the solution at 5 °C for two weeks lead to the formation of dark purple crystals of **3**.

A thermal ellipsoid plot of **1** is illustrated in Fig. 4.1. In all structures, the two cobalt centers are bridged by three dibenzylphosphinate ligands. This ligand is very flexible and is capable of bridging at various lengths as illustrated in the Co to Co atom distances in these compounds which are 4.265(2), 4.278(1) and 4.0313(7) Å for **1-3**, respectively. Complexes **1** and **2** were arranged with the octahedrally coordinated Co atom arranged on a 3-fold axis

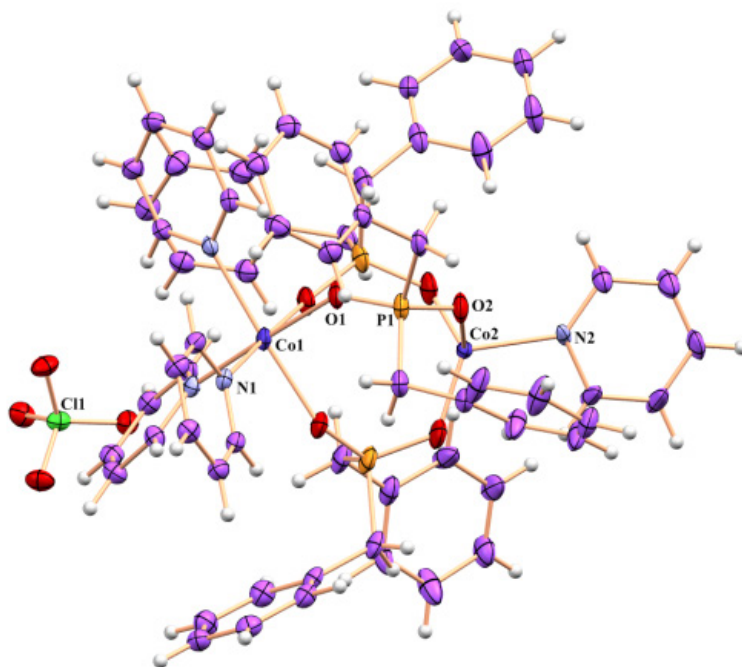


Figure 4.1. Thermal ellipsoid drawing of **1** (one orientation). Selected bond distances (Å) and angles (°) are as follows: Co(1)–O(1), 2.103(2); Co(1)–N(1), 2.192(2); Co(2)–O(2), 1.813(17); Co(2)–N(2), 2.045(4); O(1)^a–Co(1)–O(1), 91.18(8); O(1)^a–Co(1)–N(1), 86.86(9); O(1)^b–Co(1)–N(1), 177.33(8); O(1)–Co(1)–N(1), 87.04(8); N(1)–Co(1)–N(1)^a, 94.85(7); O(2)–Co(2)–O(2)^b, 125.65(13); O(2)–Co(2)–N(2), 103.6(7); O(2)–Co(2)–O(2)^a, 106.3(7); O(2)^b–Co(2)–O(2)^a, 106.0(6); O(2)^b–Co(2)–N(2), 111.3(8); N(2)–Co(2)–O(2)^a, 101.6(2); Symmetry transformation codes; ^a –y,x–y,z; ^b –x+y,–x,z.

and the tetrahedrally coordinated Co atom located slightly off the 3-fold axis. In **1**, three py ligands complete the octahedral geometry at one end and the other end has one py coordinated. The complex is positively charged and is balanced by a [ClO₄][–] anion as illustrated in Fig. 1. Compound **2** has a similar octahedral geometry with three py ligands but at the other site one chloride ligand completes the tetrahedral arrangement. This complex also has the Co atoms and the Cl ligand situated on a 3-fold axis but both benzyl groups were disordered. Compound **3** has a nitrate ligand coordinated in a bidentate

manner together with one py ligand at the Co oct site and one py ligand at the other. Ring strain in the four-membered ring of the nitrate ligand is responsible for the longer Co–O distances at Co(2)–O(7), 2.188(3) and Co(2)–O(8), 2.211(3) Å compared to the other Co–O distances at the octahedral site in **3** which range from 2.031(2) to 2.069(2) Å.²⁰ This complex did contain the shortest Co to Co distance at 4.0313(7) Å within compounds **1-3** which all feature octahedral and tetrahedral Co centers. The bridging phosphinate ligands are asymmetrically bonded in that the Co–O atom distances are significantly longer at the octahedral site in comparison to those at the tetrahedral end, i.e., 2.103 (2) and 2.102 (4) compared to 1.813 (17) and 1.973 (5) Å for **1** and **2** respectively. The disorder in these molecules hindered a more accurate determination but for **3**, the distances at 2.031 (2), 2.032(3) and 2.069(2) at the octahedral end were also significantly longer than those at the tetrahedral site at 1.955 (2) 1.933 (2), and 1.940 (2) Å for Co–O bonds on phosphinate ligands P(1), P(2) and P(3) respectively, all presumably due to steric reasons.

The $\chi_M T$ values for **1** and **2** were determined at room temperature using a Johnson Matthey Guoy balance to be 5.56 and 6.59 emu K mol⁻¹, respectively. These values are larger than the spin-only value for two high-spin cobalt(II) sites (3.75 emu K mol⁻¹) and suggest that there is a contribution of orbital angular momentum typical of the local ⁴T₁ term.²¹ The temperature dependent magnetic susceptibility data χ_M on complex **1** was obtained over the temperature range 2.0 to 300 K under a 1000 Oe measuring field and this is illustrated in Fig. 2 together with the $\chi_M T$ dependence. At 300 K, the value for $\chi_M T$ values for **1** was 5.813 compared to the 5.575 emu K mol⁻¹ reported for

$[(\text{MeCN})_5\text{Co}(\text{NCS})\text{Co}(\text{NCS})_3]$.⁵ As shown in Fig. 2, $\chi_M T$ vs T for **1** decreases slowly from 5.813 at 300 K to 4.575 at 50 K and then more rapidly to 2.254 emu K mol⁻¹ at 2 K. We were unable to determine a satisfactory fit to the data using the Curie-Weiss equation, but this is not surprising as the analysis of high-spin cobalt(II) complexes is known to be difficult.²²⁻²⁸ A fit of the data in both cases was obtained using the equations presented as Supporting Information. This analysis involved the consideration of the g factor and temperature independent paramagnetism, TIP, for the tetrahedral cobalt(II) ion; the spin-orbit coupling factor λ , the orbital reduction factor κ , and a distortion parameter ν defined as $\Delta/(\kappa\lambda)$ for the octahedral cobalt(II) ion and the intramolecular exchange interaction J and the Weiss constant θ to describe the intermolecular exchange interaction. In general, it is difficult to separate the intramolecular interaction from the intermolecular interaction. In particular, when J is negative, it is almost impossible to determine J and θ correctly. Table 1 lists the analysis of **1** and that for the complex $[\text{Co}(\text{NCMe})_5\text{Co}(\text{NCS})_4]$ ⁵ for comparison purposes.

Table 4.1. Magnetic parameters.^a

Complex	g	TIP	λ , cm ⁻¹	κ	ν	Δ , cm ⁻¹	J , cm ⁻¹	θ , K	R_χ^b , 10 ⁻⁵	$R_{\chi T}^c$, 10 ⁻⁵
1	2.25	0.0007	-173	0.93	-3.9	630	0.15	-1.8	2.5	5.8
$\text{Co}_2(\text{L})_5(\text{L}')_4$	2.17	0.0007	-155	0.89	-3.7	510	-2.62	-0.1	15	16

^a Calculated as in Supporting Information

$$^b R_\chi = \sum (\chi_{M,\text{calc}} - \chi_{M,\text{obs}})^2 / \sum (\chi_{M,\text{obs}})^2$$

$$^c R_{\chi T} = \sum (\chi_M T_{\text{calc}} - \chi_M T_{\text{obs}})^2 / \sum (\chi_M T_{\text{obs}})^2$$

^d L = MeCN, L' = NCS, reference⁵.

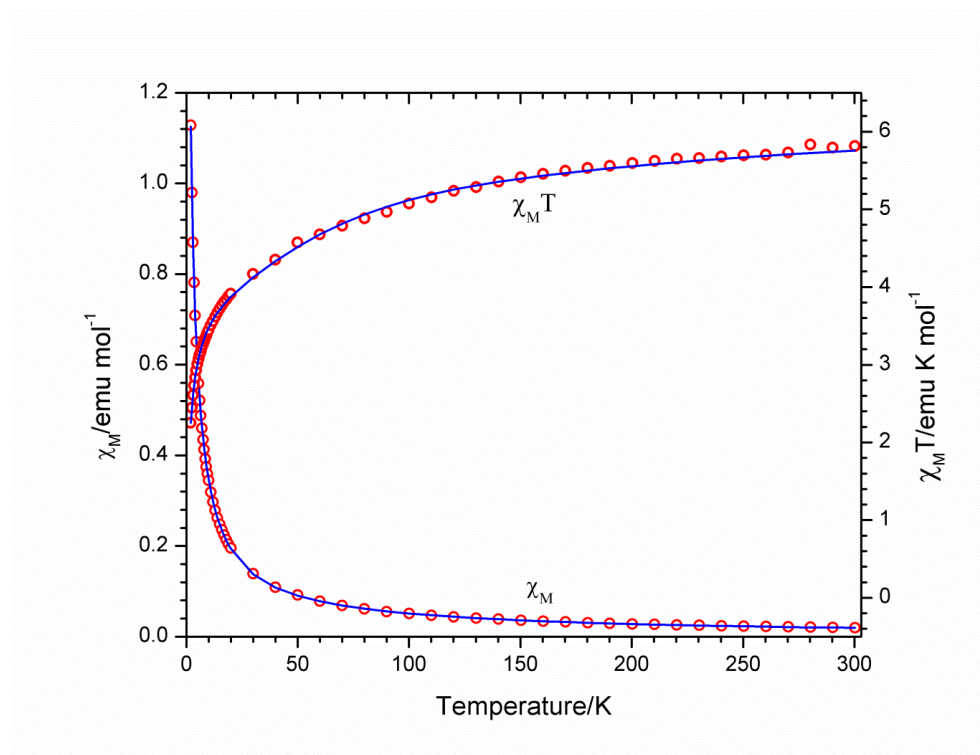


Figure 4.2. Temperature dependence of χ_M vs T and $\chi_M T$ vs T for **1** with data represented by open circles and the solid line the fit obtained using the parameters described in the text.

If the calculation for the fit of the low-temperature data modified J without consideration of θ , the quality of the fit was not good; however, this improved when θ was used instead of J . Interestingly, when J and θ were simultaneously optimized, J became positive (but small at 0.15 cm^{-1}), and the lowest R_χ value (i.e., even higher fitting quality) was obtained and in the final calculation, TIP was also considered. The value for the spin-orbit parameter λ of -173 cm^{-1} for **1** is noteworthy for the theoretical value for the free cobalt(II) ion is expected to be $\sim -172 \text{ cm}^{-1}$.²⁹ That for κ at 0.93 is also close to that for the free cobalt(II) ion.³⁰ Both of these parameters were calculated to be slightly less for

[Co(NCMe)₅Co(NCS)₄].⁵ The values for Δ at 630 and 510 cm⁻¹ for **1** and [Co(NCMe)₅Co(NCS)₄] respectively are normal for octahedral high-spin cobalt(II) complexes (~200 - ~800 cm⁻¹).³¹ For **1**, the negative ν value of -3.9 and the Δ value of 627.5 suggest that the octahedral Co(II) ion is trigonally compressed and this is also consistent with the crystal structure of **1** where O(1)^a-Co(1)-O(1) and N(1)-Co(1)-N(1)^a are larger than 90° and O(1)^a-Co(1)-N(1) and O(1)-Co(1)-N(1) are smaller than 90°.³² In conclusion, for [Co(NCMe)₅Co(NCS)₄]⁵, if J is assumed to be 0, $|\theta|$ becomes large and unreasonable. Therefore, the sign and magnitude of the J value at -2.62 cm⁻¹ in Table 1 are suggestive of antiferromagnetic interactions. However, in the case of **1**, the value of J at 0.15 cm⁻¹ while small is slightly positive and thus there is a possibility that the intramolecular interaction is weakly ferromagnetic.

Supporting information. Equations for the magnetic analysis and CIF files for 1-3 (CCDC 840142-4). This material available at <http://pubs.acs.org> and the CIF files from the Director, CCDC, 12 Union Road, Cambridge CB2 1EZ, U.K.

Corresponding Author

*E-mail: rluck@mtu.edu. Tel: (906)487 2309

Notes

The authors declare no competing financial interest.

Acknowledgements

Financial support by Michigan Technological University is gratefully acknowledged.

The variable temperature magnetic data for $[\text{Co}(\text{NCMe})_5\text{Co}(\text{NCS})_4]$ was supplied by Jack Guy DaSilva from the laboratory of Professor Joel S. Miller.

References

1. Chiari, B.; Cinti, A.; Crispu, O.; Demartin, F.; Pasini, A.; Piovesana, O. *J. Chem. Soc., Dalton Trans.* **2001**, 3611-3616
2. Panja, A.; Eichhorn, D. M. *J. Coord. Chem.* **2009**, 62, 2600-2609.
3. Li, W.; Zhan, S.-z.; Wang, J.-g.; Yan, W.-y.; Deng, Y.-f. *Inorg. Chem. Commun.* **2008**, 11, 681-683.
4. Tan, X.-w.; Xie, X.-h.; Chen, J.-y.; Zhan, S.-z. *Inorg. Chem. Commun.* **2010**, 13, 1455-1458.
5. Shurdha, E.; Moore, C. E.; Rheingold, A. L.; Miller, J. S. *Inorg. Chem.* **2011**, 50, 10546-10548.
6. Feng, L.; Maass, J. S.; Luck, R. L. *Inorg. Chim. Acta* **2011**, 373, 85-92.
7. Jimtaisong, A.; Feng, L.; Sreehari, S.; Bayse, C. A.; Luck, R. L. *J. Cluster Sci.* **2008**, 19, 181-195.
8. Maass, J. S.; Chen, Z.; Zeller, M.; Luck, R. L. *Dalton Transactions* **2011**, 40.

9. Maass, J. S.; Zeller, M.; Holmes, D.; Bayse, C. A.; Luck, R. L. *J. Cluster Sci.* **2011**, 22, 193-210.
10. Brechin, E. K.; Coxall, R. A.; Parkin, A.; Parsons, S.; Tasker, P. A.; Winpenny, R. E. P. *Angew. Chem., Int. Ed.* **2001**, 40, 2700-2703.
11. Chandrasekhar, V.; Boomishankara, R.; Sasikumara, P.; Nagarajan, L.; Cordes, A. W. Z. *Anorg. Allg. Chem.* **2005**, 631, 2727-2732.
12. Eichelberger, J. L.; Gillman, H. D. *Inorganic coordination polymers. XXI. Manganese(II), cobalt(II), nickel(II), copper(II), and zinc(II) bis(N-phenylaminomethyl) phosphinates. Effects of coordinating side groups*; Pennwalt Corp.: 1977; p 18 pp.
13. Giancotti, V.; Ripamonti, A. *Chim. Ind. (Milan)* **1966**, 48, 1065-70.
14. Giancotti, V.; Ripamonti, A. *J. Chem. Soc. A* **1969**, 706-13.
15. Gillman, H. D.; Eichelberger, J. L. *Inorg. Chim. Acta* **1977**, 24, 31-4.
16. Giordano, F.; Randaccio, L.; Ripamonti, A. *Chem. Commun.* **1967**, 19-20.
17. Rose, S. H.; Block, B. P. *J. Am. Chem. Soc.* **1965**, 87, 2076-7.
18. McAlpin, J. G.; Stich, T. A.; Ohlin, C. A.; Surendranath, Y.; Nocera, D. G.; Casey, W. H.; Britt, R. D. *J. Am. Chem. Soc.* **2011**, 133, 15444-15452.

19. 1, L. *Crystal data for 1: C₆₂H₆₂Co₂N₄O₆P₃•ClO₄, M = 1269.38, hexagonal, a = 13.5260(10) Å, b = 13.5260(10) Å, c = 57.341(4) Å, α = 90°, β = 90°, γ = 120°, V = 9085.2(11) Å³, T = 100(2) K, space group R3[−], Z = 6, 14927 reflections measured, 5028 independent reflections (R_{int} = 0.0311). The final R₁ values were 0.0518 (I > 2σ(I)). The final wR(F₂) values were 0.1126 (I > 2σ(I)). The final R₁ values were 0.0849 (all data). The final wR(F₂) values were 0.1328 (all data). The goodness of fit on F₂ was 1.018. .*
20. Driessen, W. L.; de Graaff, R. A. G.; Parlevliet, F. J.; Reedijk, J.; de Vos, R. M. *Inorg. Chim. Acta* **1994**, 216, 43-49.
21. Sakiyama, H.; Adams, H.; Fenton, D. E.; Cummings, L. R.; McHugh, P. E.; Okawa, H. *Open Journal of Inorganic Chemistry* **2011**, 1, 33-38.
22. Kahn, O. *Molecular Magnetism*. VCH: 1993; p 380 pp.
23. Lloret, F.; Julve, M.; Cano, J.; Ruiz-Garcia, R.; Pardo, E. *Inorg. Chim. Acta* **2008**, 361, 3432-3445.
24. Sakiyama, H. *J. Chem. Software* **2001**, 7, 171-178.
25. Sakiyama, H. *Inorg. Chim. Acta* **2006**, 359, 2097-2100.
26. Sakiyama, H. *J. Comput. Chem., Jpn.* **2007**, 6, 123-134.
27. Sakiyama, H. *Inorg. Chim. Acta* **2007**, 360, 715-716.

28. Tone, K.; Sakiyama, H.; Mikuriya, M.; Yamasaki, M.; Nishida, Y. *Inorg. Chem. Commun.* **2007**, *10*, 944-947.
29. Figgis, B. N.; Hitchman, M. A. *Ligand Field Theory and its Application*. Wiley-VCH: New York, 2000.
30. Lines, M. E. *The Journal of Chemical Physics* **1971**, *55*, 2977-2984.
31. Figgis, B. N.; Gerloch, M.; Lewis, J.; Mabbs, F. E.; Webb, G. A. *J. Chem. Soc., A* **1968**, 2086-93.
32. Stiefel, E. I.; Brown, G. F. *Inorg. Chem.* **1972**, *11*, 434-436.

Supplemental Data

Syntheses and structures of three complexes of formulae $[\text{L}_3\text{Co}(\mu_2\text{-O}_2\text{P}(\text{Bn})_2)_3\text{CoL}'][\text{L}'']$, featuring octahedral and tetrahedral cobalt(II) geometries; variable temperature magnetic susceptibility measurement and analysis on $[(\text{py})_3\text{Co}(\mu_2\text{-O}_2\text{PBn}_2)_3\text{Co}(\text{py})][\text{ClO}_4]$

John S. Maass,^a Matthias Zeller,^b Tanya M. Breault,^c Bart M. Bartlett,^c Hiroshi Sakiyama,^d and Rudy L. Luck^{a,*}

^a*Department of Chemistry, Michigan Technological University, 1400 Townsend Drive, Houghton, MI 49931, USA*

^b*Department of Chemistry, Youngstown State University, 1 University Plaza, Youngstown, OH 44555, USA*

^c*Department of Chemistry, University of Michigan, 930 N. University Avenue, Ann Arbor, MI 48109-1055 USA.*

^d*Department of Material and Biological Chemistry, Faculty of Science, Yamagata University, 1-4-12 Kojirakawa, Yamagata 990-8560, Japan*

Supplementary material

General Method

Chemicals were purchased from Aldrich Chemicals and solvents were used as received. Elemental analyses were conducted by Galbraith Laboratories, Knoxville, TN. IR spectra on complexes **1-3** were recorded on a PerkinElmer Spectrum One spectrometer (neat). Room temperature magnetic measurements were conducted on a Johnson Matthey Auto MSB instrument. Dibenzylphosphinic acid was prepared according to the cited literature.¹

*Synthesis of $[(\text{py})_3\text{Co}(\mu_2\text{-O}_2\text{PBn}_2)_3\text{Co}(\text{py})][\text{ClO}_4]$, **1***

0.201 g (3.58 mmol) of KOH, 0.886 g (3.58 mmol) of dibenzylphosphinic acid and 0.1 mL of pyridine were dissolved in 18 mL of ethanol. This solution was then added dropwise to a stirring solution of 0.874 g (2.38 mmol) $\text{Co}(\text{ClO}_4)_2 \cdot 6\text{H}_2\text{O}$ and 0.4 mL of

pyridine in 20 mL of ethanol. The solution turned from pink to blue when the addition was complete. The solution was left overnight upon which a blue precipitate formed which was filtered off and wash with ethanol until it was colorless assuming containing mainly KClO_4 . 1 mL of pyridine was then added to the blue filtrate which was then allowed to concentrate overnight yielding 0.723 g (0.57 mmol, 15.86 % yield based on $\text{Co}(\text{ClO}_4)_2 \cdot 6\text{H}_2\text{O}$ of $[(\text{py})_3\text{Co}(\mu_2\text{-O}_2\text{P}(\text{Bn})_2)_3\text{Co}(\text{py})][\text{ClO}_4]$, **1**, as a blue crystalline solid. Anal. Calcd. for $\text{C}_{62}\text{H}_{62}\text{O}_{10}\text{N}_4\text{P}_3\text{Co}_2\text{Cl} \cdot 0.25\text{CH}_2\text{Cl}_2$: C, 57.93; H, 4.88. Found: C, 58.64; H, 4.93.

*Synthesis of $[(\text{py})_3\text{Co}(\mu_2\text{-O}_2\text{P}(\text{Bn})_2)_3\text{Co}(\text{Cl})]$, **2***

0.046 g (0.820 mmol) of KOH, 0.203 g (0.820 mmol) of dibenzylphosphinic acid and 0.1 mL of pyridine were dissolved in 10 mL of ethanol. This solution was then added dropwise to a stirring solution of 0.130 g (0.547 mmol) $\text{CoCl}_2 \cdot 6\text{H}_2\text{O}$ and 0.2 mL of pyridine in 10 mL of ethanol. A blue precipitate formed after 4 hours which was filtered off and wash with 5 mL of ethanol yielding 0.197 g (0.171 mmol, 63.77 % yield based on $\text{CoCl}_2 \cdot 6\text{H}_2\text{O}$ of $[(\text{py})_3\text{Co}(\mu_2\text{-O}_2\text{P}(\text{Bn})_2)_3\text{Co}(\text{Cl})]$ **2**, as a blue crystalline solid.

*Synthesis of $[(\text{py})(\mu_2\text{-NO}_3)\text{Co}(\mu_2\text{-O}_2\text{P}(\text{Bn})_2)_3\text{Co}(\text{py})]$, **3***

0.100 g (0.261 mmol) of $\text{Co}(\text{acac})_2\text{NO}_2(\text{py})$ and 0.129 g (0.522 mmol) of dibenzylphosphinic acid were dissolved in 10 mL of chloroform forming a red solution which was heated to reflux and left overnight. The solution had turned green the next day which was then cooled to room temperature and filtered. The filtrate was then layered with pentane and kept cold in a freezer. After 2 weeks, large purple x-ray quality crystals were obtained.

Magnetic susceptibility measurements

The sample was prepared by weighing 71.9 mg of compound **1** into a gelatin capsule. 118.6 mg of eicosane was then added to stabilize the powder in an inert waxy matrix. Susceptibility was recorded as a function of temperature from 2.0 to 300 K under a 1000 Oe measuring field using a SQUID magnetometer. A control experiment in which only

eicosane was measured was used to correct the data for the diamagnetic gram susceptibility of the eicosane. (-9.739×10^{-7} emu/g). This measurement also corrected for the constant contribution from the drinking straw and capsule with the assumption that the mass of the gelatin capsule is constant (in all of the measurements, the capsule mass is 47(1) mg) and that the density of the straw is constant.

After these corrections, the data were converted from gram susceptibility to molar susceptibility then corrected for the diamagnetic contribution of your sample as determined from Pascal's constants, -7.3862×10^{-4} emu/mol.² The effective moment at room temperature is determined to be 6.6 Bohr magnetons, ($\mu_{\text{eff}} = 2.82 \cdot [(XT)^{1/2}]$), very similar to what was measured with a Gouy balance measurement at room temperature.

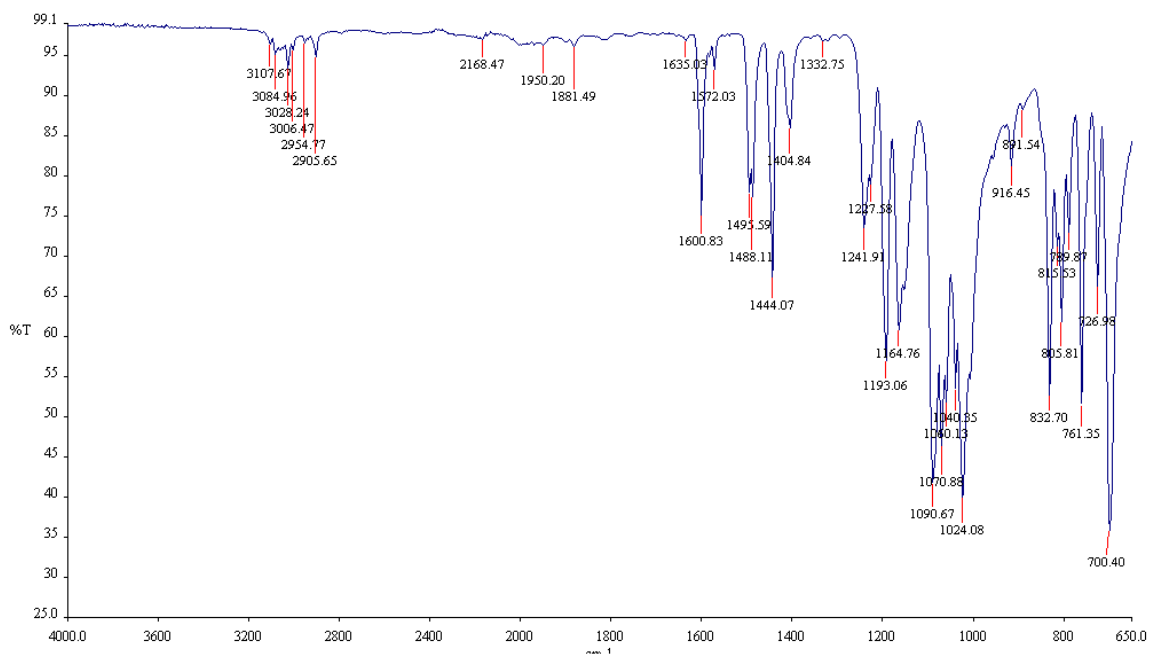


Figure 4.S1. FTIR spectra of complex 1 (neat).

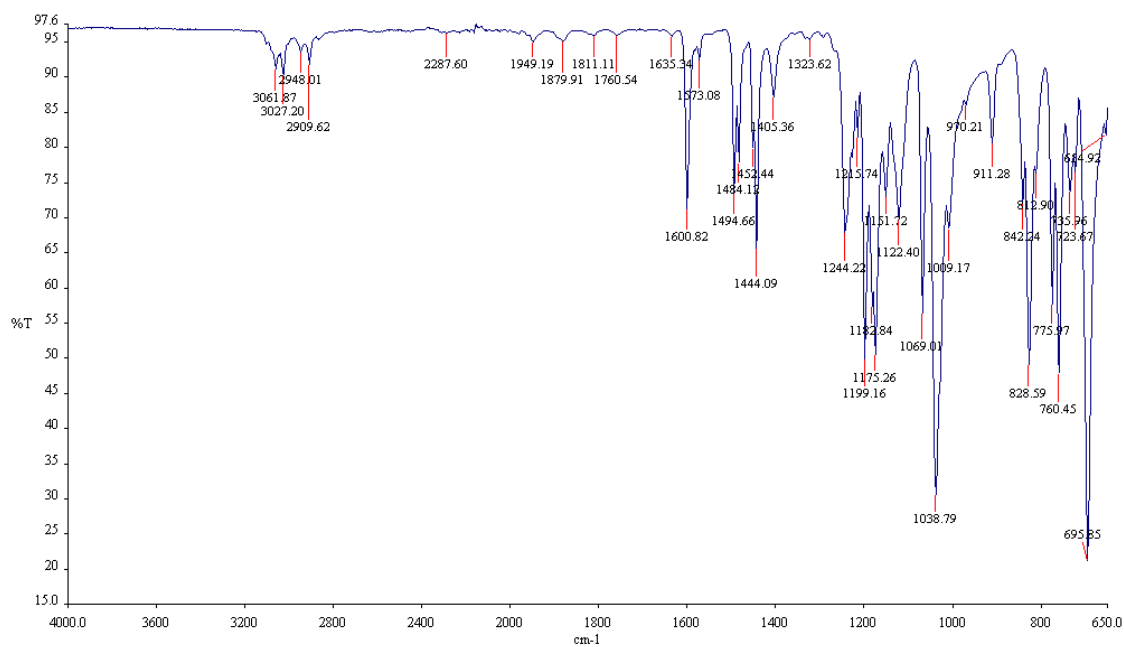


Figure 4.S2. FTIR spectra of complex 2 (neat).

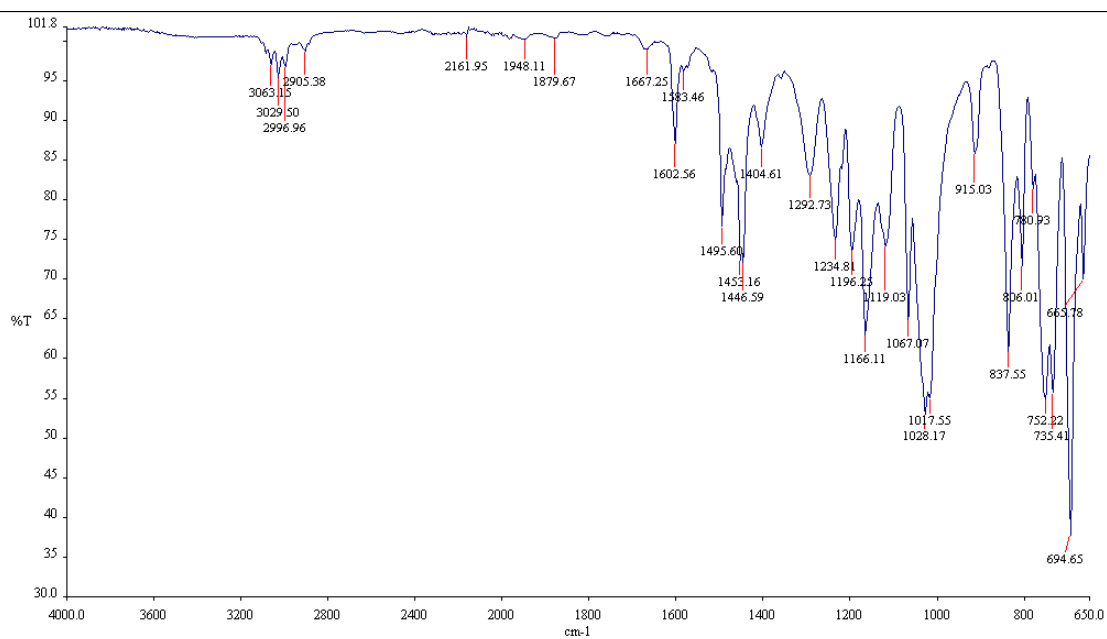


Figure 4.S3. FTIR spectra of complex 3 (neat).

Magnetic susceptibility equations for dinuclear high-spin cobalt(II) complexes considering the exchange interaction between tetrahedral and octahedral cobalt(II) ions.³

Equations expressing the relationship between a parameter set (κ , λ , Δ) and Zeemann coefficients for an octahedral cobalt(II) ion were obtained using the Hamiltonian below.

$$\mathbf{H} = \Delta(\mathbf{L}_z^2 - 2/3) - (3/2)\kappa\lambda\mathbf{L}\cdot\mathbf{S} + \beta[-(3/2)\kappa\mathbf{L}_u + g_e\mathbf{S}_u]\cdot\mathbf{H}_u \quad (u = x, y, z)$$

Considering the isotropic exchange interaction, the magnetic susceptibility equation was obtained based on the Hamiltonian $\mathbf{H} = -J\mathbf{S}_{3/2}\cdot\mathbf{S}_{1/2}$, where $\mathbf{S}_{3/2}$ was the local spin operator for a tetrahedral cobalt(II) ion and $\mathbf{S}_{1/2}$ was the local spin operator for the effective 1/2 spin of an octahedral cobalt(II) ion. The full equation was obtained combining the magnetic susceptibility equation and the equations of the Zeemann coefficients.

$$\chi_M = \frac{\chi_z + 2\chi_x}{3}$$

$$\chi_{z(x)} = N \frac{F_{1,z(x)}}{F_2} + \text{TIP}$$

$$\begin{aligned} F_{1,z(x)} = & \frac{5}{4} \sum_{n=\pm 1} \left[\frac{\left(\frac{1}{2} E_{z(x),n}^{(1)} + \frac{3}{4} g \beta \right)^2}{k(T-\theta)} - 2 E_{z(x),n}^{(2)} \right] \exp\left[\frac{-E_n^{(0)} + \frac{5}{4} J}{k T}\right] \\ & + \frac{1}{4} \sum_{n=\pm 1} \left[\frac{\left(-\frac{1}{2} E_{z(x),n}^{(1)} + \frac{5}{4} g \beta \right)^2}{k(T-\theta)} - 2 E_{z(x),n}^{(2)} \right] \exp\left[\frac{-E_n^{(0)} - \frac{25}{12} J}{k T}\right] \\ & + \sum_{n \neq \pm 1} \left[\frac{\left(E_{z(x),n}^{(1)} \right)^2}{k(T-\theta)} - 2 E_{z(x),n}^{(2)} \right] \exp\left[\frac{-E_n^{(0)}}{k T}\right] \end{aligned}$$

($n = \pm 1, \pm 2, \pm 3, \pm 4, \pm 5, \pm 6$)

$$F_2 = \frac{5}{8} \sum_{n=\pm 1} \exp\left[\frac{-E_n^{(0)} + \frac{5}{4}J}{kT}\right] + \frac{3}{8} \sum_{n=\pm 1} \exp\left[\frac{-E_n^{(0)} - \frac{25}{12}J}{kT}\right] + \sum_{n \neq \pm 1} \exp\left[\frac{-E_n^{(0)}}{kT}\right]$$

($n = \pm 1, \pm 2, \pm 3, \pm 4, \pm 5, \pm 6$)

$$v = \frac{\Delta}{\kappa \lambda}$$

$$E_{\pm 1}^{(0)} = -\frac{2c_2^2 \Delta}{3} - 3\sqrt{\frac{3}{2}} c_1 c_2 \kappa \lambda - 3\sqrt{2} c_2 c_3 \kappa \lambda + c_3^2 \left(\frac{\Delta}{3} + \frac{3\kappa \lambda}{4}\right) + c_1^2 \left(\frac{\Delta}{3} + \frac{9\kappa \lambda}{4}\right)$$

$$E_{\pm 2}^{(0)} = -\frac{2c_4^2 \Delta}{3} - 3\sqrt{\frac{3}{2}} c_4 c_5 \kappa \lambda + c_5^2 \left(\frac{\Delta}{3} - \frac{3\kappa \lambda}{4}\right)$$

$$E_{\pm 3}^{(0)} = -\frac{2c_7^2 \Delta}{3} - 3\sqrt{\frac{3}{2}} c_6 c_7 \kappa \lambda - 3\sqrt{2} c_7 c_8 \kappa \lambda + c_8^2 \left(\frac{\Delta}{3} + \frac{3\kappa \lambda}{4}\right) + c_6^2 \left(\frac{\Delta}{3} + \frac{9\kappa \lambda}{4}\right)$$

$$E_{\pm 4}^{(0)} = -\frac{2c_{10}^2 \Delta}{3} - 3\sqrt{\frac{3}{2}} c_9 c_{10} \kappa \lambda - 3\sqrt{2} c_{10} c_{11} \kappa \lambda + c_{11}^2 \left(\frac{\Delta}{3} + \frac{3\kappa \lambda}{4}\right) + c_9^2 \left(\frac{\Delta}{3} + \frac{9\kappa \lambda}{4}\right)$$

$$E_{\pm 5}^{(0)} = -\frac{2c_{12}^2 \Delta}{3} - 3\sqrt{\frac{3}{2}} c_{12} c_{13} \kappa \lambda + c_{13}^2 \left(\frac{\Delta}{3} - \frac{3\kappa \lambda}{4}\right)$$

$$E_{\pm 6}^{(0)} = \frac{\Delta}{3} - \frac{9\kappa \lambda}{4}$$

$$c_1 = \frac{d_1}{|d_1|} \sqrt{d_1^2 / (d_1^2 + d_2^2 + d_3^2)}$$

$$c_2 = \frac{d_2}{|d_2|} \sqrt{d_2^2 / (d_1^2 + d_2^2 + d_3^2)}$$

$$c_3 = \frac{d_3}{|d_3|} \sqrt{d_3^2 / (d_1^2 + d_2^2 + d_3^2)}$$

$$c_4 = \frac{d_4}{|d_4|} \sqrt{d_4^2 / (d_4^2 + d_5^2)}$$

$$c_5 = \frac{d_5}{|d_5|} \sqrt{d_5^2 / (d_4^2 + d_5^2)}$$

$$c_6 = \frac{d_6}{|d_6|} \sqrt{d_6^2 / (d_6^2 + d_7^2 + d_8^2)}$$

$$c_7 = \frac{d_7}{|d_7|} \sqrt{d_7^2 / (d_6^2 + d_7^2 + d_8^2)}$$

$$c_8 = \frac{d_8}{|d_8|} \sqrt{d_8^2 / (d_6^2 + d_7^2 + d_8^2)}$$

$$c_9 = \frac{d_9}{|d_9|} \sqrt{d_9^2 / (d_9^2 + d_{10}^2 + d_{11}^2)}$$

$$c_{10} = \frac{d_{10}}{|d_{10}|} \sqrt{d_{10}^2 / (d_9^2 + d_{10}^2 + d_{11}^2)}$$

$$c_{11} = \frac{d_{11}}{|d_{11}|} \sqrt{d_{11}^2 / (d_9^2 + d_{10}^2 + d_{11}^2)}$$

$$c_{12} = \frac{d_{12}}{|d_{12}|} \sqrt{d_{12}^2 / (d_{12}^2 + d_{13}^2)}$$

$$c_{13} = \frac{d_{13}}{|d_{13}|} \sqrt{d_{13}^2 / (d_{12}^2 + d_{13}^2)}$$

$$d_1 = \sqrt{6}/V_1$$

$$d_2 = -1$$

$$d_3 = \sqrt{8}/(V_1 + 2)$$

$$d_4 = 1$$

$$d_5 = \frac{3 - 4v - \sqrt{225 - 24v + 16v^2}}{6\sqrt{6}}$$

$$d_6 = \sqrt{6}/V_2$$

$$d_7 = -1$$

$$d_8 = \sqrt{8}/(V_2 + 2)$$

$$d_9 = \sqrt{6}/V_3$$

$$d_{10} = -1$$

$$d_{11} = \sqrt{8}/(V_3 + 2)$$

$$d_{12} = 1$$

$$d_{13} = \frac{3 - 4v + \sqrt{225 - 24v + 16v^2}}{6\sqrt{6}}$$

$$\begin{aligned}
q &= -18225 - 2484v - 1161v^2 - 72v^3 - 16v^4 \\
V_1 &= \frac{-15 - 4v}{9} - \\
&\quad \frac{-441 - 48v - 16v^2}{9\sqrt[3]{-3861 - 2376v - 288v^2 - 64v^3 + 36\sqrt{3}\sqrt{q}}} + \\
&\quad \frac{\sqrt[3]{-3861 - 2376v - 288v^2 - 64v^3 + 36\sqrt{3}\sqrt{q}}}{9}
\end{aligned}$$

$$\begin{aligned}
w &= -18225 - 2484v - 1161v^2 - 72v^3 - 16v^4 \\
V_2 &= \frac{-15 - 4v}{9} + \\
&\quad \frac{(1 - \sqrt{3}i)(-441 - 48v - 16v^2)}{18\sqrt[3]{-3861 - 2376v - 288v^2 - 64v^3 + 36\sqrt{3}\sqrt{w}}} - \\
&\quad \frac{(1 + \sqrt{3}i)\sqrt[3]{-3861 - 2376v - 288v^2 - 64v^3 + 36\sqrt{3}\sqrt{w}}}{18}
\end{aligned}$$

$$\begin{aligned}
k &= -18225 - 2484v - 1161v^2 - 72v^3 - 16v^4 \\
V_3 &= \frac{-15 - 4v}{9} + \\
&\quad \frac{(1 + \sqrt{3}i)(-441 - 48v - 16v^2)}{18\sqrt[3]{-3861 - 2376v - 288v^2 - 64v^3 + 36\sqrt{3}\sqrt{k}}} - \\
&\quad \frac{(1 - \sqrt{3}i)\sqrt[3]{-3861 - 2376v - 288v^2 - 64v^3 + 36\sqrt{3}\sqrt{k}}}{18}
\end{aligned}$$

$$E_{z,1}^{(1)} = -E_{z,-1}^{(1)} = \frac{1}{2} c_2^2 g_e \beta + c_3^2 \beta \left(-\frac{g_e}{2} - \frac{3\kappa}{2} \right) + c_1^2 \beta \left(\frac{3g_e}{2} + \frac{3\kappa}{2} \right)$$

$$E_{z,2}^{(1)} = -E_{z,-2}^{(1)} = \frac{3}{2} c_4^2 g_e \beta + c_5^2 \beta \left(\frac{g_e}{2} - \frac{3\kappa}{2} \right)$$

$$E_{z,3}^{(1)} = -E_{z,-3}^{(1)} = \frac{1}{2} c_7^2 g_e \beta + c_8^2 \beta \left(-\frac{g_e}{2} - \frac{3\kappa}{2} \right) + c_6^2 \beta \left(\frac{3g_e}{2} + \frac{3\kappa}{2} \right)$$

$$E_{z,4}^{(1)} = -E_{z,-4}^{(1)} = \frac{1}{2} c_{10}^2 g_e \beta + c_{11}^2 \beta \left(-\frac{g_e}{2} - \frac{3\kappa}{2}\right) + c_9^2 \beta \left(\frac{3g_e}{2} + \frac{3\kappa}{2}\right)$$

$$E_{z,5}^{(1)} = -E_{z,-5}^{(1)} = \frac{3}{2} c_{12}^2 g_e \beta + c_{13}^2 \beta \left(\frac{g_e}{2} - \frac{3\kappa}{2}\right)$$

$$E_{z,6}^{(1)} = -E_{z,-6}^{(1)} = \beta \left(\frac{3g_e}{2} - \frac{3\kappa}{2}\right)$$

$$\begin{aligned} E_{z,\pm 1}^{(2)} = & \left[\frac{1}{2} c_2 c_7 g_e \beta + c_3 c_8 \beta \left(-\frac{g_e}{2} - \frac{3\kappa}{2}\right) + c_1 c_6 \beta \left(\frac{3g_e}{2} + \frac{3\kappa}{2}\right) \right]^2 / \\ & \left[-\frac{2c_2^2 \Delta}{3} + \frac{2c_7^2 \Delta}{3} - 3\sqrt{\frac{3}{2}} c_1 c_2 \kappa \lambda - 3\sqrt{2} c_2 c_3 \kappa \lambda + 3\sqrt{\frac{3}{2}} c_6 c_7 \kappa \lambda + 3\sqrt{2} c_7 c_8 \kappa \lambda + \right. \\ & \left. c_3^2 \left(\frac{\Delta}{3} + \frac{3\kappa \lambda}{4}\right) - c_8^2 \left(\frac{\Delta}{3} + \frac{3\kappa \lambda}{4}\right) + c_1^2 \left(\frac{\Delta}{3} + \frac{9\kappa \lambda}{4}\right) - c_6^2 \left(\frac{\Delta}{3} + \frac{9\kappa \lambda}{4}\right) \right] + \\ & \left[\frac{1}{2} c_2 c_{10} g_e \beta + c_3 c_{11} \beta \left(-\frac{g_e}{2} - \frac{3\kappa}{2}\right) + c_1 c_9 \beta \left(\frac{3g_e}{2} + \frac{3\kappa}{2}\right) \right]^2 / \\ & \left[-\frac{2c_2^2 \Delta}{3} + \frac{2c_{10}^2 \Delta}{3} - 3\sqrt{\frac{3}{2}} c_1 c_2 \kappa \lambda - 3\sqrt{2} c_2 c_3 \kappa \lambda + 3\sqrt{\frac{3}{2}} c_9 c_{10} \kappa \lambda + 3\sqrt{2} c_{10} c_{11} \kappa \lambda + \right. \\ & \left. c_3^2 \left(\frac{\Delta}{3} + \frac{3\kappa \lambda}{4}\right) - c_{11}^2 \left(\frac{\Delta}{3} + \frac{3\kappa \lambda}{4}\right) + c_1^2 \left(\frac{\Delta}{3} + \frac{9\kappa \lambda}{4}\right) - c_9^2 \left(\frac{\Delta}{3} + \frac{9\kappa \lambda}{4}\right) \right] \end{aligned}$$

$$\begin{aligned} E_{z,\pm 2}^{(2)} = & \left[\frac{3}{2} c_4 c_{12} g_e \beta + c_5 c_{13} \beta \left(\frac{g_e}{2} - \frac{3\kappa}{2}\right) \right]^2 / \\ & \left[-\frac{2c_4^2 \Delta}{3} + \frac{2c_{12}^2 \Delta}{3} - 3\sqrt{\frac{3}{2}} c_4 c_5 \kappa \lambda + 3\sqrt{\frac{3}{2}} c_{12} c_{13} \kappa \lambda + c_5^2 \left(\frac{\Delta}{3} - \frac{3\kappa \lambda}{4}\right) - c_{13}^2 \left(\frac{\Delta}{3} - \frac{3\kappa \lambda}{4}\right) \right] \end{aligned}$$

$$\begin{aligned}
E_{z,\pm 3}^{(2)} = & \left[\frac{1}{2} c_2 c_7 g_e \beta + c_3 c_8 \beta \left(-\frac{g_e}{2} - \frac{3\kappa}{2} \right) + c_1 c_6 \beta \left(\frac{3g_e}{2} + \frac{3\kappa}{2} \right) \right]^2 / \\
& \left[\frac{2c_2^2 \Delta}{3} - \frac{2c_7^2 \Delta}{3} + 3\sqrt{\frac{3}{2}} c_1 c_2 \kappa \lambda + 3\sqrt{2} c_2 c_3 \kappa \lambda - 3\sqrt{\frac{3}{2}} c_6 c_7 \kappa \lambda - 3\sqrt{2} c_7 c_8 \kappa \lambda - \right. \\
& c_3^2 \left(\frac{\Delta}{3} + \frac{3\kappa \lambda}{4} \right) + c_8^2 \left(\frac{\Delta}{3} + \frac{3\kappa \lambda}{4} \right) - c_1^2 \left(\frac{\Delta}{3} + \frac{9\kappa \lambda}{4} \right) + c_6^2 \left(\frac{\Delta}{3} + \frac{9\kappa \lambda}{4} \right) \Big] + \\
& \left[\frac{1}{2} c_7 c_{10} g_e \beta + c_8 c_{11} \beta \left(-\frac{g_e}{2} - \frac{3\kappa}{2} \right) + c_6 c_9 \beta \left(\frac{3g_e}{2} + \frac{3\kappa}{2} \right) \right]^2 / \\
& \left[-\frac{2c_7^2 \Delta}{3} + \frac{2c_{10}^2 \Delta}{3} - 3\sqrt{\frac{3}{2}} c_6 c_7 \kappa \lambda - 3\sqrt{2} c_7 c_8 \kappa \lambda + 3\sqrt{\frac{3}{2}} c_9 c_{10} \kappa \lambda + 3\sqrt{2} c_{10} c_{11} \kappa \lambda + \right. \\
& c_8^2 \left(\frac{\Delta}{3} + \frac{3\kappa \lambda}{4} \right) - c_{11}^2 \left(\frac{\Delta}{3} + \frac{3\kappa \lambda}{4} \right) + c_6^2 \left(\frac{\Delta}{3} + \frac{9\kappa \lambda}{4} \right) - c_9^2 \left(\frac{\Delta}{3} + \frac{9\kappa \lambda}{4} \right) \Big]
\end{aligned}$$

$$\begin{aligned}
E_{z,\pm 4}^{(2)} = & \left[\frac{1}{2} c_2 c_{10} g_e \beta + c_3 c_{11} \beta \left(-\frac{g_e}{2} - \frac{3\kappa}{2} \right) + c_1 c_9 \beta \left(\frac{3g_e}{2} + \frac{3\kappa}{2} \right) \right]^2 / \\
& \left[\frac{2c_2^2 \Delta}{3} - \frac{2c_{10}^2 \Delta}{3} + 3\sqrt{\frac{3}{2}} c_1 c_2 \kappa \lambda + 3\sqrt{2} c_2 c_3 \kappa \lambda - 3\sqrt{\frac{3}{2}} c_9 c_{10} \kappa \lambda - 3\sqrt{2} c_{10} c_{11} \kappa \lambda - \right. \\
& c_3^2 \left(\frac{\Delta}{3} + \frac{3\kappa \lambda}{4} \right) + c_{11}^2 \left(\frac{\Delta}{3} + \frac{3\kappa \lambda}{4} \right) - c_1^2 \left(\frac{\Delta}{3} + \frac{9\kappa \lambda}{4} \right) + c_9^2 \left(\frac{\Delta}{3} + \frac{9\kappa \lambda}{4} \right) \Big] + \\
& \left[\frac{1}{2} c_7 c_{10} g_e \beta + c_8 c_{11} \beta \left(-\frac{g_e}{2} - \frac{3\kappa}{2} \right) + c_6 c_9 \beta \left(\frac{3g_e}{2} + \frac{3\kappa}{2} \right) \right]^2 / \\
& \left[\frac{2c_7^2 \Delta}{3} - \frac{2c_{10}^2 \Delta}{3} + 3\sqrt{\frac{3}{2}} c_6 c_7 \kappa \lambda + 3\sqrt{2} c_7 c_8 \kappa \lambda - 3\sqrt{\frac{3}{2}} c_9 c_{10} \kappa \lambda - 3\sqrt{2} c_{10} c_{11} \kappa \lambda - \right. \\
& c_8^2 \left(\frac{\Delta}{3} + \frac{3\kappa \lambda}{4} \right) + c_{11}^2 \left(\frac{\Delta}{3} + \frac{3\kappa \lambda}{4} \right) - c_6^2 \left(\frac{\Delta}{3} + \frac{9\kappa \lambda}{4} \right) + c_9^2 \left(\frac{\Delta}{3} + \frac{9\kappa \lambda}{4} \right) \Big]
\end{aligned}$$

$$\begin{aligned}
E_{z,\pm 5}^{(2)} = & \left[\frac{3}{2} c_4 c_{12} g_e \beta + c_5 c_{13} \beta \left(\frac{g_e}{2} - \frac{3\kappa}{2} \right) \right]^2 / \\
& \left[\frac{2c_4^2 \Delta}{3} - \frac{2c_{12}^2 \Delta}{3} + 3\sqrt{\frac{3}{2}} c_4 c_5 \kappa \lambda - 3\sqrt{\frac{3}{2}} c_{12} c_{13} \kappa \lambda - c_5^2 \left(\frac{\Delta}{3} - \frac{3\kappa \lambda}{4} \right) + c_{13}^2 \left(\frac{\Delta}{3} - \frac{3\kappa \lambda}{4} \right) \right]
\end{aligned}$$

$$E_{z,\pm 6}^{(2)} = 0$$

$$E_{x,1}^{(1)} = -E_{x,-1}^{(1)} = c_2^2 g_e \beta + \sqrt{3} c_1 c_3 g_e \beta - \frac{3c_2 c_3 \beta \kappa}{\sqrt{2}}$$

$$E_{x,\pm 2}^{(1)} = 0$$

$$E_{x,3}^{(1)} = -E_{x,-3}^{(1)} = c_7^2 g_e \beta + \sqrt{3} c_6 c_8 g_e \beta - \frac{3 c_7 c_8 \beta \kappa}{\sqrt{2}}$$

$$E_{x,4}^{(1)} = -E_{x,-4}^{(1)} = c_{10}^2 g_e \beta + \sqrt{3} c_9 c_{11} g_e \beta - \frac{3 c_{10} c_{11} \beta \kappa}{\sqrt{2}}$$

$$E_{x,\pm 5}^{(1)} = 0$$

$$E_{x,\pm 6}^{(1)} = 0$$

$$\begin{aligned}
E_{x,\pm 1}^{(2)} = & \left(\frac{1}{2} \sqrt{3} c_2 c_4 g_e \beta + c_3 c_5 g_e \beta - \frac{3 c_1 c_4 \beta \kappa}{2 \sqrt{2}} - \frac{3 c_2 c_5 \beta \kappa}{2 \sqrt{2}} \right)^2 / \\
& \left[-\frac{2 c_2^2 \Delta}{3} + \frac{2 c_4^2 \Delta}{3} - 3 \sqrt{\frac{3}{2}} c_1 c_2 \kappa \lambda - 3 \sqrt{2} c_2 c_3 \kappa \lambda + 3 \sqrt{\frac{3}{2}} c_4 c_5 \kappa \lambda - \right. \\
& \left. c_5^2 \left(\frac{\Delta}{3} - \frac{3 \kappa \lambda}{4} \right) + c_3^2 \left(\frac{\Delta}{3} + \frac{3 \kappa \lambda}{4} \right) + c_1^2 \left(\frac{\Delta}{3} + \frac{9 \kappa \lambda}{4} \right) \right] + \\
& \left(\frac{1}{2} \sqrt{3} c_2 c_{12} g_e \beta + c_3 c_{13} g_e \beta - \frac{3 c_1 c_{13} \beta \kappa}{2 \sqrt{2}} - \frac{3 c_2 c_{13} \beta \kappa}{2 \sqrt{2}} \right)^2 / \\
& \left[-\frac{2 c_2^2 \Delta}{3} + \frac{2 c_{12}^2 \Delta}{3} - 3 \sqrt{\frac{3}{2}} c_1 c_2 \kappa \lambda - 3 \sqrt{2} c_2 c_3 \kappa \lambda + 3 \sqrt{\frac{3}{2}} c_{12} c_{13} \kappa \lambda - \right. \\
& \left. c_{13}^2 \left(\frac{\Delta}{3} - \frac{3 \kappa \lambda}{4} \right) + c_3^2 \left(\frac{\Delta}{3} + \frac{3 \kappa \lambda}{4} \right) + c_1^2 \left(\frac{\Delta}{3} + \frac{9 \kappa \lambda}{4} \right) \right] + \\
& \left(c_2 c_7 g_e \beta + \frac{1}{2} \sqrt{3} (c_3 c_6 + c_1 c_8) g_e \beta - \frac{3 (c_3 c_7 + c_2 c_8) \beta \kappa}{2 \sqrt{2}} \right)^2 / \\
& \left[-\frac{2 c_2^2 \Delta}{3} + \frac{2 c_7^2 \Delta}{3} - 3 \sqrt{\frac{3}{2}} c_1 c_2 \kappa \lambda - 3 \sqrt{2} c_2 c_3 \kappa \lambda + 3 \sqrt{\frac{3}{2}} c_6 c_7 \kappa \lambda + 3 \sqrt{2} c_7 c_8 \kappa \lambda + \right. \\
& \left. c_3^2 \left(\frac{\Delta}{3} + \frac{3 \kappa \lambda}{4} \right) - c_8^2 \left(\frac{\Delta}{3} + \frac{3 \kappa \lambda}{4} \right) + c_1^2 \left(\frac{\Delta}{3} + \frac{9 \kappa \lambda}{4} \right) - c_6^2 \left(\frac{\Delta}{3} + \frac{9 \kappa \lambda}{4} \right) \right] + \\
& \left(c_2 c_{10} g_e \beta + \frac{1}{2} \sqrt{3} (c_3 c_9 + c_1 c_{11}) g_e \beta - \frac{3 (c_3 c_{10} + c_2 c_{11}) \beta \kappa}{2 \sqrt{2}} \right)^2 / \\
& \left[-\frac{2 c_2^2 \Delta}{3} + \frac{2 c_{10}^2 \Delta}{3} - 3 \sqrt{\frac{3}{2}} c_1 c_2 \kappa \lambda - 3 \sqrt{2} c_2 c_3 \kappa \lambda + 3 \sqrt{\frac{3}{2}} c_9 c_{10} \kappa \lambda + 3 \sqrt{2} c_{10} c_{11} \kappa \lambda + \right. \\
& \left. c_3^2 \left(\frac{\Delta}{3} + \frac{3 \kappa \lambda}{4} \right) - c_{11}^2 \left(\frac{\Delta}{3} + \frac{3 \kappa \lambda}{4} \right) + c_1^2 \left(\frac{\Delta}{3} + \frac{9 \kappa \lambda}{4} \right) - c_9^2 \left(\frac{\Delta}{3} + \frac{9 \kappa \lambda}{4} \right) \right]
\end{aligned}$$

$$\begin{aligned}
E_{x,\pm 2}^{(2)} = & \left(\frac{1}{2} \sqrt{3} c_5 g_e \beta - \frac{3 c_4 \beta \kappa}{2 \sqrt{2}} \right)^2 / \\
& \left[-\frac{\Delta}{3} - \frac{2 c_4^2 \Delta}{3} + \frac{9 \kappa \lambda}{4} - 3 \sqrt{\frac{3}{2}} c_4 c_5 \kappa \lambda + c_5^2 \left(\frac{\Delta}{3} - \frac{3 \kappa \lambda}{4} \right) \right] + \\
& \left(\frac{1}{2} \sqrt{3} c_2 c_4 g_e \beta + c_3 c_5 g_e \beta - \frac{3 c_1 c_4 \beta \kappa}{2 \sqrt{2}} - \frac{3 c_2 c_5 \beta \kappa}{2 \sqrt{2}} \right)^2 / \\
& \left[\frac{2 c_2^2 \Delta}{3} - \frac{2 c_4^2 \Delta}{3} + 3 \sqrt{\frac{3}{2}} c_1 c_2 \kappa \lambda + 3 \sqrt{2} c_2 c_3 \kappa \lambda - 3 \sqrt{\frac{3}{2}} c_4 c_5 \kappa \lambda + \right. \\
& \left. c_5^2 \left(\frac{\Delta}{3} - \frac{3 \kappa \lambda}{4} \right) - c_3^2 \left(\frac{\Delta}{3} + \frac{3 \kappa \lambda}{4} \right) - c_1^2 \left(\frac{\Delta}{3} + \frac{9 \kappa \lambda}{4} \right) \right] + \\
& \left(\frac{1}{2} \sqrt{3} c_4 c_7 g_e \beta + c_5 c_8 g_e \beta - \frac{3 c_4 c_6 \beta \kappa}{2 \sqrt{2}} - \frac{3 c_5 c_7 \beta \kappa}{2 \sqrt{2}} \right)^2 / \\
& \left[-\frac{2 c_4^2 \Delta}{3} + \frac{2 c_7^2 \Delta}{3} - 3 \sqrt{\frac{3}{2}} c_4 c_5 \kappa \lambda + 3 \sqrt{\frac{3}{2}} c_6 c_7 \kappa \lambda + 3 \sqrt{2} c_7 c_8 \kappa \lambda + \right. \\
& \left. c_5^2 \left(\frac{\Delta}{3} - \frac{3 \kappa \lambda}{4} \right) - c_8^2 \left(\frac{\Delta}{3} + \frac{3 \kappa \lambda}{4} \right) - c_6^2 \left(\frac{\Delta}{3} + \frac{9 \kappa \lambda}{4} \right) \right] + \\
& \left(\frac{1}{2} \sqrt{3} c_4 c_{10} g_e \beta + c_5 c_{11} g_e \beta - \frac{3 c_4 c_9 \beta \kappa}{2 \sqrt{2}} - \frac{3 c_5 c_{10} \beta \kappa}{2 \sqrt{2}} \right)^2 / \\
& \left[-\frac{2 c_4^2 \Delta}{3} + \frac{2 c_{10}^2 \Delta}{3} - 3 \sqrt{\frac{3}{2}} c_4 c_5 \kappa \lambda + 3 \sqrt{\frac{3}{2}} c_9 c_{10} \kappa \lambda + 3 \sqrt{2} c_{10} c_{11} \kappa \lambda + \right. \\
& \left. c_5^2 \left(\frac{\Delta}{3} - \frac{3 \kappa \lambda}{4} \right) - c_{11}^2 \left(\frac{\Delta}{3} + \frac{3 \kappa \lambda}{4} \right) - c_9^2 \left(\frac{\Delta}{3} + \frac{9 \kappa \lambda}{4} \right) \right]
\end{aligned}$$

$$\begin{aligned}
E_{x,\pm 3}^{(2)} = & \left(\frac{1}{2} \sqrt{3} c_4 c_7 g_e \beta + c_5 c_8 g_e \beta - \frac{3 c_4 c_6 \beta \kappa}{2 \sqrt{2}} - \frac{3 c_5 c_7 \beta \kappa}{2 \sqrt{2}} \right)^2 / \\
& \left[\frac{2 c_4^2 \Delta}{3} - \frac{2 c_7^2 \Delta}{3} + 3 \sqrt{\frac{3}{2}} c_4 c_5 \kappa \lambda - 3 \sqrt{\frac{3}{2}} c_6 c_7 \kappa \lambda - 3 \sqrt{2} c_7 c_8 \kappa \lambda - \right. \\
& \left. c_5^2 \left(\frac{\Delta}{3} - \frac{3 \kappa \lambda}{4} \right) + c_8^2 \left(\frac{\Delta}{3} + \frac{3 \kappa \lambda}{4} \right) + c_6^2 \left(\frac{\Delta}{3} + \frac{9 \kappa \lambda}{4} \right) \right] + \\
& \left(\frac{1}{2} \sqrt{3} c_7 c_{12} g_e \beta + c_8 c_{13} g_e \beta - \frac{3 c_6 c_{12} \beta \kappa}{2 \sqrt{2}} - \frac{3 c_7 c_{13} \beta \kappa}{2 \sqrt{2}} \right)^2 / \\
& \left[-\frac{2 c_7^2 \Delta}{3} + \frac{2 c_{12}^2 \Delta}{3} - 3 \sqrt{\frac{3}{2}} c_6 c_7 \kappa \lambda - 3 \sqrt{2} c_7 c_8 \kappa \lambda + 3 \sqrt{\frac{3}{2}} c_{12} c_{13} \kappa \lambda - \right. \\
& \left. c_{13}^2 \left(\frac{\Delta}{3} - \frac{3 \kappa \lambda}{4} \right) + c_8^2 \left(\frac{\Delta}{3} + \frac{3 \kappa \lambda}{4} \right) + c_6^2 \left(\frac{\Delta}{3} + \frac{9 \kappa \lambda}{4} \right) \right] + \\
& \left(c_2 c_7 g_e \beta + \frac{1}{2} \sqrt{3} (c_3 c_6 + c_1 c_8) g_e \beta - \frac{3 (c_3 c_7 + c_2 c_8) \beta \kappa}{2 \sqrt{2}} \right)^2 / \\
& \left[\frac{2 c_2^2 \Delta}{3} - \frac{2 c_7^2 \Delta}{3} + 3 \sqrt{\frac{3}{2}} c_1 c_2 \kappa \lambda + 3 \sqrt{2} c_2 c_3 \kappa \lambda - 3 \sqrt{\frac{3}{2}} c_6 c_7 \kappa \lambda - 3 \sqrt{2} c_7 c_8 \kappa \lambda - \right. \\
& \left. c_3^2 \left(\frac{\Delta}{3} + \frac{3 \kappa \lambda}{4} \right) + c_8^2 \left(\frac{\Delta}{3} + \frac{3 \kappa \lambda}{4} \right) - c_1^2 \left(\frac{\Delta}{3} + \frac{9 \kappa \lambda}{4} \right) + c_6^2 \left(\frac{\Delta}{3} + \frac{9 \kappa \lambda}{4} \right) \right] + \\
& \left(c_7 c_{10} g_e \beta + \frac{1}{2} \sqrt{3} (c_8 c_9 + c_6 c_{11}) g_e \beta - \frac{3 (c_8 c_{10} + c_7 c_{11}) \beta \kappa}{2 \sqrt{2}} \right)^2 / \\
& \left[-\frac{2 c_7^2 \Delta}{3} + \frac{2 c_{10}^2 \Delta}{3} - 3 \sqrt{\frac{3}{2}} c_6 c_7 \kappa \lambda - 3 \sqrt{2} c_7 c_8 \kappa \lambda + 3 \sqrt{\frac{3}{2}} c_9 c_{10} \kappa \lambda + 3 \sqrt{2} c_{10} c_{11} \kappa \lambda + \right. \\
& \left. c_8^2 \left(\frac{\Delta}{3} + \frac{3 \kappa \lambda}{4} \right) - c_{11}^2 \left(\frac{\Delta}{3} + \frac{3 \kappa \lambda}{4} \right) + c_6^2 \left(\frac{\Delta}{3} + \frac{9 \kappa \lambda}{4} \right) - c_9^2 \left(\frac{\Delta}{3} + \frac{9 \kappa \lambda}{4} \right) \right]
\end{aligned}$$

$$\begin{aligned}
E_{x,\pm 4}^{(2)} = & \left(\frac{1}{2} \sqrt{3} c_4 c_{10} g_e \beta + c_5 c_{11} g_e \beta - \frac{3 c_4 c_9 \beta \kappa}{2 \sqrt{2}} - \frac{3 c_5 c_{10} \beta \kappa}{2 \sqrt{2}} \right) / \\
& \left[\frac{2 c_4^2 \Delta}{3} - \frac{2 c_{10}^2 \Delta}{3} + 3 \sqrt{\frac{3}{2}} c_4 c_5 \kappa \lambda - 3 \sqrt{\frac{3}{2}} c_9 c_{10} \kappa \lambda - 3 \sqrt{2} c_{10} c_{11} \kappa \lambda - \right. \\
& \left. c_5^2 \left(\frac{\Delta}{3} - \frac{3 \kappa \lambda}{4} \right) + c_{11}^2 \left(\frac{\Delta}{3} + \frac{3 \kappa \lambda}{4} \right) + c_9^2 \left(\frac{\Delta}{3} + \frac{9 \kappa \lambda}{4} \right) \right] + \\
& \left(\frac{1}{2} \sqrt{3} c_{10} c_{12} g_e \beta + c_{11} c_{13} g_e \beta - \frac{3 c_9 c_{12} \beta \kappa}{2 \sqrt{2}} - \frac{3 c_{10} c_{13} \beta \kappa}{2 \sqrt{2}} \right) / \\
& \left[-\frac{2 c_{10}^2 \Delta}{3} + \frac{2 c_{12}^2 \Delta}{3} - 3 \sqrt{\frac{3}{2}} c_9 c_{10} \kappa \lambda - 3 \sqrt{2} c_{10} c_{11} \kappa \lambda + 3 \sqrt{\frac{3}{2}} c_{12} c_{13} \kappa \lambda - \right. \\
& \left. c_{13}^2 \left(\frac{\Delta}{3} - \frac{3 \kappa \lambda}{4} \right) + c_{11}^2 \left(\frac{\Delta}{3} + \frac{3 \kappa \lambda}{4} \right) + c_9^2 \left(\frac{\Delta}{3} + \frac{9 \kappa \lambda}{4} \right) \right] + \\
& \left(c_2 c_{10} g_e \beta + \frac{1}{2} \sqrt{3} (c_3 c_9 + c_1 c_{11}) g_e \beta - \frac{3 (c_3 c_{10} + c_2 c_{11}) \beta \kappa}{2 \sqrt{2}} \right) / \\
& \left[\frac{2 c_2^2 \Delta}{3} - \frac{2 c_{10}^2 \Delta}{3} + 3 \sqrt{\frac{3}{2}} c_1 c_2 \kappa \lambda + 3 \sqrt{2} c_2 c_3 \kappa \lambda - 3 \sqrt{\frac{3}{2}} c_9 c_{10} \kappa \lambda - 3 \sqrt{2} c_{10} c_{11} \kappa \lambda - \right. \\
& \left. c_3^2 \left(\frac{\Delta}{3} + \frac{3 \kappa \lambda}{4} \right) + c_{12}^2 \left(\frac{\Delta}{3} + \frac{3 \kappa \lambda}{4} \right) - c_1^2 \left(\frac{\Delta}{3} + \frac{9 \kappa \lambda}{4} \right) + c_9^2 \left(\frac{\Delta}{3} + \frac{9 \kappa \lambda}{4} \right) \right] + \\
& \left(c_7 c_{10} g_e \beta + \frac{1}{2} \sqrt{3} (c_8 c_9 + c_6 c_{11}) g_e \beta - \frac{3 (c_8 c_{10} + c_7 c_{11}) \beta \kappa}{2 \sqrt{2}} \right) / \\
& \left[\frac{2 c_7^2 \Delta}{3} - \frac{2 c_{10}^2 \Delta}{3} + 3 \sqrt{\frac{3}{2}} c_6 c_7 \kappa \lambda + 3 \sqrt{2} c_7 c_8 \kappa \lambda - 3 \sqrt{\frac{3}{2}} c_9 c_{10} \kappa \lambda - 3 \sqrt{2} c_{10} c_{11} \kappa \lambda - \right. \\
& \left. c_8^2 \left(\frac{\Delta}{3} + \frac{3 \kappa \lambda}{4} \right) + c_{11}^2 \left(\frac{\Delta}{3} + \frac{3 \kappa \lambda}{4} \right) - c_6^2 \left(\frac{\Delta}{3} + \frac{9 \kappa \lambda}{4} \right) + c_9^2 \left(\frac{\Delta}{3} + \frac{9 \kappa \lambda}{4} \right) \right]
\end{aligned}$$

$$\begin{aligned}
E_{x,\pm 5}^{(2)} = & \left(\frac{1}{2} \sqrt{3} c_{13} g_e \beta - \frac{3 c_{12} \beta \kappa}{2 \sqrt{2}} \right)^2 / \\
& \left[-\frac{\Delta}{3} - \frac{2 c_{12}^2 \Delta}{3} + \frac{9 \kappa \lambda}{4} - 3 \sqrt{\frac{3}{2}} c_{12} c_{13} \kappa \lambda + c_{13}^2 \left(\frac{\Delta}{3} - \frac{3 \kappa \lambda}{4} \right) \right] + \\
& \left(\frac{1}{2} \sqrt{3} c_2 c_{12} g_e \beta + c_3 c_{13} g_e \beta - \frac{3 c_1 c_{12} \beta \kappa}{2 \sqrt{2}} - \frac{3 c_2 c_{13} \beta \kappa}{2 \sqrt{2}} \right)^2 / \\
& \left[\frac{2 c_2^2 \Delta}{3} - \frac{2 c_{12}^2 \Delta}{3} + 3 \sqrt{\frac{3}{2}} c_1 c_2 \kappa \lambda + 3 \sqrt{2} c_2 c_3 \kappa \lambda - 3 \sqrt{\frac{3}{2}} c_{12} c_{13} \kappa \lambda + \right. \\
& \left. c_{13}^2 \left(\frac{\Delta}{3} - \frac{3 \kappa \lambda}{4} \right) - c_3^2 \left(\frac{\Delta}{3} + \frac{3 \kappa \lambda}{4} \right) - c_1^2 \left(\frac{\Delta}{3} + \frac{9 \kappa \lambda}{4} \right) \right] + \\
& \left(\frac{1}{2} \sqrt{3} c_7 c_{12} g_e \beta + c_8 c_{13} g_e \beta - \frac{3 c_6 c_{12} \beta \kappa}{2 \sqrt{2}} - \frac{3 c_7 c_{13} \beta \kappa}{2 \sqrt{2}} \right)^2 / \\
& \left[\frac{2 c_7^2 \Delta}{3} - \frac{2 c_{12}^2 \Delta}{3} + 3 \sqrt{\frac{3}{2}} c_6 c_7 \kappa \lambda + 3 \sqrt{2} c_7 c_8 \kappa \lambda - 3 \sqrt{\frac{3}{2}} c_{12} c_{13} \kappa \lambda + \right. \\
& \left. c_{13}^2 \left(\frac{\Delta}{3} - \frac{3 \kappa \lambda}{4} \right) - c_8^2 \left(\frac{\Delta}{3} + \frac{3 \kappa \lambda}{4} \right) - c_6^2 \left(\frac{\Delta}{3} + \frac{9 \kappa \lambda}{4} \right) \right] + \\
& \left(\frac{1}{2} \sqrt{3} c_{10} c_{12} g_e \beta + c_{11} c_{13} g_e \beta - \frac{3 c_9 c_{12} \beta \kappa}{2 \sqrt{2}} - \frac{3 c_{10} c_{13} \beta \kappa}{2 \sqrt{2}} \right)^2 / \\
& \left[\frac{2 c_{10}^2 \Delta}{3} - \frac{2 c_{12}^2 \Delta}{3} + 3 \sqrt{\frac{3}{2}} c_9 c_{10} \kappa \lambda + 3 \sqrt{2} c_{10} c_{11} \kappa \lambda - 3 \sqrt{\frac{3}{2}} c_{12} c_{13} \kappa \lambda + \right. \\
& \left. c_{13}^2 \left(\frac{\Delta}{3} - \frac{3 \kappa \lambda}{4} \right) - c_{11}^2 \left(\frac{\Delta}{3} + \frac{3 \kappa \lambda}{4} \right) - c_9^2 \left(\frac{\Delta}{3} + \frac{9 \kappa \lambda}{4} \right) \right]
\end{aligned}$$

$$\begin{aligned}
E_{x,\pm 6}^{(2)} = & \left(\frac{1}{2} \sqrt{3} c_5 g_e \beta - \frac{3 c_4 \beta \kappa}{2 \sqrt{2}} \right)^2 / \\
& \left[\frac{\Delta}{3} + \frac{2 c_4^2 \Delta}{3} - \frac{9 \kappa \lambda}{4} + 3 \sqrt{\frac{3}{2}} c_4 c_5 \kappa \lambda - c_5^2 \left(\frac{\Delta}{3} - \frac{3 \kappa \lambda}{4} \right) \right] + \\
& \left(\frac{1}{2} \sqrt{3} c_{13} g_e \beta - \frac{3 c_{12} \beta \kappa}{2 \sqrt{2}} \right)^2 / \\
& \left[\frac{\Delta}{3} + \frac{2 c_{12}^2 \Delta}{3} - \frac{9 \kappa \lambda}{4} + 3 \sqrt{\frac{3}{2}} c_{12} c_{13} \kappa \lambda - c_{13}^2 \left(\frac{\Delta}{3} - \frac{3 \kappa \lambda}{4} \right) \right]
\end{aligned}$$

References

1. Boyd, E. A.; Boyd, M. E. K.; Kerrigan, F. *Tetrahedron Lett.* **1996**, 37, 5425-5426.
2. Bain, G. A.; Berry, J. F. *J. Chem. Educ.* **2008**, 85, 532.
3. Sakiyama, H. *Inorg. Chim. Acta* **2006**, 359, 2097-2100.

Chapter 5 Conclusion

1.1 Conclusion

This dissertation has primarily dealt with the coordination chemistry of bis(benzyl)phosphinate with vanadium, tungsten and cobalt. Our interest in the coordination chemistry of the bis(benzyl)phosphinate ligand stems from our assumption that it is sterically unique when compared to other phosphinates and should yield new coordination compounds. Although only the synthesis and physical properties of these compounds were explored in this work, the catalytic applications of these compounds remain to be discovered.

VO(acac)₂ reacted with bis(benzyl)phosphinic acid in the presence of water or pyridine to form (V₃(μ₃-O)O₂)(μ₂-O₂P(CH₂C₆H₅)₂)₆(H₂O)(**1**) or (V₃(μ₃-O)O₂)(μ₂-O₂P(CH₂C₆H₅)₂)₆(py)(**2**). These trimeric clusters are non-classical metal triangles in which the central core has C_{2v} symmetry rather than the more symmetrical D_{2h} symmetry of classical metal triangles. The crystal structure of **1** was found to be highly disordered over three positions. In an attempt to remove the disorder of the core, the pyridine derivative of the product was synthesized using VO(acac)₂py in ethanol heated to 120 °C. This reaction pathway lead to a mixture of both compounds in the form of a co-crystal consisting of **1**(21.6(6)%) and **2**(78.3(6)%). Pure **2** was made starting from VO(acac)₂ and pyridine in dry methylene chloride and its crystal structure was analyzed. These two compounds contain characteristic absorptions in their FTIR spectra at about 995 and 1025 cm⁻¹ of intensity 1:2 which are most likely due to the vanadium oxide bond and may be indicative of the non-classical arrangement. Attempts to reproduce these compounds using different phosphinic acids such as 2-hydroxyisophosphindoline-2-oxide or

diphenylphosphinic acid resulted in the formation of insoluble polymers. Room temperature magnetic susceptibility measurements of the trimers and polymeric compounds gave the spin only values for d^1 metal centers. The variable temperature magnetic measurements of **2** showed that the compound obeys Curie's Law between 2 and 4 °K and displays very weak magnetic interactions over the temperature range 0 to 300 °K. TGA studies of the trimers showed that both of them decomposed into amorphous solids, confirmed by powder diffraction, at around 600 °C.

The tetranuclear compound, $V_4(\mu_3-O)_4(\mu_2-O_2P(Bn)_2)_4(O_4)$, was obtained when $(V_3(\mu_3-O)O_2)(\mu_2-O_2P(CH_2C_6H_5)_2)_6(H_2O)$ was oxidized with either O_2 or $tBuOOH$ in the presence of water. An analogous tungsten species formulated as $W_4(\mu_3-O)_4(\mu_2-O_2P(Bn)_2)_4(O_4)$ was also synthesized by reacting bis(benzyl)phosphinic acid with $W(CO)_6$ in a mixture of THF and ethanol. The tungsten cubane is isoelectronic with the previously synthesised molybdenum cubane $Mo_4(\mu_3-O)_4(\mu_2-O_2P(Bn)_2)_4(O_4)$ and is isolobal with the vanadium and molybdenum cubanes. The molybdenum and tungsten cubanes contain metal-metal bonds of lengths 2.6261(5) and 2.6354(5) Å. The vanadium cubane contains no such bond since the vanadium is in the zero oxidation state which results in considerably different bond lengths and angles when compared to the other two cubanes. The potential catalytic applications of both of these cubanes in areas such as epoxidations, oxidations and alcohol isomerizations remains to be explored.

The reaction between the bis(benzyl)phosphinate ligand and cobalt(II) resulted in three different dimeric compounds which are formulated as $[py_3Co(\mu_2-O_2P(Bn)_2)_3Copy][ClO_4^-](1')$, $py_3Co(\mu_2-O_2P(Bn)_2)_3CoCl(2')$ and $py(\mu_2-NO_3)Co(\mu_2-$

$\text{O}_2\text{P}(\text{Bn})_2)_3\text{Copy}(\mathbf{3'})$. In each dimer one cobalt center exists in a tetrahedral coordination environment and the other in an octahedral. The X-ray diffraction data for each compound revealed that the Co to Co distances in these three compounds are 4.0313(7) Å for $\mathbf{3'}$, 4.265(2) Å for $\mathbf{1'}$ and 4.278(1) Å for $\mathbf{2'}$. This variation in distances could yield different magnetic properties. Only $\mathbf{1'}$ has had its variable temperature magnetic susceptibility measured which revealed a small J of 0.15 cm^{-1} which implies only weak exchange interactions between the cobalt centers.

Appendix

License agreement for Chapter 2

Rightslink® by Copyright Clearance Center



RightsLink®

Home

Account
Info

Help



ACS Publications Title:
High quality. High impact.

Syntheses, X-ray Structural Characterizations, and Thermal Stabilities of Two Nonclassical Trinuclear Vanadium(IV) Complexes, $(V_3(\mu_3-O)_2(\mu_2-O_2P(CH_2C_6H_5)_2)_6(H_2O))$ and $(V_3(\mu_3-O)_2(\mu_2-O_2P(CH_2C_6H_5)_2)_6(py))$, and Polymeric Complexes of Stoichiometry $(VO(O_2PR)_2)_\infty$, $R_2 = Ph_2$ and $o-(CH_2)_2(C_6H_4)$

Author: John S. Maass, Zhichao Chen, Matthias Zeller, Floriana Tuna, Richard E. P. Winpenny, and Rudy L. Luck

Publication: Inorganic Chemistry

Publisher: American Chemical Society

Date: Mar 1, 2012

Copyright © 2012, American Chemical Society

Logged in as:

john.maass

LOGOUT

PERMISSION/LICENSE IS GRANTED FOR YOUR ORDER AT NO CHARGE

This type of permission/license, instead of the standard Terms & Conditions, is sent to you because no fee is being charged for your order. Please note the following:

- Permission is granted for your request in both print and electronic formats, and translations.
- If figures and/or tables were requested, they may be adapted or used in part.
- Please print this page for your records and send a copy of it to your publisher/graduate school.
- Appropriate credit for the requested material should be given as follows: "Reprinted (adapted) with permission from (COMPLETE REFERENCE CITATION). Copyright (YEAR) American Chemical Society." Insert appropriate information in place of the capitalized words.
- One-time permission is granted only for the use specified in your request. No additional uses are granted (such as derivative works or other editions). For any other uses, please submit a new request.

BACK

CLOSE WINDOW

Copyright © 2012 Copyright Clearance Center, Inc. All Rights Reserved. [Privacy statement](#).
Comments? We would like to hear from you. E-mail us at customercare@copyright.com

License agreement for Chapter 3

Dear John

The Royal Society of Chemistry (RSC) hereby grants permission for the use of your paper(s) specified below in the printed and microfilm version of your thesis. You may also make available the PDF version of your paper(s) that the RSC sent to the corresponding author(s) of your paper(s) upon publication of the paper(s) in the following ways: in your thesis via any website that your university may have for the deposition of theses, via your university's Intranet or via your own personal website. We are however unable to grant you permission to include the PDF version of the paper(s) on its own in your institutional repository. The Royal Society of Chemistry is a signatory to the STM Guidelines on Permissions (available on request).

Please note that if the material specified below or any part of it appears with credit or acknowledgement to a third party then you must also secure permission from that third party before reproducing that material.

Please ensure that the thesis states the following:

Reproduced by permission of The Royal Society of Chemistry

and include a link to the paper on the Royal Society of Chemistry's website.

Please ensure that your co-authors are aware that you are including the paper in your thesis.

Regards

Gill Cockhead

Publishing Contracts & Copyright Executive

Gill Cockhead (Mrs), Publishing Contracts & Copyright Executive

Royal Society of Chemistry, Thomas Graham House

Science Park, Milton Road, Cambridge CB4 0WF, UK

Tel [+44 \(0\) 1223 432134](tel:+44%201223432134) *begin of the skype highlighting* [+44 \(0\) 1223 432134](tel:+44%201223432134) *end of the skype highlighting*, Fax [+44 \(0\) 1223 423623](tel:+44%201223423623)

<http://www.rsc.org>

License agreement for Chapter 4

Rightslink® by Copyright Clearance Center



RightsLink®

Home

Account
Info

Help



ACS Publications Title:
High quality. High impact.

Syntheses and Structures of Three Complexes of Formulas $[L_3Co(\mu_2-O_2P(Bn)_2)_3CoL'] [L'']$, Featuring Octahedral and Tetrahedral Cobalt(II) Geometries; Variable-Temperature Magnetic Susceptibility Measurement and Analysis on $[(py)_3Co(\mu_2-O_2P(Bn)_2)_3Co(py)] [ClO_4]$

Author: John S. Maass, Matthias Zeller, Tanya M. Breault, Bart M. Bartlett, Hiroshi Sakiyama, and Rudy L. Luck

Publication: Inorganic Chemistry

Publisher: American Chemical Society

Date: May 1, 2012

Copyright © 2012, American Chemical Society

Logged in as:

john.maass

LOGOUT

PERMISSION/LICENSE IS GRANTED FOR YOUR ORDER AT NO CHARGE

This type of permission/license, instead of the standard Terms & Conditions, is sent to you because no fee is being charged for your order. Please note the following:

- Permission is granted for your request in both print and electronic formats, and translations.
- If figures and/or tables were requested, they may be adapted or used in part.
- Please print this page for your records and send a copy of it to your publisher/graduate school.
- Appropriate credit for the requested material should be given as follows: "Reprinted (adapted) with permission from (COMPLETE REFERENCE CITATION). Copyright (YEAR) American Chemical Society." Insert appropriate information in place of the capitalized words.
- One-time permission is granted only for the use specified in your request. No additional uses are granted (such as derivative works or other editions). For any other uses, please submit a new request.

BACK

CLOSE WINDOW

Copyright © 2012 Copyright Clearance Center, Inc. All Rights Reserved. [Privacy statement](#).
Comments? We would like to hear from you. E-mail us at customer@copyright.com